Fluorometric Monitoring of the Properties of Proteins Entrapped in Sol-Gel Derived Matrices

Kulwinder Flora

A thesis submitted to the Department of Chemistry, Brock University

in partial fulfillment of the requirements for the degree of

Master of Science

Brock University, St. Catharines, ON

August 1998

Abstract

The successful development of stable biosensors incorporating entrapped proteins suffers from poor understanding of the properties of the entrapped biomolecules. This thesis reports on the use of fluorescence spectroscopy to investigate the properties of proteins entrapped in sol-gel processed silicate materials. Two different single tryptophan (Trp) proteins were investigated in this thesis, the Ca^{2+} binding protein cod III parvalbumin (C3P) and the salicylate binding protein human serum albumin (HSA). Furthermore, the reactive single cysteine (Cys) residue within C3P and HSA were labelled with the probes iodoacetoxynitrobenzoxadiazole (C3P) and acrylodan (C3P and HSA) to further examine the structure, stability and function of the free and entrapped proteins. The results show that both C3P and HSA can be successfully entrapped into sol-gel-derived matrices with retention of function and conformational flexibility.

Acknowledgments

I would like to thank firstly my thesis supervisor, Dr. John Brennan for all of his advice, support, and patience during the past two years. I would also like to thank my committee members, Dr. Stephen Hartman, Dr. Jim McNulty and Dr. Doug Bruce for their assistance.

One never works in isolation, and this thesis is no exception. I would like to thank several collaborators who provided technical assistance including; Howard Melville for use of the liophilizer in the Earth Sciences Department at Brock University, Jhansi Lakshmi for training me on the Pore size analyzer, James Shoemaker for his assistance with diffuse reflectance IR experiments and Dr. Arthur Szabo for the use of his fluorescence lifetime instrument at the University of Windsor. A special thanks to Dr. Frank Bright and his graduate students, Gary Baker and Meagan Doody at State University of New York at Buffalo, who obtained time-resolved fluorescence and O_2 quenching data for HSA-Ac. Furthermore, I would like to acknowledge NSERC for funding of this work, and also technical services at Brock University for all of their help.

It has been a long road to get to this point and it is in thanks to many people along the way who made it worthwhile. A special thanks to a few members of H209 over the years; Lili Zheng, Bill Reid, and Emily DiBattista, Cassandra Spong and Amy Jones for all of their assistance and friendship. I would also like to thank some special friends who were always there...even on the days when things didn't work; Dr. Carl Turner, James Shoemaker, and Mike Rakic. Thank you....you all made it enjoyable to come into work

(on most days!!!). A special thanks to all of the friends who have come into my life during my 6 year sentence at Brock. You all made the time at Brock enjoyable and memorable.

I would also like to thank my family for always believing in me and supporting me throughout my educational career.

Table of Contents

List of Figures

List of Tables

Chapter 1: Introduction and Theory

1.1 Introduction to Biosensors

The development of analytical devices for monitoring chemical and biological species in complex media without the need for sample pretreatment or time consuming separation steps, has proven to be an important field of research. The field of biosensors has arisen to meet this challenge. Biosensors are devices which use biological molecules, either entrapped within or immobilized onto inorganic or organic matrices, in order to recognize specific analytes. The binding of an analyte to an entrapped protein normally is transduced into an optical, thermal, piezoelectric or electrochemical signal in order to determine the presence and/or concentration of the analyte. Thus the two main components of a biosensor are the biomolecule, which is capable of selectively binding to an analyte, and the transducer, which is able to produce a signal from the binding interaction.

Biological molecules which have been used in the development of sensors include enzymes,[1-8] lectins,[9] molecular receptors,[10] metal and oxygen binding proteins, [2,11-19] lectins, antibodies, [20-23] as well as DNA/RNA [24,25] and artificial or synthetic receptors. [26] At present, proteins are still the biomolecule most often used to provide selectivity in biosensors. While a large amount of research has been done on such sensors, many problems exist with the development of biosensors, resulting in few commercially available devices. Perhaps the most significant obstacle which exists is the successful interfacing of functional protein within or to the physical transducer. There are many immobilization methods which have been investigated, including physical adsorption,[27] entrapment in

organic or inorganic polymer matrices,[3] covalent bonding to surfaces,[28] and cross linking of proteins after adsorption.[29] Although progress has been made in each of these areas, problems still exist with leaching, desorption, changes in function (k_m, k_{cat}, k_d) and denaturation (loss of function) of the biomolecules. Other problems include long term changes in function, which can affect calibration, and degradation of the surface over time due to proteolytic or microbial attack.

Research is now being conducted in order to understand the properties of immobilized and entrapped proteins and the factors responsible for protein denaturation. Such effects are aimed at developing better encapsulation and/or immobilization schemes which can maintain the structure of proteins and maximize both initial and long-term function. It is important to note that the three-dimensional protein structures are delicate and can easily unfold, eliminating function. Numerous solution-based studies have been done in order to characterize the structure-function relationships of proteins. However, few studies have been done with entrapped proteins. The study of structure-function relationships for entrapped proteins is a major focus of the present thesis.

1.1.1 Sol-gel Encapsulation of Biomolecules in Sol-gel Processed Materials

The preparation of silicate materials from liquid precursors has been known for over 150 years. [30] Typical processing conditions involve acid or base catalyzed hydrolysis of silane precursors in alcohol/water mixtures, gelation at low pH, and heating of the material to produce a durable, glass-like material.

In the past few years several reports have appeared which describe a modified sol-gel processing method which is suitable for the encapsulation of biomolecules into inorganic silicates derived from precursors such as tetraethylorthosilicate (TEOS) or tetramethylorthosilicate (TMOS). [2,3,11,18,19,26,31,32] Two main breakthroughs led to the successful encapsulation of biomolecules by this method. The first involved the promotion of hydrolysis by sonication of TEOS or TMOS in the presence of water and acid, thereby removing the need for an alcohol co-solvent, which is known to be detrimental to biomolecules. The second was the addition of a buffered aqueous solution to the hydrolyzed silane to bring the pH of the medium close to the physiological range and to dilute any alcohol produced during hydrolysis of the TEOS before the proteins were added. [22,26] More recent procedures add the protein directly in the buffer solution. [2,6,7,19] These modifications, combined with low temperature aging over a period of several days or weeks, have resulted in a large number of successful protein encapsulation protocols. An outline of some of the successful systems can be found in the review by Avnir *et al.* [2]

Figure 1.1 shows a simplified schematic of the chemical processes involved in protein encapsulation into sol-gel-derived glass materials. Sol-gel processing firstly involves hydrolysis of alkoxysilane monomers such as tetramethylorthosilicate (TMOS) or tetraethylorthosilicate (TEOS) under mildly acidic conditions. This product, known as a sol, is a colloidal suspension, consisting of particles of 1-100 nm. Condensation and polycondensation involve linkage of the colloids and these processes are allowed to occur at a very slow rate. Gelation, resulting in the formation of a wet, extended siloxane network, is induced by adding a buffered aqueous solution containing the desired

biomolecule. The act of gelation takes only a few minutes and the resulting product is a solid matrix containing an entrapped protein with a large amount of solvating water, and up to 50% alcohol (by volume) owing to the products of alkoxysilane hydrolysis. The wet gels are then aged (typically at 4°C to prevent the denaturation of the biomolecule), either in, buffer or in a dessciator. The condensation and polycondensation processes continue over 12-30 days, shrinking and strengthening the gel and reducing the volume of entrapped solvent.

1.	$Si(OEt)_4 + nH_2O + H^+ \rightarrow Si(OEt)_{4-n}(OH)_n + nEtOH$	Hydrolysis
2.	$2\ Si(OEt)_{4-n}(OH)_n \rightarrow (OH)_{n-1}(OEt)_{4-n}Si\text{-}O\text{-}Si\ (OEt)_{4-n}(OH)_n + H_2O$	Condensation
3.	$n\text{-}Si\text{-}O\text{-}Si \rightarrow [\text{-}Si\text{-}O\text{-}Si\text{-}O\text{-}Si\text{-}O\text{-}]_n + H_2O$	Polycondensation
4.	$[\text{-}O\text{-}Si\text{-}O\text{-}Si\text{-}O\text{-}Si\text{-}O\text{-}]_n$ + buffer + protein $\rightarrow$ entrapped protein	Gelation
5.	Condensation and polycondensation continue for weeks	Drying

Figure 1.1: Sol-gel encapsulation

Sol-gel-derived bioglasses normally have a large amount of trapped interstitial water in their pores, and this allows proteins to retain a structure and stability similar to that found in aqueous media. Sol-gel encapsulated proteins can be stable for months, [13,33] however the basis of this stability is still largely unknown. It has been proposed that the "cage" may reduce the conformational flexibility of the protein, thus prevent unfolding. [6,19] However, studies on proteins such as cytochrome C and bovine serum albumin (BSA) have suggested that substantial mobility exists within entrapped proteins. Clearly, more

work is required to determine the basis of the enhanced stability of entrapped proteins. For example, the pores of the sol-gel matrix allow for the diffusion of analytes through the matrix allowing interactions between the biomolecule and analyte to occur while retaining the entrapped protein and preventing microbial attack. Sol-gel processed biomolecules offer several advantages over other protein immobilization and entrapment methods.

Another advantage of sol-gel encapsulation is that the matrix is transparent, allowing for spectroscopic measurements of the encapsulated proteins. Thus, measurements which require ultraviolet radiation, such as ultra-violet visible absorbance and fluorescence spectroscopy, can be done to aid in the investigation of the state and function of the biological moiety within the matrix. In addition, the materials are easy to prepare, can be cast into virtually any shape (monoliths, fibers, thin films), and are easy to interface to both electrodes and optical fibers.

In 1990, Braun *et al.* [3] were the first group to successfully encapsulate biomolecules into inorganic matrices to show retention of activity and an increase in thermal stability of alkaline phosphatase. These researchers found that the restriction of the conformational flexibility of the enzyme in the gel aided in the improved stability of the enzyme. Since this initial report, many groups have conducted research on sol-gel encapsulated proteins. [2,11-19] The problems which still exist are that some proteins are able to retain there activity whereas other are not. In addition, not much is known about structure versus function relationships of entrapped proteins in sol-gel-derived materials.

To this point, few groups have examined the structure of a protein after sol-gel encapsulation. This was first done by Edminston *et al.* [19] using fluorescence techniques to

examine the structures of BSA and myoglobin (Mb) immobilized in sol-gel-derived matrices made from tetramethylorthosilicate (TMOS). It was found that BSA was able to retain its native structure upon entrapment, as shown by fluorescence spectra, while Mb was not, as indicated by absorbance spectra. BSA was able to undergo a conformational change induced by chemical denaturation and pH changes in solution, but was unable to fully undergo these conformational changes while entrapped due to restrictions in conformational flexibility of the protein. The inability to undergo full conformational motions was suggested to be due to steric restrictions imposed by the silicate matrix. However, this may also be due to the presence of an inaccessible fraction of protein which can not be reached by external reagents. This study was important since it indicated that not all proteins can be entrapped into sol-gel-derived matrices so as to retain their native form. However, the property of the matrix that allowed only some of the proteins to retain their structure was not explored in detail, and thus needs to be further examined.

The dynamic motions of entrapped proteins has also been examined in detail by Bright *et al.*[18] Both bovine serum albumin and human serum albumin were labelled with the fluorescent probe acrylodan. The decay of rotational anisotropy of the label was monitored as a function of aging the proteins in TMOS derived biogels. It was found that the probe was able to report on both the global motions of the protein, and on its local motions. However, the degree of local motion increased after 37 days of aging, suggesting that the cybotactic pocket hosting the probe actually opens as a function of aging, perhaps indicating protein unfolding. Overall, the global motion of the protein was

slower than in solution, but the protein was able to move, indicating that it was not adsorbed to the pores of the sol-gel.

Our group has successfully entrapped the small protein monellin into TEOS derived matrices using a modified sol-gel procedure.[13] Emission spectra, quenching and anisotropy data showed that the protein was entrapped in its native form. Interestingly, the anisotropy results suggested that the mobility of the solvent inside the sol-gel-derived glass was substantially reduced in comparison to solution, in agreement with the results for HSA-Ac and BSA-Ac, described above. A less mobile solvent environment may be part of the reason for the improved stability of some proteins upon entrapment.[16] This hypothesis was supported by thermal stability studies of free and entrapped monellin, which showed that there was a 14 ± 1°C increase in stability upon entrapment.[34] Further studies suggested that the sol-gel entrapment procedure can be tailored to optimize the stability of entrapped metal-ion-binding proteins by entrapping the proteins in the presence of an excess of ligand to maximize the thermodynamic stability of the protein.[17]

1.2 Thesis Motivation

1.2.1 Project Goals

Although the literature in the field of sol-gel based protein entrapment is extensive, it is clear that more information is needed regarding both the internal environment of the sol-gel matrix and properties of entrapped proteins in order to explain the effect of entrapment on protein structure, stability and function.

The research in this thesis focuses on the use of fluorescence spectroscopy to investigate the environment within the sol-gel-derived matrix into which the biological molecule is encapsulated, the structure/function relationships of entrapped proteins, and the stability of the entrapped protein to both chemical and thermal denaturation. These studies were done to provide insights into how the interior of the sol-gel-derived matrix affects the structure, conformational flexibility, thermal and chemical stability of the protein and how these parameters relate to the function of the entrapped protein. Furthermore, preliminary work on a new signal transduction method, termed fluorescent allosteic signal transduction (FAST), was also done using Cod III parvalbumin, both in solution and in the sol-gel-derived matrices.

1.2.1 Thesis Organization

This thesis is organized into 7 chapters. The first chapter gives an overall introduction to biosensors as well as information on relevant theory and techniques used in this study. Chapter 2 investigates the physical characteristics and internal environment of TEOS derived sol-gel processed materials by using two fluorescent probes, pyrene and 7-azaindole, to determine an appropriate encapsulation protocol for proteins. Chapter 3 investigates and compares the structure, stability, conformational flexibility and functionality of the small Ca^{2+} binding protein Cod III parvalbumin (Cod III parv, C3P) in solution and the sol-gel-derived matrix. The purpose of this study was to determine the effects of entrapment on the structure-function relationships of a model FAST protein, when using the sol-gel processing protocol adapted from the study in Chapter 2. Chapter

4 furthers the study described in Chapter 3 by labelling the single cysteine residue in Cod III parv with the fluorescent probes iodoacetoxynitrobenzoxadiazole (IANBD) and acrylodan (Ac) to determine if Ca^{2+} induced conformational changes are possible with the labels present, and to allow Ca^{2+} detection using a He-Cd laser-based fiber optic fluorimeter. Ac and NBD were chosen as appropriate probes since both can be excited at 442 nm, which is the output of the He-Cd laser. Chapter 5 investigates the unfolding behaviour, stability, and structure-function relationships of a much larger protein, human serum albumin (HSA), and labelled HSA(HSA-Ac). These studies were done in solution to determine the unfolding pathway of the protein. Chapter 6 extends the study described in Chapter 5 to HSA and HSA-Ac entrapped in TEOS derived materials to investigate the effects of entrapment on the structure-function relationship of a large protein, and to compare to unfolding patterns and thermodynamic stability of the free and entrapped protein. Chapter 7 provides conclusions and suggestions of future work.

1.3 Theory and Techniques used for Investigating Protein Structure and Stability

1.3.1 Ultraviolet-Visible Absorption

UV-Vis spectroscopy is a technique which is readily used for examining proteins. The amino acids phenylalanine (Phe), tyrosine (Tyr) and tryptophan (Trp) are able to absorb UV light due to the presence of aromatic rings. The absorbance of proteins with these amino acids is slightly shifted to longer wavelengths, or red-shifted, in polar environments such as water and blue shifted in non-polar environments such as the interior of a protein. However, these shifts are small, generally being less than 5 nm.

Tryptophan is the most widely used amino acid for UV-Vis absorbance experiments, mainly due to its high degree of absorbance and red-shifted absorbance relative to Phe and Tyr. With the use of Beer's Law, the concentrations of protein solutions can be obtained. Beer's Law is shown in equation 1.

$$A=\varepsilon bc \qquad (1)$$

where, A is the absorbance, ε is the molar extinction coefficient ($M^{-1}cm^{-}1$), b is the pathlength (in cm) and c is the molar (M) concentration of the solution. For tryptophan, the extinction coefficient at 280 nm is 5600 $M^{-1}\cdot cm^{-1}$, while ε_{max} of Tyr is 1440 $M^{-1}\cdot cm^{-1}$ at 277 nm. Thus, the observed absorbance can be directly related to the protein concentration if the number of tryptophans and tyrosines per protein is known. UV-Vis experiments can also be used to determine or verify protein aggregation leading to light scattering. For tryptophan, if a non-zero absorbance value is obtained at wavelengths of greater than 310 nm, scattering is taking place and thus the protein is aggregated.

1.3.2 Fluorescence Spectroscopy of Proteins

The fluorescence emission of proteins containing either extrinsic or intrinsic fluorophores can be measured. For extrinsic fluorescence the protein must be labelled with a fluorophore such as acrylodan or nitrobenzoxadiazole (NBD). Extrinsic fluorescence often has many problems associated with it. The most important is the difficulty in determining the exact location of the fluorophore. There can also be problems with determining the number of probes that get bound to the protein. This makes it difficult or even impossible to relate changes in fluorescence to changes in protein

structure. In addition, there exists the possibility of labelling at or near the active site, which destroys protein function. Fortunately, these problems of extrinsic labelling can be remedied by selectively labelling only the sulfhydryl residues on proteins with sulfhydryl reactive probes, such as acrylodan and NBD. Proteins such as human serum albumin and Cod III parvalbumin contain only one free sulfhydryl group, making it simple to place only a single label on the protein and also making it possible to know the exact location of the probe.

Intrinsic fluorescence methods involve the incorporation (or natural occurrence) of the fluorophore directly in the amino acid sequence. Intrinsic fluorescence spectroscopy is commonly used to monitor the structure and thermodynamic stability of proteins containing fluorescent amino acids with aromatic rings. Both ultraviolet absorbance and fluorescence emission data can be obtained for these amino acid residues, however Tyr and Trp are the most useful and Trp is the best of all amino acids to use due its sensitivity to the protein structure and dynamics, and to local environment.

Fluorescence spectroscopy is an essential technique in this research project. The fluorescence process can be illustrated by the Jablonski diagram, shown in Figure 1.2. Before the molecule is excited, it exists in a stable state, the singlet ground state, designated by S_0 on the diagram. The absorption of a photon of light takes place by the molecule in $\sim 10^{-15}$s, placing the molecule in an excited vibrational level of the first excited singlet state, designated as S_1. The loss of excess vibrational energy occurs over $\sim 10^{-12}$s, causing the electron to move to the lowest vibrational energy level of the excited electronic state (S_1V_0). From this state, energy may be lost by several processes. In

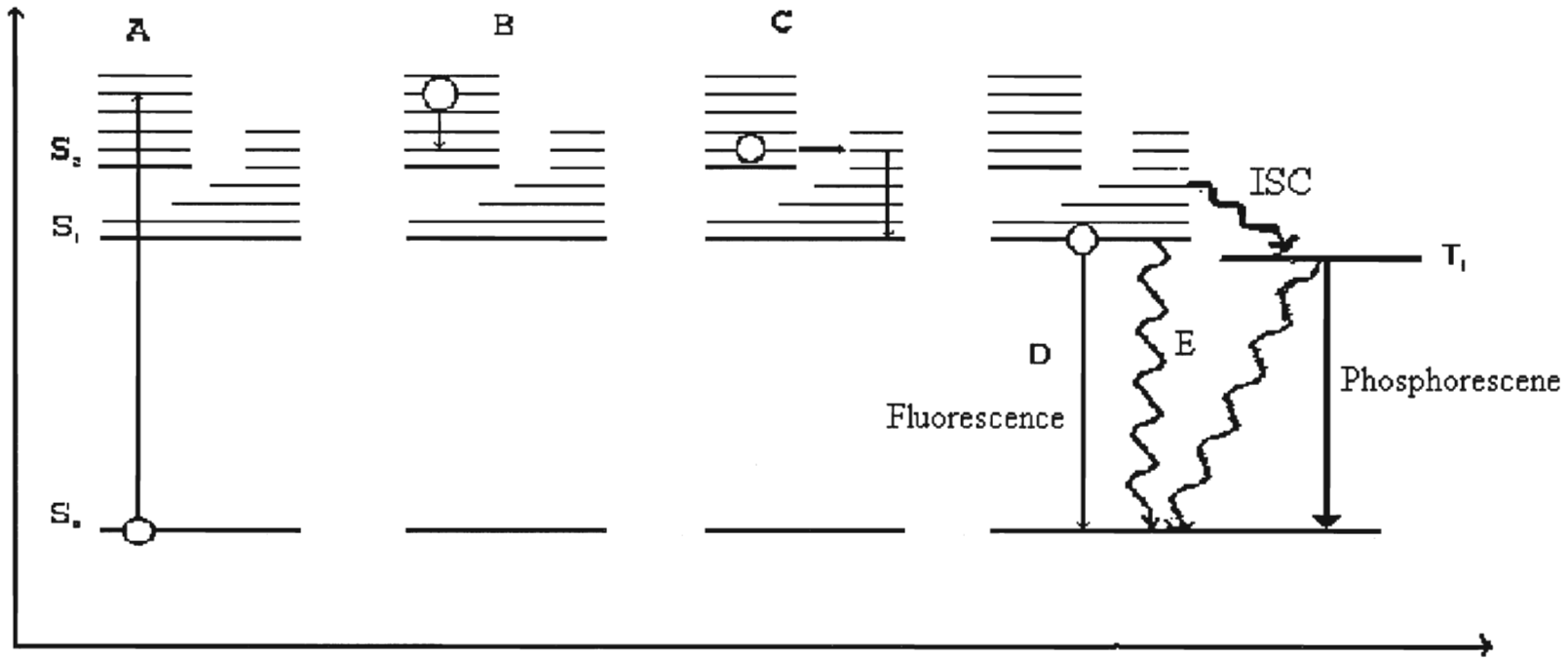

Figure 1.2: Jablonski Diagram

process D, fluorescence is shown where the molecule moves from the lowest energy level in the excited state to an excited vibrational level of the electronic ground state, by emission of a photon in 10^{-8} - 10^{-9} s. Competing processes are the loss of electronic energy as heat by internal conversion, intersystem crossing (ISC) which results in phosphorescence or further ISC, or interactions with external reagents via energy transfer and collisional quenching.

If one or more of the non-radiative processes is substantially faster than fluorescence, very little fluorescence emission will be observed. On the other hand, if the fluorescence pathway is most favourable, almost all of the excited state energy can be lost radiatively. Normally, the process of fluorescence and other processes are defined by the rate constants for radiative decay (k_r) and non-radiative decay (k_{nr}), respectively.

The efficiency of the fluorophore process is determined by the quantum yield, which is expressed in terms of the various rate constants for radiative and non-radiative decay processes, as shown by equation 2;

$$\Phi = \frac{k_r}{k_r + \Sigma k_{nr}} \qquad (2)$$

where k_r is the radiative rate constant and Σk_{nr} is the sum of all non-radiative rate constants. Hence, highly fluorescent molecules will have large quantum yield values (approaching 1.0), while weakly fluorescent species will have quantum yield values close to zero.

Fluorescence spectroscopy can provide a great deal of information when monitoring the emission of tryptophan residues in a protein. The quantitative data that can be obtained from observation of fluorescence emission include; excitation and emission wavelength envelopes and maxima, steady-state emission intensity, average intensity decay time (lifetime), steady-state anisotropy and time-resolved anisotropy decay.

Steady-state emission intensity provides useful information on proteins. Fluorescence intensity (F) is given by;

$$F=2.303I_o k\varepsilon bc\Phi \qquad (3)$$

where, I_o is the excitation intensity, ε is the extinction coefficient of the fluorophore, b is the path length of the cell, and c is the concentration of the fluorophore in $mol{\cdot}L^{-1}$, and Φ is the quantum yield. In most cases, if I_0, b, k and c are constant, then intensity determined by the quantum yield (Φ), which is given by Equation 2.

1.3.2.1 Emission Wavelength

Intensity and quantum yield are generally integrated intensities. However, there exists an envelope of intensity versus wavelength for both fluorescence excitation and emission. A useful parameter of fluorescence emission is the location of the wavelength of maximum emission intensity. The emission wavelength maximum provides information about the dipolarity of the local microenvironment, and can be used to assess the degree of solvent exposure of the tryptophan residue. Solvents have the ability to produce red shifts, or shifts to longer wavelengths (lower energy), due to their dipolarity. There are three main causes of wavelength shifts; the Stokes Shift, general solvent effects and

specific solvent effects. The Lippert equation, (4) estimates the magnitude of the wavelength shift for the general solvent effect;

$$\bar{\nu}a - \bar{\nu}f \cong \frac{2}{hc}\left(\frac{\varepsilon - 1}{2\varepsilon + 1} - \frac{n^2 - 1}{2n^2 - 1}\right)\frac{(\mu^* - \mu)^2}{a^3} + const \qquad (4)$$

where $\bar{\nu}_a$ and $\bar{\nu}_f$ represent the absorption and fluorescence energy maxima in wavenumbers (cm^{-1}), respectively, h is Planck's constant, c is the speed of light, ε is the dielectric constant of the solvent, n is the solvent refractive index, a is the radius of the fluorophore cavity within the solvent, μ and μ^* are the dipole moments of the ground and excited states of the fluorophore, respectively, and *const* represents the inherent Stokes shift due to vibrational relaxation of the electron in the excited electronic state following adsorption. Based on the Lippert equation, more polar solvents results in larger ($\bar{\nu}a - \bar{\nu}f$) thus a lower emission energy or red-shift. This is valid only if the difference in dipole moments of the ground and excited states in non-zero. Specific solvent interactions occur between the fluorophore and solvent and are more complicated. Such interactions include hydrogen bonding and excited state reactions.

1.3.2.2 Fluorescence Lifetimes

The fluorescence lifetime (τ) is a measure of the time required for a collection of excited molecules to decay to 1/e of their initial intensity. Equations 5 and 6 describe the lifetimes for a simple, single component decay following excitation with a direct δ-function;

$$I(t) = I_o e^{-t/\tau} \tag{5}$$

where

$$\tau = \frac{1}{k_r + \Sigma k_{nr}} \tag{6}$$

In these equations, I is the intensity at time t, I_o is the initial intensity at time zero and τ is the fluorescence lifetime, given by (6). All other terms have been described previously. For several different probes, or one type of probe in many environments, the fluorescence decay is more complex, and is described by the sum of discrete decay components as shown in equation 7;

$$I(\lambda, t) = \sum_i \alpha_i(\lambda) \exp(-t / \tau_i) \tag{7}$$

where τ_i is the decay time of the ith component and $\alpha_i(\lambda)$ is the pre-exponential factor at emission wavelength λ. The fractional fluorescence of component i at wavelength λ ($f_i(\lambda)$) can be calculated as follows;

$$f_i(\lambda) = (\alpha_i(\lambda)\tau_i \Big/ \sum_i \alpha_i(\lambda)\tau_i) \tag{8}$$

where α_i is the normalized, pre-exponential factor describing the contribution of each τ_i to the total decay. The mean fluorescence lifetime is found by;

$$< \tau >= \sum_i \left(\frac{\alpha_i \tau_i^2}{\sum_i \alpha_i \tau_i} \right) = \sum_i f_i \tau_i \tag{9}$$

The mean lifetime is important for this project because the fluorescence intensity decay kinetics of Trp in proteins is normally multi-exponential. Lifetimes provide information about the rate constants k_r and k_{nr} as well as an indication of dynamic quenching

processes. It is possible to find k_r and k_{nr} from the following relationships, if Φ and $<\tau>$ are known.

$$\Phi = \frac{\tau_s}{\tau_r}, \qquad k_{nr} = \frac{1}{\tau_s} - \frac{1}{\tau_r}, \qquad k_r = \frac{1}{\tau_r}, \qquad \text{where} \qquad <\tau> = \tau_s \tag{10}$$

1.3.2.3 Anisotropy

Quantum yields, emission and excitation wavelengths, and fluorescence lifetimes generally give information on parameters such as structure or distribution of structures. However, these techniques provide no information on mobility and or overall protein dynamics. To get such information, polarized light is used to measure the fluorescence anisotropy. The fluorescence anisotropy (r) can be defined as the ratio of the polarized component to the total intensity of light (I_T), as given by;

$$r = \frac{I_{\parallel} - I_{\perp}}{I_{\parallel} + 2I_{\perp}} \tag{11}$$

When polarized light is passed into a sample, light which is emitted is measured through parallel and perpendicular polarizers. Here, $I_{\parallel}$ is the emitted light intensity parallel to the incident polarized light and $I_{\perp}$ is the emitted light intensity perpendicular to the incident polarized light direction. The total emitted light intensity (I_T) is given by equation 12;

$$I_T = I_{\parallel} + 2I_{\perp} \tag{12}$$

Once light passes through the excitation monochromator, the resulting light is partially polarized. This causes the rotation of the exciting polarizer to yield different intensities in

the horizontal and vertical positions. To determine the true intensity ratio ($I_{\parallel}/I_{\perp}$), a ratio of sensitivities of the detection system for horizontally and vertically polarized light needs to be determined. This parameter is known as the G-factor, which represents the ratio of sensitivity for the vertically polarized light divided by the sensitivity of the horizontally polarized light. [35]

The value of the anisotropy can be used to obtain the average rotational correlation time (ϕ) if the mean fluorescence lifetime and limiting anisotropy (r_0) are known;

$$r = \frac{r_0}{1+(\tau/\phi)} \tag{13}$$

When r=0, the protein is fully mobile, when $r=r_0$ then the protein is immobile. Accordingly, if ϕ is low, the moiety rotates quickly, while if ϕ is high, then the motion is slow.

Decay of Fluorescence Anisotropy

Time-resolved measurements can give more information on the components underlying an average parameter. Time-resolved fluorescence anisotropy can provide insight into the mobility of the fluorescent reporter group and the mobility of the entire protein. In the case of fluorescently-labelled proteins, there are rotational components which can be assigned to local reorientation of the probe and to global motions of the entire biomolecule. If one assumes that the protein undergoes isotropic rotational motion, then the observed time-resolved decay of anisotropy ($r(t)$) is described by a double exponential decay of the form;

$$r(t) = r_0[\beta_1 \exp(-t/\phi_1) + \beta_2 \exp(-t/\phi_2)] \tag{14}$$

In the situation where this local probe motion is faster than the global motion of the entire protein, the local rotational motion of the probe, ϕ_L is given as $1/(1/\phi_1 + 1/\phi_2)$, where ϕ_1 reflects the global reorientation of the entire protein. The terms β_1 and β_2 represent the fractional contributions to the total anisotropy decay from the "global" and "local" motions, respectively ($\Sigma\beta_i=1$).

A semi-angle (θ) can be associated with the cone within which the probe is able to precess during its excited-state fluorescence lifetime, given by:

$$\theta = \cos^{-1}[0.5(8(\beta_2)^{1/2} + 1)^{1/2} - 1] \qquad (15)$$

If the environment surrounding the probe is totally restrictive to the local probe motion, θ will approach 0°. In contrast, complete freedom to rotationally reorient will result in a θ value of 90°. Intermediate θ values reflect partial freedom of the probe to reorient within its cybotactic region.

1.3.2.4 Quenching

In addition to structure and dynamics, other experiments can be done to probe the conformation of a protein and accessibility of a reporter group. The method commonly used to probe the solvent accessibility of tryptophan residues in the protein is acrylamide quenching. The structure of acrylamide is shown in Figure 1.3.

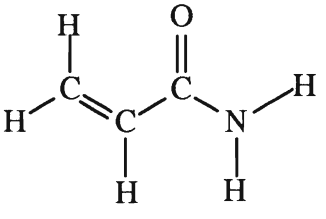

Figure 1.3: Structure of Acrylamide

The amount of quenching observed correlates with the degree of solvent exposure of Trp. Fluorescence quenching experiments involve adding a substance which can interact with the fluorophore to result in a decrease in the fluorescence intensity or fluorescence lifetimes of the probe. For proteins, both dynamic and static quenching processes can occur.

Dynamic quenching results from collisions between the quencher and the fluorophore in the excited state which occurs through the process of diffusion. As a result, the fluorophore undergoes non-radiative decay and the quantum yield and lifetime both decrease. Molecular contact between the fluorophore and quencher is usually required for deactivation of the excited fluorophore through dynamic quenching, although exceptions do exist (ie., energy transfer). The Stern-Volmer equation describes the dynamic quenching process;

$$F_0/F = \tau_o/\tau = 1 + K_{sv}[Q] = 1 + k_q\tau_o[Q] \qquad (16)$$

where F_o is the fluorescence intensity in the absence of the quencher, F is the fluorescence intensity in the presence of the quencher, $[Q]$ is the molar concentration of the quencher, K_{sv} is the Stern Volmer quenching constant for the collisional process (M^{-1}), k_q is the bimolecular quenching constant ($M^{-1}.s^{-1}$), and τ_0 and τ are the lifetimes in the absence and presence of the quencher, respectively.

Static quenching involves the instantaneous deactivation of an excited fluorophore by a quencher which is located within an active volume element at the time of excitation of the fluorophore. In this case, diffusion of Q and F are not necessary for a quenching

interaction to occur and hence only F is affected, but not τ. The volume element is the volume of the sphere as described by equation 17.

$$V = \frac{4}{3}\pi r^3 \tag{17}$$

Typically, the active volume of the sphere surrounding the fluorophore has a radius reaction distance of about 10 angstroms. Static quenching generally occurs in combination with dynamic quenching and is evident if a Stern-Volmer plot shows an upward curvature. A modified version of the Stern-Volmer equation, (Eqn. 18) can be used to account for static quenching;

$$\frac{F_0}{Fe^{V[Q]}} = 1 + K_{SV}[Q] = 1 + k_q\tau_0[Q] \tag{18}$$

where $e^{V[Q]}$ accounts for the static quenching.

1.3.2.5 Energy Transfer Measurements

Proteins containing two labels can give further information about the protein. In this thesis project, both HSA and Cod III parvalbumin contain a single Trp residue and also a free cysteine residue which can be labelled. The presence of two fluorescent species within the protein allows for energy transfer between the label and the Trp residue. The efficiency of energy transfer (E) as a function of distance between probes (R) can be described using equation (19);

$$E = \left(1 - \frac{\Phi_{DA}}{\Phi_D}\right) = \left(1 - \frac{\tau_{DA}}{\tau_D}\right) = \frac{R_0^6}{R^6 + R_0^6} \tag{19}$$

where R_0 represents the distance at which energy transfer is 50% efficient, Φ_{DA} and τ_{DA} are the quantum yield and fluorescence lifetime of the donor in the presence of the acceptor, and Φ_D and τ_D are the unquenched donor quantum yield and lifetime in the absence of acceptor. The value of R_0 (in nanometers) is obtained from equation (20);

$$R_0 = 9.79x10^2(Jn^{-4}\kappa^2\Phi_D)^{1/6} \qquad (20)$$

where J is the overlap integral, n is the refractive index of the solution and κ^2 is the orientation factor between the donor and acceptor electronic transition dipole moments. The overlap integral is determined using equation (21):

$$J = \frac{F_D(\lambda)\varepsilon_A(\lambda)\lambda^4 d\lambda}{F_D(\lambda)d\lambda} \qquad (21)$$

where $F_D(\lambda)$ is the emissive rate of the donor at each wavelength, ε_A is the molar extinction coefficient of the acceptor, λ is the wavelength and $d\lambda$ is the wavelength interval (usually 1 nm).

1.3.3 Protein Structure and Stability

The following Table shows the spectroscopic properties of the aromatic amino acids.

	ABSORBANCE			FLUORESCENCE	
	λ_{max} (nm)	Molar Absorptivity ($M^{-1}cm^{-1}$)		λ_{max} (nm)	Quantum Yield
Phenylalanine	257.4	197		282	0.04
Tyrosine	274.6	1420		303	0.21
Tryptophan	279.8	5600		348	0.20

Table 1.1: The spectroscopic properties of the aromatic amino acids at neutral pH. [36]

As indicated in Table 1.1, phenylalanine has both a low ε_{max} and quantum yield, making its fluorescence difficult to detect. Tyrosine is not sensitive to its environment in solution and has a low ε_{max}. Tryptophan is the most photosensitive amino acid due to the indole ring which makes it the largest and most fluorescent side chain in proteins.

Depending on the excitation wavelength, it is possible to have all three amino acids present, but only have Trp fluorescence excited (ie., if λ_{ex} is 292 nm or greater). This is not true for Tyr fluorescence, which can only be observed independently if Trp is not present. Phe fluorescence will only be seen if both Tyr and Trp are absent. It is due to this selectivity as well as its high absorbance and quantum yield properties that tryptophan is the most widely studied intrinsic amino acid in proteins. Figure 1.4 shows the aromatic amino acid tryptophan, with the charges that are present at pH 7.

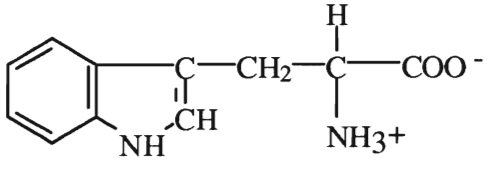

Figure 1.4: Structure of Tryptophan

When using fluorescence to study proteins, it is ideal to analyze proteins containing a single tryptophan or a single label. This is because the lifetime, wavelength and intensity studies become much more complicated if more than one fluorophore is present. Tryptophan is the amino acid which occurs least frequently, thus proteins do not normally contain more than a few tryptophans. Single Trp proteins are commercially available or can be isolated and thus were used in this study. The proteins used also contained single cysteine residues which were labelled using NBD and/or acrylodan.

The determination of the amino acid sequence is the most basic step in characterizing the structure of a protein. The amino acid sequence of a protein is called the primary structure. The secondary structure of a protein describes the local conformation of the polypeptide backbone, such as the formation of α-helices and β-sheets. The tertiary structure is the overall organization of the folded polypeptide chain. The quaternary structure is the 3-dimensional association of the individual subunits of the protein. Cod III parvalbumin is a small single domain protein containing 108 amino acid residues whereas human serum albumin has 585 amino acid residues forming 3 domains, each split into a 2 subdomains (IA,B, II A,B and III A,B).

Many research groups are examining how and why specific proteins fold the way they do. Another avenue being researched, in contrast with protein folding, is how the stability of a folded protein to chemical and thermal denaturation can be maximized. Such studies generally examine the unfolding of proteins. Maximization of the chemical and thermal stability of proteins has many important applications, including improving the performance of enzyme reactors, affinity columns and biosensors. This research project is geared towards understanding the factors which affect the chemical and thermal stability of entrapped proteins, with the ultimate goal of developing of a new generation of more stable biosensors.

1.3.3.1 Thermodynamics of Protein Unfolding

1.3.3.1.1 Thermal Denaturation

Fluorescence-based protein unfolding curves are generally obtained by two different denaturation methods. In the first case, the fluorescence signal (usually steady-state intensity or anisotropy) is monitored as a function of temperature. In thermal denaturation, the temperature is increased to cause the structural changes in the protein. The energy is added in the form of heat to drive the protein over an energy barrier for unfolding. The resulting unfolding curve is analyzed by non-linear fitting to the equation described by Eftink; [15]

$$F_T = \frac{F_{0N} + s_N T + [F_{0U} + s_U T]\exp\{[-\Delta H^0_{un} + T\Delta S^0_{un}]/RT\}}{1+\exp\{-[\Delta H^0_{un} + T\Delta S^0_{un}]/RT\}} \qquad (22)$$

where F_T is the measured intensity (or anisotropy) at some temperature T, and R is the gas constant. The remaining six terms are fitting parameters, where F_{0N} and F_{0U} are the fluorescence intensity (or anisotropy) of the native and unfolded states, respectively, s_N and s_U are the baseline slopes of the native and unfolded states as a function of temperature, respectively, and ΔH^0_{un} and ΔS^0_{un} are the enthalpy change and entropy change for the unfolding reaction, respectively. The free energy change for unfolding (ΔG_{un}) is then determined by using equation (23);

$$\Delta G_{un}(T_r) = \Delta H^0_{un} - T_r \Delta S^0_{un} + \Delta C_{p,un}[(T_r - T_{un}) - T\ln(T_r / T_{un})] \qquad (23)$$

where T_r is a reference temperature (usually 20°C), T_{un} is the temperature of unfolding (given by $\Delta H^0_{un} / \Delta S^0_{un}$) and $\Delta C_{p,un}$ is differential heat capacity for unfolding, which

accounts for the temperature sensitivity of the entropy and enthalpy terms on going from T_r to T_{un}.

1.3.3.1.2 Chemical Denaturation

The second method used to unfold proteins is the addition of a chemical denaturant such as urea or guanidine hydrochloride (GdHCl). The structures of GdHCl and urea are shown in Figure 1.5.

Guanidine Hydrochloride Urea

Figure 1.5: Structure of Guanidine Hydrochloride and Urea

In this case, the steady-state fluorescence intensity or anisotropy of the protein is monitored as the concentration of the chemical denaturant is increased. The unfolding transitions are usually fit using the equation given by Santoro and Bolen; [37]

$$F_D = \frac{(F_N + m_N[D]) + (F_U + M_U[D]\exp\{-\Delta G_{(F\rightarrow U)} / RT + m_G[D]/RT\}}{1+\exp[-(\Delta G_{(F\rightarrow U)} / RT + m_G[D]/RT)]} \qquad (24)$$

where F_D is the value of the fluorescence intensity (or anisotropy) at a given concentration of denaturant, $[D]$, R is the gas constant and T is the temperature. Once again, the remaining six terms are fitting parameters, where F_N and F_U are the values of the intensity or anisotropy extrapolated to zero concentration of denaturant for the native and unfolded states, respectively, m_N and m_U are the slopes for the dependencies of F_N and F_U on

denaturant concentration, $\Delta G_{(F\rightarrow U)}$ is the free energy of unfolding, and m_G is the slope describing the dependence of $\Delta G_{(F\rightarrow U)}$ on denaturant concentration. The transition midpoint ($D_{1/2}$) values can be calculated by dividing $\Delta G_{(F\rightarrow U)}$ by $-m_G$. The stability can be correlated to the ability of the protein to withstand the entrapment protocol as well as to examine effects of the internal environment after entrapment.

1.4 Fiber Optic Sensing

Optical sensing is one method used to transduce binding events. For remote sensing, the development of optical fiber sensors has proved to be advantageous when coupled with fluorescence detection techniques. Fiber optic sensors can work in extrinsic or intrinsic modes. In extrinsic mode, the fiber is not directly used to get the spectrometric signal, but only as a light pipe. On the other hand, with intrinsic mode fibers, the fiber is used as a waveguide and the biomolecule is evanescently excited as described below. An optical fiber consists of three components, as shown in Figure 1.6. [38] These components are a core of refractive index n_1, which is surrounded by a cladding of lower refractive index, n_2. The cladding is further protected by a jacket.

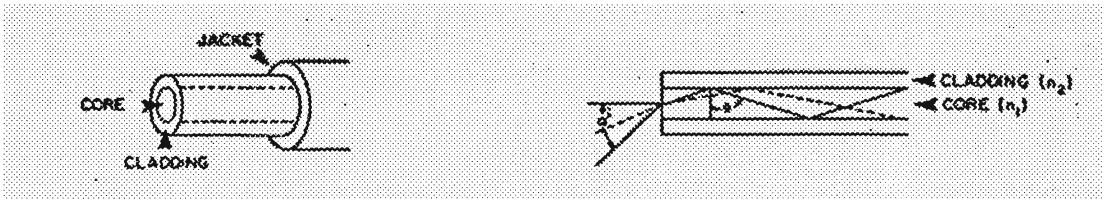

Figure 1.6: Schematic of an optical fiber

Fluorescence which is excited and collected via optical fibers is based on total internal reflection (TIR). In order for TIR to take place, n_1 must be greater than n_2. The critical angle (α_c) may be defined by Snell's Law, equation 1.

$$\alpha_c=\sin^{-1}(n_1/n_2) \qquad (25)$$

Above the critical angle, total internal reflection takes place. The inherent sensitivity of fiber optic based sensing is due to the field of evanescent radiation emitting from the surface of the fiber. An evanescent wave (EW) is an electric field which exponentially decays from the film fiber interface into the film. The evanescent wave decays to zero exponentially as a function of distance, δ, from the film and fiber as shown in equation 26.[39]

$$E=E_s\exp[-\delta/dp] \qquad (26)$$

where E_S is the electric field at the surface, d_p is the penetration depth which is the distance of the electric field to 1/e of E_S. The penetration depth is given by equation 27. [39]

$$d_p= \lambda/[2\pi n_2((n_1/n_2)^2\sin^2\alpha-1)^{1/2}] \qquad (27)$$

Typically, excitation of 442 nm gives a penetration depth of ~225nm.

1.5 Proteins Used in this Study

Two proteins containing a single tryptophan (Trp) residue as well as a single sulfhydryl group were used in this study; Cod III parvalbumin (C3P) in Figure 1.7 [40] (note: Cod III parvalbumin is structurally analogous to Carp Parvalbumin) and human serum albumin (HSA), as shown in Figure 1.8.[41] The single Trp residue is important when investigating intrinsic fluorescence since multiple residues make it difficult to interpret

fluorescence spectra and lifetimes become complicated. It is also important that both of these proteins contain a single free sulfhydryl group which can be labelled with a fluorescent probe in order to conduct further analysis of the unfolding and binding patterns of the proteins. Another reason that these two proteins were chosen were to represent small single domain proteins (C3P) and large multidomain protein molecules (HSA). By encapsulating a small and a large protein molecule, the effects of sol-gel encapsulation on the structure, stability, dynamics and conformational motions of small and large biomolecules can be better understood. Furthermore, both of these proteins have been studied in solution and their crystal structures are known. Another important factor of these proteins is that they both have the ability to bind analytes, allowing for investigation of their binding ability after encapsulation.

In this work, the structural stability of the proteins Cod III parvalbumin and HSA were first examined in aqueous solution. The basis for this study was to gain knowledge about the stability of proteins in solution, and eventually extend these studies to proteins encapsulated in sol-gels. Such a study can determine whether protein structure can be maintained or improved in sol-gel-derived glasses with the addition of thermal and chemical stress and whether the binding ability can be retained in the silicate matrix.

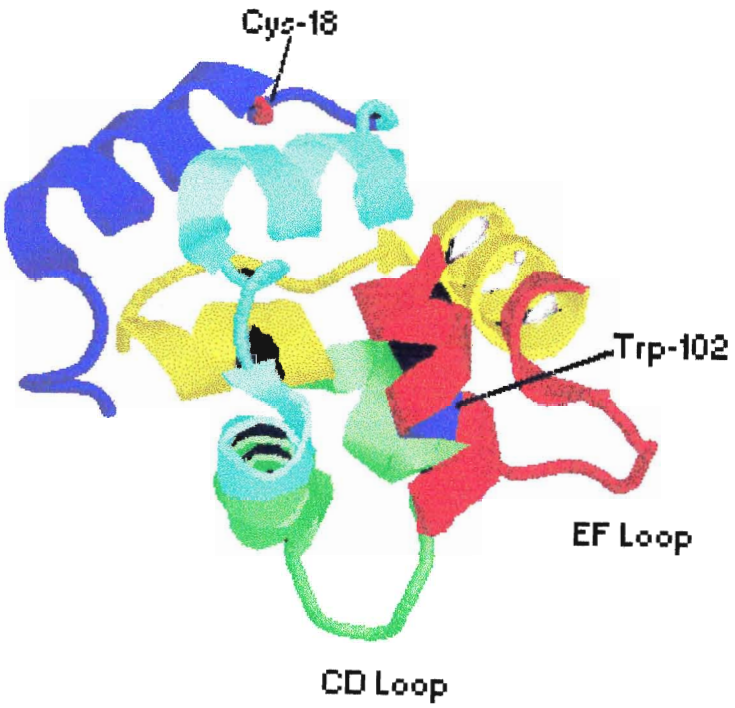

Figure 1.7 Crystal structure of Cod III Parvalbumin [40]

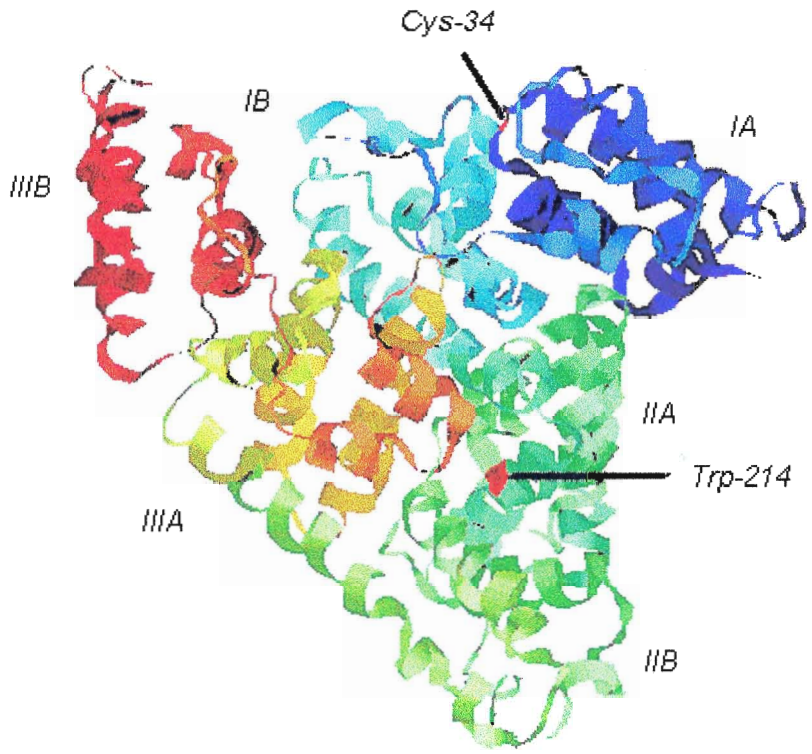

Figure 1.8 Structure of human serum albumin [41]

1.6 References for Chapter 1

1)Yamanaka, S. A.; Bguyen, N. P.; Dunn, B.; Valentine, J. S.; Zink, J. I. *J. Sol-Gel Sci. and Tech.* **1996**, *7*, 117.

2)Avnir, D.; Braun, S.; Lev, O.; Ottolenghi, M. *Chem. Mater.* **1994**, *6*, 1605.

3)Braun, S.; Rappoport, S.; Zusman, R.; Avnir, D.; Ottolenghi, M. *Mater. Lett.* **1990**, *10*, 1.

4)Tatsu, Y.; Yamashita, K.; Yamaguchi, M.; Yamamura, S.; Yamamoto, H.; Yoshikawa, S. *Chem. Lett.* **1992**, 1615.

5)Coche-Guerente, L.; Cosnier, S.; Labbe, P. *Chem. Mater.* **1997**, *9*, 1348.

6)Braun, S.; Shtelzer, S.; Rappoport, S.; Avnir, D.; Ottolenghi, M. *J. Non-Cryst. Solids.* **1992**, *147&148*, 739.

7)Yamanaka, S. A.; Nishida, F.; Ellerby, L. M.; Nishida, C. R.; Dunn, B.; Valentine, J. S.; Zink, J. I. *Chem. Mater.* **1992**, *4*, 495.

8)Reetz, M. T.; Zonta, A.; Simpelkamp, J. *Biotech. and Bioeng.* **1995**, *49*, 527.

9)Krull, U.J.; Brennan, J.D.; Hosein, S.; Hougham, B.D.; Vandenberg, E.T. *Analyst* **1989**, *115*, 147

10)Heckl, W.M.; Thompson, M.; Mohwald, H. *Langmuir* **1989**, *5*, 390.

11)Dave, B. C.; Miller, J. M.; Dunn, B.; Valentine, J. S.; Zink, J. I. *J. Sol-Gel Sci. and Tech.* **1997**, *8*, 629.

12)Chen, Z.; Kaplan, D. L.; Yang, K.; Kumar, J.; Marx, K. A.; Tripathy, S. K. *J. Sol-Gel Sci. and Tech.* **1996**, *7*, 99.

13)Ellerby, L. M.; Nishida, C. R.; Nishida, F.; Yamanaka, S. A.; Dunn, B.; Valentine, J.S.; Zink, J. I. *Science* **1992**, *255*, 1113.

14)Zusman, R.; Beckman, D. A.; Zusman, I.; Brent, R. L. *Anal. Biochem.* **1992**, *201*, 103.

15)Eftink, M. R. *Biophys. J.* **1994**, *66*, 482.

16)Zheng, L.; Reid, W. R.; Brennan, J. D. *Anal. Chem.* **1997**, *69*, 3940.

17)Zheng, L.; Flora, K.; Brennan, J. D. *Chem. Mater.* **1998**, accepted with revisions.

18)Jordan, J. D.; Dunbar, R. A.; Bright, F. V. *Anal. Chem.* **1995**, *67*, 2436.

19)Edminston, P. L.; Wambolt, C. L.; Smith, M. K.; Saavedra, S. S. *J. Coll. Int. Sci.* **1994**, *163*, 395.

20)Roux, C.; Livage, J.; Farhati, K.; Monjour, L. *J. of Sol-Gel Sci. and Tech.* **1997**, *8*, 663.

21)Bronshtein, A.; Aharonson, N.; Avnir, D.; Turniansky, A.; Alstein, M. *Chem. Mater.* **1997**, *9*, 2632.

22)Wang, R.; Narang, U.; Prasad, P. N.; Bright, F. V. *Anal. Chem.* **1993**, *65*, 2671.

23)Turniansky, A.; Avnir, D.; Bronshtein, A.; Aharonson, N.; Altstein, M. *J. Sol-Gel Sci. and Tech.* **1996**, *7*, 135.

24)Vo-Dinh, T.; Houck, K.; Stokes, D. L. *Anal. Chem.* **1996**, *66*, 3379.

25)Abel, A. P.; Weller, M. G.; Duveneck, G. L.; Ehrat, M.; Widmer, M. *Anal. Chem.* **1996**, *68*, 2905.

26)Lundgren, J. S.; Bright, F. V. *Anal. Chem.* **1996**, *68*, 3377.

27)Okahata, Y.; Ebato, H. *Anal. Chem.* **1991**, *63*, 203.

28)Tromberg, B. J.; Sepaniak, M. J.; Vo-Dinh, T.; Griffin, G. D. *Anal. Chem.* **1987**, *59*, 1226.

29)Bhatia, S. K.; Shriver-Lake, L. C.; Prior, K. J.; Georger, J. H.; Calvert, J. M.; Bredehorst, R.; Ligler, F. S. *Anal. Biochem.* **1989**, *178*, 408.

30)Ebelmen, M. *Ann. Chimie. Phys.* **1846**, *16*, 129.

31)Narang, U.; Rahman, M. H.; Wang, J. H.; Prasad, P. N.; Bright, F. V. *Anal. Chem.* **1995**, *67*, 1935.

32)Miller, J. M.; Dunn, B.; Valentine, J. S.; Zink, J. I. *J. Non-Cryst. Solids*. **1996**, *220*, 279.

33)Shtelzer, S.; Rappoport, S.; Avnir, D.; Ottolenghi, M.; Braun, M. *Appl. Biochem.* **1992**, *15*, 227.

34)Zheng, L; Brennan, J.D. *The Analyst* **1998**, *123*, 1735.

35)Lakowicz, J. *Principles of Fluorescence Spectroscopy*; Lakowicz, J., Ed.; Plenum Press: New York, 1983, p. 10.

36)Creighton, T. E. *Proteins Structures and Molecular Properties*; 2 ed.; W.H. Freeman and Company: New York, 1993.

37)Santoro, M. M.; Bolen, D. W. *Biochem.* **1988**, *27*, 8063.

38)Vo-Dinh, T.; Griffith, G. D.; Ambrose, K. R. *Appl. Spec.* **1986**, *40*, 696.

39)Love, W.F; Button, L.J; Slovacek R.E. *Biosensors and Fiberoptics*; The Humana Press Inc.:, 1991, p. 141.

40) Brookhaven Protein Data Bank. http://www.pdb.bnl.gov/pdb-bin/pdbids (4CPV)

41) Brookhaven Protein Data Bank. http://www.pdb.bnl.gov/pdb-bin/pdbids (1UOR)

Chapter 2: The Effect of Preparation and Aging Conditions on the Fluorescence Properties of 7-Azaindole and Pyrene Entrapped in Tetraethylorthosilicate Derived Matrices

2.1 Introduction

Over the past few decades, numerous protocols have been developed to entrap biomolecules. As discussed in Chapter 1, many aspects of protein stability have to be considered in the preparation of sol-gel derived matrices. These parameters will affect both protein stability, and the properties of the final material. Key aspects in the preparation of silicate glass matrices by the sol-gel method are the type and ratio of starting materials and the methods used for gelation and aging of the matrices. Numerous sol-gel protocols have been developed,[1] but almost all share some common characteristics. Most protocols use low pH conditions to initiate hydrolysis and many use large quantities of alcohol as a co-solvent to aid in the mixing of species during hydrolysis.[2-8] Many protocols also allow gelation and aging to occur at low pH values.[4-8] Unfortuneately, both low pH values and high ethanol concentrations can have deleterious effects in cases where sol-gel derived matrices are used to entrap biological compounds such as proteins.[9] In the past few years several reports have appeared which describe a modified sol-gel processing method which is suitable for the encapsulation of biomolecules into monoliths derived from tetraethylorthosilicate (TEOS) or tetramethylorthosilicate (TMOS), as noted in Chapter 1.[9-22]

Efficient encapsulation of active biomolecules represents a major advance in the area of sol-gel science. However, very little is known about how the modified sol-gel processing method affects properties of the final material. A large amount of work has been done to determine the final characteristics of sol-gel derived materials which were prepared with added ethanol and aged at low pH values, including pore-size, transparency, degree of

crosslinking, hardness and stability to dehydration and rehydration.[23-26] However, very little has been reported for materials prepared by sonication of precursors in the absence of alcohol followed by addition of buffer to promote gelation. A detailed study of the physical and chemical characteristics of such materials is required in order to address questions such as how the ratio of silane-to-buffer solution used for gelation and the conditions used for aging affect the evolution of the matrix during aging and the final characteristics of the materials. A better understanding of the internal physical and chemical characteristics and the internal environment of these materials is necessary in order to develop optimal processing conditions for entrapment of biomolecules.

A technique which has been used extensively to obtain information about the internal environment of sol-gel derived materials is fluorescence spectroscopy.[27-34] This is mainly due to the low limits of detection and the large amount of information available from fluorescence techniques. In the present study, the fluorescent probes used to examine the microenvironment of the sol-gel derived matrices were pyrene and 7-azaindole (7AI), whose structures are shown in Figures 2.1 and 2.2 respectively. Pyrene has been widely used in studies of sol-gel derived materials.[35-37] Usually, the ratio of the emission peaks at 393 nm and 373 nm (I_3/I_1) is used to characterize the polarity of the internal environment,[35,36] while the excimer emission is used to probe the changes in the local concentration of the probe during aging and drying.[37]

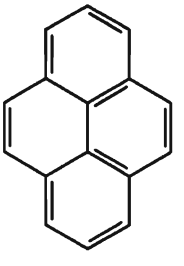

Figure 2.1: Structure of Pyrene

7-Azaindole has been much less widely applied to the study of sol-gel systems. In fact, there is only one previous report describing the use of 7AI for examining sol-gel derived matrices.[3] The photophysical behaviour of 7AI has been thoroughly examined in the past few years,[38-43] and it has been shown to be sensitive to a number of parameters, including pH,[39] polarity[41] and the presence of protic solvents.[40,42] 7AI has an emission maximum at approximately 385 nm in water and 355 nm in ethanol.[41] The protonated form, which exists below pH 4.5, shows a much broader spectral contour and has an emission maximum at approximately 445 nm.[38,39]

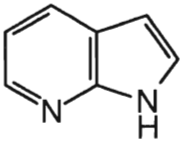

Figure 2.2: Structure of 7-Azaindole

The probe has two emitting forms in protic solvents, a normal form (maximum at 385 nm in water) and a tautomeric form at ~520 nm which results from an excited state proton transfer reaction.[42,43] This tautomer form is not observable when 7AI is in water but becomes more pronounced when 7AI is in alcoholic solvents.[42,43] Thus, 7AI can be used to obtain qualitative information regarding the local alcohol or water concentration.

Another advantage of using 7AI to probe the internal environment of sol-gel derived matrices is that in certain cases where a high Si-OH content is present, the emission peak shifts to a characteristic wavelength between 410 nm and 415 nm as the matrix dries.[3] This is thought to be due to the adsorption of the 7AI, via the two nitrogens in the ring system, onto

hydroxyl groups present at the surface of the pores within the silicate matrix.[3] This indicates that 7AI can also be used to monitor both the expulsion of solvent from the sol-gel derived matrices and the presence of silanol groups within the matrix, potentially providing a method to obtain qualitative information regarding the degree of crosslinking.

Another useful probe for characterizing sol-gel derived materials is pyranine (8-hydroxypyrene-1,3,6-trisulfonic acid, trisodium salt), as shown in structure 2.3. This probe is able to quantitate the amount of ethanol present in the pore liquid, by ratioing the emission peaks at 515 nm, which is indicative of water, and 438 nm, which is indicative of ethanol.[44] The purpose of this probe was to understand and confirm the results obtained using 7AI when investigating internal ethanol content.

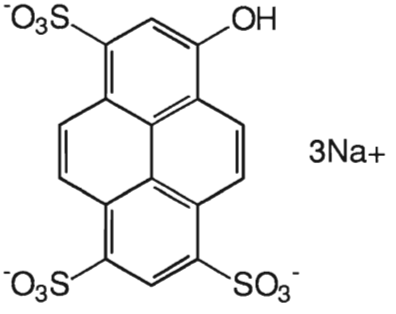

Figure 2.3. Structure of Pyranine

In this chapter, the use of 7AI and pyrene to follow the changes in the internal environmental of TEOS derived matrices during aging and drying is described. The effect of parameters such as the volume of buffer solution used to promote gelation and the conditions under which the materials were aged (i.e. in a dry state or an aqueous state) were examined while other parameters, such as the pH and concentration of the buffer solution, were left constant. The aging conditions are especially important since numerous protocols have been reported for sol-gel based bioencapsulation, including dry-aging, in air,[10-14,17,18] washing the

freshly formed gel to remove ethanol followed by dry-aging[45] and aging in the presence of buffer.[20,46] The physical characteristics of the dry materials, including the pore-size, optical clarity, hardness, and dehydration/rehydration stability, were also examined and correlated to the fluorescence results.

2.2 Experimental

2.2.1 Chemicals

Tetraethylorthosilicate (TEOS, 99.999+%) was obtained from Aldrich Chemicals (Milwaukee, Wisconsin). 7-azaindole, pyrene and polymethacrylate fluorimeter cuvettes were obtained from Sigma Chemicals (St. Louis, Missouri). Pyranine (8-hydroxypyrene-1,3,6-trisulfonic acid, trisodium salt) was purchased from Molecular Probes (Oregon, USA). Water used for preparation of buffers was distilled and deionized through a Barnstead E-Pure three cartridge organic-free water purification system. All other chemicals were of analytical grade and were used without further purification.

2.2.2 Preparation of Sol-Gel Monoliths

TEOS was hydrolyzed by mixing 9.0 mL of the silane, 2.8 mL of cold deionized water and 0.2 mL of 0.1 N hydrochloric and sonicating the solution in ice water until a clear, single phase solution was formed (approximately 2 hours). The hydrolyzed solution was stored for 7 days at -20°C before use to ensure complete hydrolysis of the TEOS.[45,47] Following hydrolysis, the silane solution was mixed with a phosphate buffer solution (10 mM, pH 8.20, 100 mM KCl) containing 20 mM of the appropriate fluorophore in a disposable

$1cm^2$ polymethacrylate cuvette. The ratio of hydrolyzed TEOS to buffer was varied from 1:1 to 10:1 (by volume) while maintaining the total volume of the mixture at 1.5 mL. The TEOS:buffer mixture was vortexed at low speed to ensure proper mixing and was then allowed to gel with the cuvette in an upright position. Dry-aged monoliths were washed twice with 2 mL of buffer solution 10 mins after gelation (1 minute per wash step) to remove residual ethanol and to ensure that the internal pH and buffer levels were to close to the values of the phosphate buffer solution. The monoliths were then were drained, the cuvette was capped with Parafilm and several small holes (*ca.* 1 mm diameter) were punched in the film. The monoliths were then allowed to dry for a period of several months at room temperature.

Wet-aged monoliths were washed as described above and then had approximately 2 mL of the phosphate buffer solution added approximately 10 minutes after gelation. These monoliths were then capped with Parafilm and were allowed to age for 10 days in the buffer with an exchange of buffer each day. The buffer solutions used for the exchanges contained 20 mM of the 7AI or pyrene probe to avoid leaching of the entrapped probe from the monoliths. After 10 days the buffer was removed and the monoliths were allowed to allowed to dry for several months in a manner identical to that used for the dry-aged monoliths.

2.2.3 Fluorescence Spectroscopy of Sol-Gel Monoliths

Fluorescence spectra were collected using instrumentation which is described in detail elsewhere.[46] Samples containing 7AI were excited at 290 nm and emission was collected from 310 nm to 600 nm. Samples containing pyrene were excited at 340 nm with emission collected from 350 nm to 600 nm. All spectra were collected in 1 nm increments with 4 nm

excitation and emission bandpasses using an integration time of 0.5s per point. Appropriate blanks were subtracted from each sample and the spectra were corrected for deviations in the emission monochromator throughput and photomultiplier tube (PMT) response.

For dry-aged monoliths, spectra were collected on a daily basis at approximately 24 hr intervals, starting 30 minutes after gelation and continuing until there were no further changes in the mass of the samples or in the spectral characteristics (usually 15 and 25 days for dry-aged and 28 and 10 days for wet-aged for equilibration of mass and spectral appearance). For wet-aged monoliths, spectra were collected daily from samples that had the surrounding phosphate buffer solution removed just prior to collection of spectra to avoid contributions from fluorophores which were present in solution. After collection of the spectra, 2 mL of a fresh phosphate buffer solution (containing 20 mM of the appropriate probe) was added to dilute any residual alcohol while avoiding leaching of the probes from the monoliths during aging. After 10 days (at which point no further changes in spectra were observed), the buffer was removed and the monoliths were capped with Parafilm and allowed to dry in air, with spectra collected every 2 or 3 days until no further changes in the spectra occurred (*ca.* 25 days). Both wet-aged and dry-aged samples were left to age until a total of 140 days had elapsed since gelation, with spectra being collected at various times between days 25 and 140. Physical testing was done on day 140.

2.2.4 Infrared Spectroscopy

Representative infrared spectra were collected from wet-aged and dry-aged monoliths using an ATI-Mattson Research Series FTIR spectrometer with a diffuse reflectance accessory. The samples were prepared with a 3:1 TEOS:buffer ratio and aged 140 days. The

samples were crushed and were degassed by heating at 120°C for 60 minutes before spectra were collected. A total of 1024 scans were collected in absorbance mode from 4000 cm^{-1} to 400 cm^{-1} with a resolution of 4 cm^{-1} for each sample.

2.2.5 Optical Transparency

The optical transparency of the fully dried monoliths was examined by UV-Vis transmittance measurements using an ATI Unicam UV-4 spectrophotometer. The transmittance of TEOS derived monoliths was examined by placing the monolith in a quartz cuvette in the sample path with an empty cuvette in the reference path. Transmittance curves were collected from 240 nm to 400 nm in 0.2 nm increments using a scan speed of 30 nm per minute and a bandpass of 1.5 nm. Transmittance values reported are those obtained at 400 nm.

2.2.6 Hardness

Hardness was tested qualitatively by scratching the surface of the monoliths with various substances using the Moh's hardness scale. The substances used were talc (1), gypsum (2), calcite (3), copper (3.5), fluorite (4), apatite (5), orthoclase (6) and quartz (7). The number given in parentheses increases as the hardness of the compound increases. A number was assigned to the sol-gel derived materials based on the substance for which both the sol-gel and the substance scratched each other, or neither scratched the other.

2.2.7 Dehydration/Rehydration Behaviour

The dehydration behaviour was tested by simply examining the number of cracks which developed in the various monoliths as drying proceeded. If there were between 0 and 2 cracks, the stability was judged to be good, if there were 3-5 cracks, stability was judged to be moderate, while samples with greater than 5 cracks were judged to have poor stability. Rehydration stability was determined by rapidly adding 2 mL of buffer solution to the cuvette containing the monolith. Again, the stability was judged by the number of cracks formed during rehydration, using the qualitative scale described above.

2.2.8 Pore Size Analysis

Pore size analysis of completely dried monoliths was performed on a Coulter SA3100 surface area/pore size analyzer. Before analysis, the monoliths (either with or without encapsulated probes) were crushed to a fine powder and outgassed at 120°C for 60 minutes to remove air and bound water from the surface of the powder. The pressure was measured as nitrogen was adsorbed and desorbed at a constant temperature of -196°C. From the resulting isotherm, the average pore size and distribution of sizes was determined using the BJH (Barrett, Joyner and Halenda) calculation.[48]

2.3. Results and Discussion

2.3.1 Physical Properties

The hydrolyzed TEOS was mixed with buffer in volumetric ratios of 1:1 up to 4:1 TEOS:buffer. These ratios cover the range generally used to prepare sol-gel materials for bioencapsulation.[9-20] Gelation times for the 1:1, 2:1, 3:1 and 4:1 systems were 2 mins, 10

mins, 35 mins and 100 mins, respectively. Given the combination of hydrolysis and condensation reactions and the long incubation time for the sol before addition of buffer, it is extremely difficult to accurately determine the ratio of alcohol:water in the freshly formed gels. Pyranine provides information on ethanol:water ratios, therefore giving quantitative information on pore liquid composition. Pyranine was encapsulated within all 4 types of preparation conditions. It was found that there is initially 36%, 46%, 54% and 62% ethanol in the blocks of type 1:1, 2:1, 3:1 and 4:1, respectively. The pyranine data showed that after 2 days of washing, the ethanol has been washed away, since the emission peak at 438 nm had diminished.

For the wet-aged samples, 2.0 mL of buffer was added after gelation, resulting in the minimum water:silane molar ratios changing to 64:1 45:1, 39:1 and 28:1 for the 1:1, 2:1, 3:1 and 4:1 systems, respectively. In this case, the volume percentage of ethanol (after equilibration) is between 14% (1:1 system) and 23% (4:1 system). Hence, a substantial dilution of the ethanol occurs immediately. Removal and replacement of the surrounding buffer at 24 hour intervals results in further dilution of ethanol, with the ratios changing to 6 - 9% after 1 exchange, 2 - 4% after 2 exchanges, and 1.0 - 1.5% after 3 exchanges for the 1:1 to 4:1 systems, respectively. Hence, three buffer exchanges will effectively dilute the ethanol to the point where it should have no influence on the spectroscopic signals observed from 7AI or pyrene. These results are consistent with the ones found for pyranine.

Following gelation, the monoliths were aged for 10 days with or without buffer solution present and then a further 130 days in air, at which point several physical properties were measured. For optical biosensors, the matrix used to entrap the proteins should show good optical clarity, good physical strength (as measured by hardness), resistance to fracture

upon dehydration and rehydration and as large a pore-size as possible to allow facile entry of analytes. [46] Each of these properties was tested for both dry-aged and wet-aged monoliths at each ratio of silane-to-water. The results are shown in Table 2.1. Several interesting trends are apparent. First, the transparency of the monoliths increased with the amount of water initially present for dry-aged systems and was good for all wet-aged systems. Firstly, the resistance to abrasion for each of the materials did not appear to depend on the amount of water used for gelation. Secondly, the dehydration stability was good for all wet-aged monoliths, but was dependent on the TEOS:buffer ratio for dry-aged systems, increasing with the amount of water used for gelation. Third, the rehydration stability of wet-aged monoliths was moderate in all cases (minor cracking), while the rehydration stability of dry-aged monoliths was moderate at best and decreased dramatically with an increasing TEOS:buffer ratio. In fact, the addition of water to dry-aged monoliths made with a 3:1 or 4:1 TEOS:buffer ratio resulted in complete fragmentation, with small pieces of glass violently dislodging from the monolith until only tiny fragments remained. Finally, the relative pore-size of the dry-aged monoliths decreased as the silane:buffer ratio increased. On the other hand, the relative pore-size of the wet-aged monoliths was fairly constant and was up to 2-fold larger in diameter than the pore-sizes of the dry-aged monoliths.

The results from the dry-aged samples are consistent with larger amounts of water resulting in longer drying times, thus allowing more time for the structure of the monolith to evolve. Larger amounts of water during aging are known to promote dissolution and reprecipitation of silica, providing an increase in the strength of the "neck" regions which connect individual sol particles, and promoting the growth of more stable structures within the matrix through the process of coarsening. [26,49,50] Increases in the amount of coarsening

can also result in larger pores and a more even distribution of pore-sizes, reducing capillary stresses and resulting in the improved stability to dehydration and rehydration. [24-26,51] Together, these factors indicate that a material with improved optical and mechanical characteristics is obtained as the level of water increases.

Table 2.1. Physical properties of TEOS derived monoliths which were wet-aged or dry-aged for 10 days followed by dry-aging for 130 days.

TEOS:H_2O (v/v)	Final Clarity	Dehydration Stability	Rehydration Stability	Hardness (Mohs Scale)[c]	Pore-size (nm)[d]
1:1 D[a]	Transparent	Good	Moderate	3.5	4.01 ± 0.30
2:1 D	Transparent	Good	Moderate	4	3.52 ± 0.21
3:1 D	Translucent[b]	Moderate	Poor	4	3.39 ± 0.14
4:1 D	Translucent[b]	Moderate	Poor	4	3.33 ± 0.11
1:1 W	Transparent	Good	Moderate	3.5	7.43 ± 0.45
2:1 W	Transparent	Good	Moderate	3.5	6.61 ± 0.53
3:1 W	Transparent	Good	Moderate	3.5	6.51 ± 0.48
4:1 W	Transparent	Good	Moderate	3.5	6.49 ± 0.24

a) D = dry-aged, W = wet-aged, b) the translucence was the result of small air bubbles which were entrapped in the monoliths during mixing of the silane and buffer, c) all hardness measurements are ± 0.5 units, and are the average obtained from measurements of three samples for each TEOS:buffer ratio, d) errors are standard deviations obtained from measurement of three different samples of identical composition.

For wet-aged monoliths, there was a minimum of a 28-fold molar excess of water-to-silane for each system and the amount of water was constant for 10 days, thus altering the initial aging conditions. In all cases where monoliths were wet-aged, the dehydration stability was such that no cracking appeared, and was similar to that observed for dry-aged systems which were aged with an initial R-value of 12:1 or higher. On the other hand, the rehydration stability of wet-aged monoliths was better than that obtained from any of the dry-aged monoliths. In this case, the monoliths were forced to respond to rapid changes in water content, causing a different response. The results indicate that the better rehydration stability

for wet-aged monoliths is the direct result of the presence of excess water during aging. This behaviour indicates that the larger pores and smaller proportion of silanol groups (as suggested by IR experiments, described below) for samples aged with larger amounts of water have the effect of decreasing the capillary stresses during rehydration, resulting in an improvement in rehydration stability.

2.3.2 Infrared Spectroscopy

To further examine the properties of the dried samples, infrared absorbance spectra were collected for the wet-aged and dry-aged samples which were prepared with a 1:1 to 4:1 TEOS:buffer ratio. Representative spectra collected for wet-aged and dry-aged materials prepared with a 3:1 TEOS:buffer ratio are shown in Figure 2.4. The ratio of two regions of these spectra are of interest; the Si-OH stretching regions between 3000 and 3700 cm^{-1} and at 950 cm^{-1}, and the Si-O-Si stretching region at ~490 cm^{-1}.[52] The IR spectra show that the wet-aged sample had relatively low amplitude absorption bands in the Si-OH stretching region between 3200 and 3700 cm^{-1}, and had larger amplitude bands in the 490 cm^{-1} region. On the other hand, the spectrum of the dry-aged sample has larger amplitude absorption bands in both the 3000-3500 cm^{-1} range and at 950 cm^{-1} relative to the Si-O-Si band at 490 cm^{-1} when sample. This result indicates that dry-aged samples have a larger proportion of silanol groups compared to wet-aged samples.

A second comparison can be made as a function of the silane:buffer ratio used for gelation. The ratio of bands corresponding to Si-OH (3200 and 3700 cm^{-1}) and Si-O-Si (490 cm^{-1}) groups indicated that the ratio of silanol groups to siloxane groups increased as the amount of water used for gelation decreased, suggesting that the use of larger amounts of

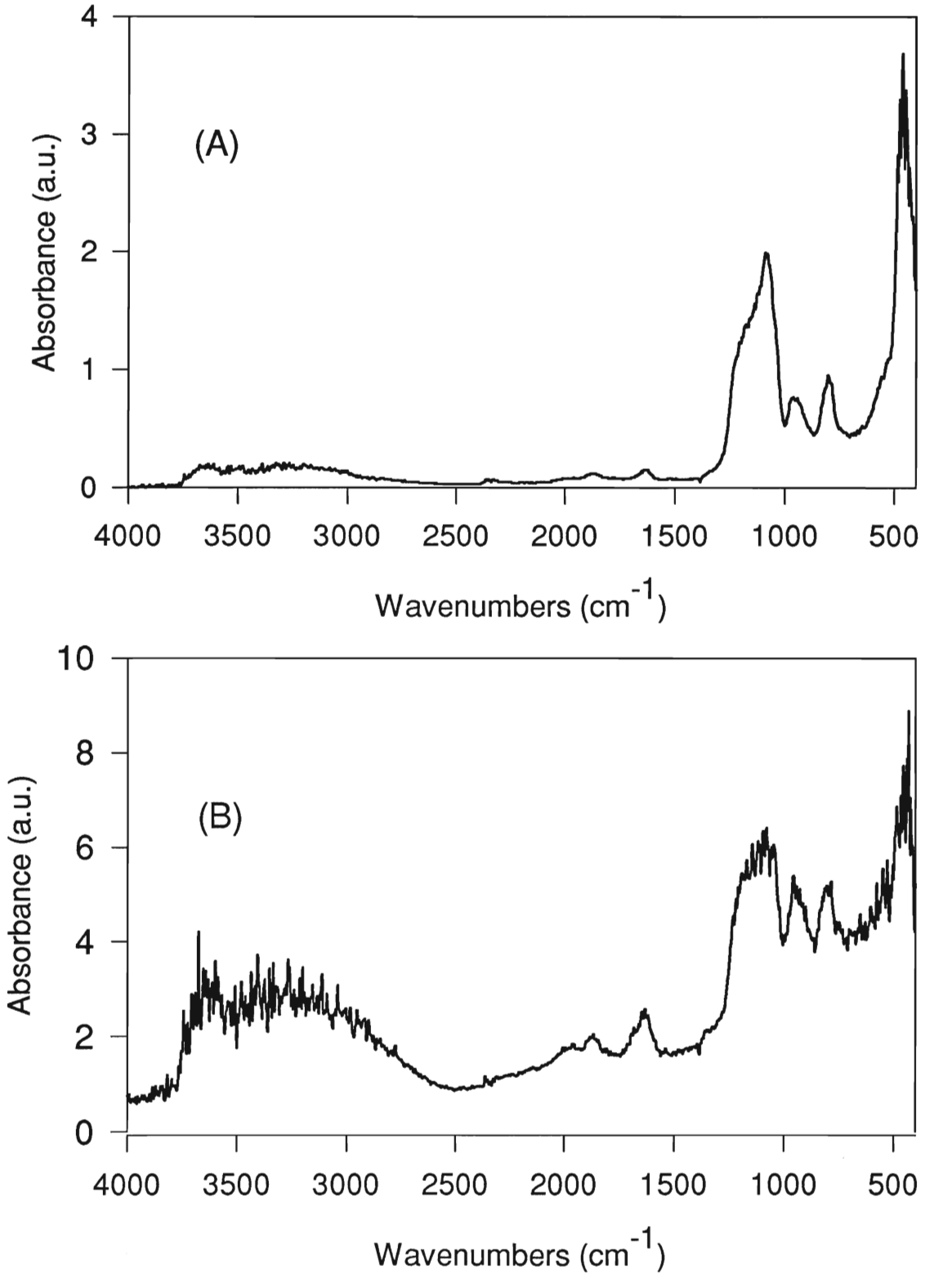

Figure 2.4. Diffuse reflectance infrared spectra of TEOS derived monoliths prepared with a 3:1 TEOS:buffer ratio for gelation. The samples were crushed to powder form and dried at 120°C for 60 minutes before spectra were collected. (A) wet-aged monolith, (B) dry-aged monolith.

water for gelation led to an increase in crosslinking. These results are in agreement with the expected increase in coarsening and increased cross-linking as the ratio of water:silane used during aging was increased.

2.3.3 Fluorescence Measurements on Wet-Aged Monoliths

The differences in the physical properties and IR spectra of the various samples indicated that the internal environment of the different systems evolved in different ways during aging and drying, prompting us to further examine these changes during the aging and drying cycles. Initial studies involved the fluorescent probe 7-azaindole. Representative spectra of 7AI as a function of aging time for monoliths formed with a silane:buffer ratio of 1:1 are shown in Figure 2.5. Spectral properties are listed in Table 2.2. When the matrices were formed, the initial fluorescence emission maxima were between 367 nm and 372 nm for all compositions. Representative emission maxima and full-width-at-half-maximum (FWHM) values obtained on our instrument for different volume percentages of ethanol in water are as follows: 0% = 384 nm (76 nm); 20% = 377 nm (75 nm); 40% = 370 nm (70 nm); 60% = 367 nm (67 nm); 80% = 364 nm (65 nm); 100% =355 nm (61 nm). The emission wavelength and FWHM of the entrapped 7AI indicated that the internal environment of the monoliths initially had a polarity similar to that of a solution containing between 30% and 60% ethanol for the wet-aged systems, [49,50] even though the calculated amount of ethanol was as low as ~14%. The inital values of ethanol are in the range of 36%-62% and 10%-20% after one 24 hour long washing step, as given by pyranine. Given the discrepancy between the emission maxima in ethanol:water mixtures and in the sol-gel derived matrices, it is clear that the wavelength maximum of 7AI is not reporting solely on the amount of ethanol present.

Table 2.2. Fluorescence characteristics of wet-aged TEOS derived monoliths containing 20 μM 7-azaindole or pyrene as a function of drying time.

Probe	Aging time	Wavelength or amplitude ratio 1:1[a,b]	Wavelength or amplitude ratio 2:1	Wavelength or amplitude ratio 3:1	Wavelength or amplitude ratio 4:1
7-azaindole	Initial nm	368 (71)[c]	367 (73)	367 (72)	372 (72)
	10 days[d]	394 (101)	397 (101)	398 (101)	399 (102)
	25 days	396 (104)	397 (99)	396 (101)	396 (100)
	55 days	403 (104)	401 (101)	400 (97)	398 (101)
	90 days	386 (124)	391 (99)	393 (103)	400 (104)
	104 days	392 (125)	396 (101)	397 (114)	389 (121)
	116 days	395 (130)	396 (100)	394 (105)	391 (123)
	126 days	389 (124)	394 (98)	393 (113)	391 (122)
	140 days	392 (111)	392 (98)	392 (110))	392 (118)
Pyrene	Initial I_3/I_1	0.87	0.89	0.88	0.90
	10 days[b]	0.88	0.88	0.90	0.92
	25 days	0.93	0.94	0.94	1.00
	55 days	1.09	1.00	1.05	1.00
	90 days	0.96	0.99	0.98	0.95
	104 days	0.96	0.91	0.93	0.93
	116 days	0.90	0.92	0.97	0.96
	126 days	0.95	0.96	0.96	0.95
	140 days	0.89	0.93	0.94	0.89

a) all values represent the average emission wavelength maximum and spectral full-width-at-half-maximum (FWHM) values from three different samples of identical composition, b) typical errors in emission maxima for 7AI are ± 1 nm or less, typical errors in FWHM for 7AI are ± 3 nm or less, typical errors in the amplitude ratio for pyrene are ± 0.02 or less, c) the number in brackets is the FWHM, in nanometers, d) buffer was removed at day 10.

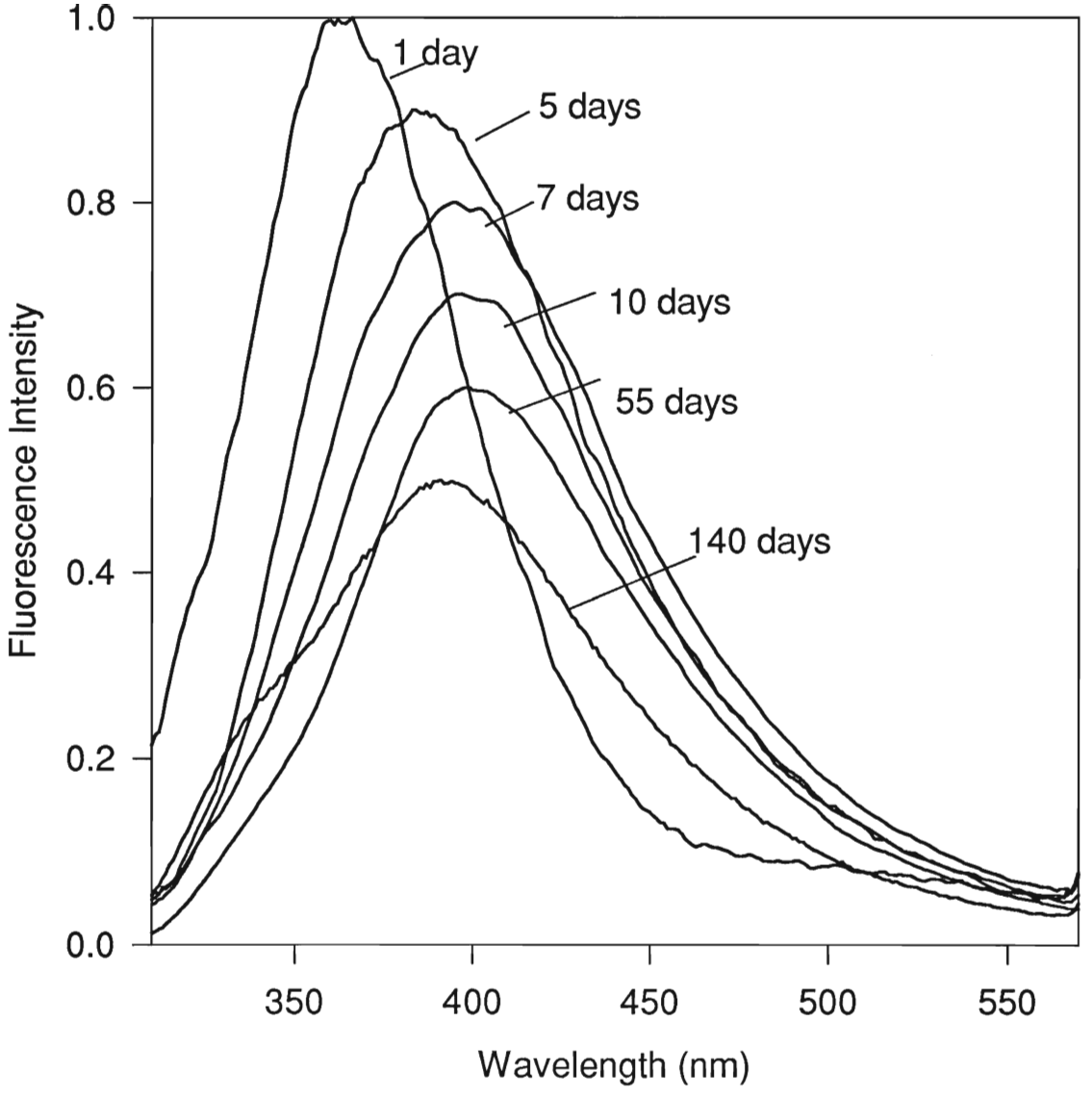

Figure 2.5. Fluorescence spectra of 7AI collected at various times during wet-aging of TEOS derived monoliths prepared with a 3:1 TEOS:buffer ratio for gelation. The intensity values have been scaled to allow easier visualization of the differences between the spectra.

Figure 2.6 shows the evolution of the fluorescence maximum during aging of each system. For all TEOS:buffer ratios the fluorescence emission maximum red-shifted in a similar manner over the first seven days, evolving from *ca.* 370 nm to between 394 nm and 399 nm, after which the emission maximum remained constant. During this time, the FWHM value increased to ~101 nm for all systems. The wavelength shift and the increase in the FWHM value are consistent with the internal environment slowly shifting toward higher polarity as ethanol is removed. However, the final values for both the emission maximum and the FWHM are *larger* than the values obtained in water. These spectral values are clearly indicative of specific interactions involving hydrogen-bonding between the sol-gel matrix and the probe. This interpretation is in agreement with the results obtained by Matsui,[3] and also agrees with results obtained by Bright and co-workers who studied the emission of prodan in TMOS derived matrices.[4] The spectral broadening indicates that the probe exists in a distribution of environments, with some fraction of the probe solvated by the entrapped solvent.

At day 10 the buffer was removed and the monoliths were aged and dried in air. Table 2.2 shows that the emission maximum for all samples continues to shift over time, reaching values as high as 403 nm, with minimal changes in the FWHM over the first 55 days. Beyond day 55 the FWHM values increased for most samples while the emission maximum slowly blue-shifted. This behaviour is consistent with the removal of entrapped water such that the probe environment becomes dehydrated, producing a blue-shift in the emission maximum.[4,27,41] The final spectral widths were in all cases between 25 nm and 40 nm greater than the initial values, indicating that there was a distribution of final environments for the entrapped probe, in agreement with previous reports.[4] The emission maxima of the final

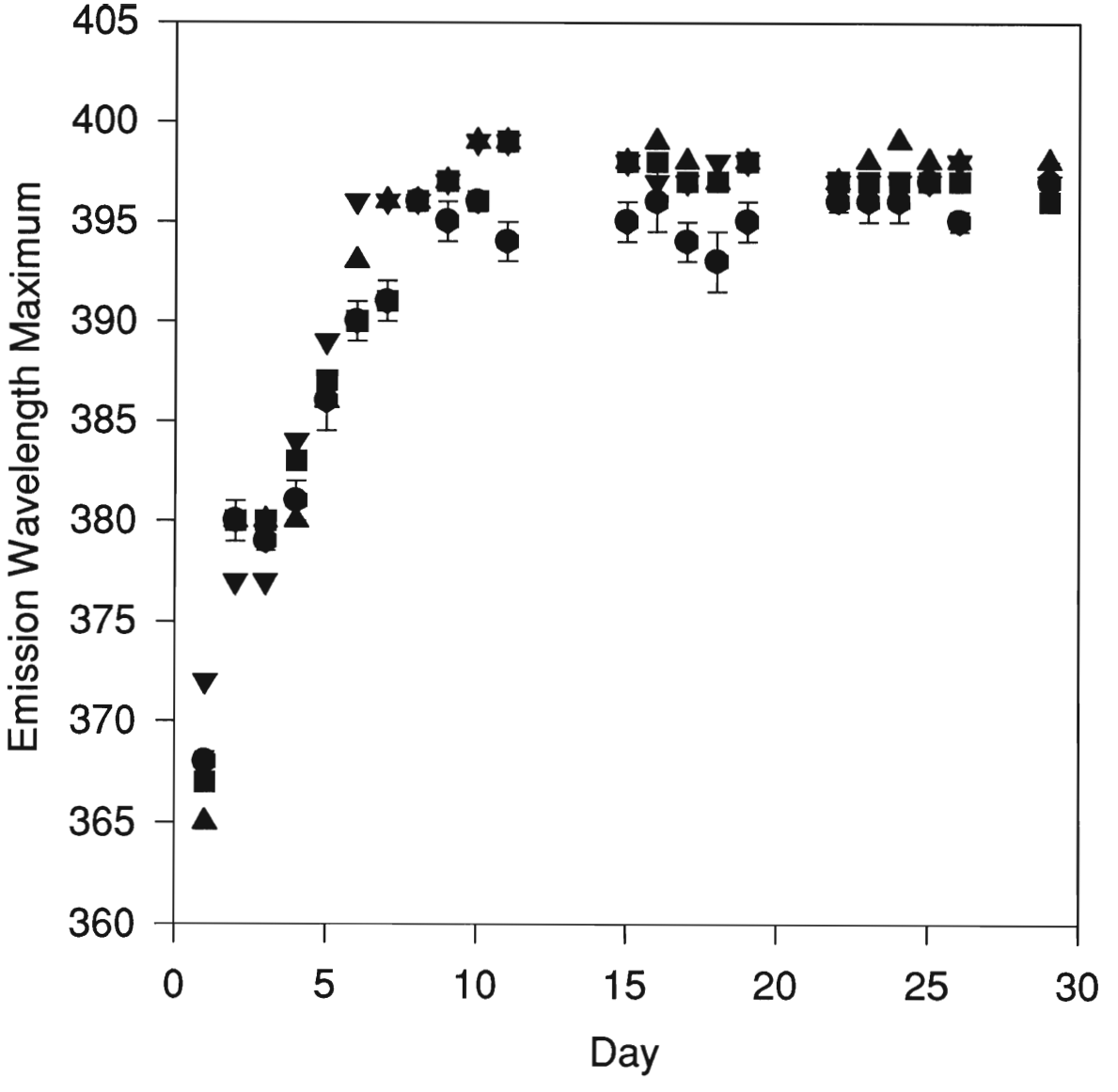

Figure 2.6. Effect of aging conditions on 7AI emission wavelength during the first 25 days of wet-aging for TEOS derived monoliths prepared with different TEOS:buffer ratios for gelation. (●) 1:1 TEOS:buffer, (■) 2:1 TEOS:buffer, (▲) 3:1 TEOS:buffer, (▼) 4:1 TEOS:buffer. Representative error bars have been included for the 1:1 TEOS:buffer system. Similar error values are obtained for all other ratios.

states in each system were 8 nm red-shifted from the value in water, indicating that there were specific interactions of the probe with the silane (adsorption via hydrogen-bonding to silanols).[3] The final states for each TEOS:buffer ratio show similar emission maxima, and all show some degree of spectral broadening, which indicates that the final environment was affected mainly by the presence of an excess amount of buffer during the first 10 days rather than the initial gelation conditions.

Complementary studies with the molecular probe pyrene were done in wet-aged monoliths to compare with the 7AI results. A series of representative spectra for TEOS monoliths containing pyrene are shown in Figure 2.7. For these spectra, the maximum amplitude of the third vibronic band compared to the first vibronic band (I_3/I_1) was used as a measure of the environmental polarity. Figure 2.8a shows the evolution of the ratio of vibronic bands during aging for each of the samples measured. The amplitude ratios are listed in Table 2.2. The initial ratio of the amplitudes of the third and first vibronic bands was approximately 0.88 for all systems studied. For comparison, a ratio of 0.86 corresponds to an environment with a polarity similar to that of ethanol.[2] This result corresponds very closely to the result obtained from 7AI, and confirms that there was a significant amount of ethanol present initially.

As the monoliths aged over the first 10 days, with daily buffer exchanges, the ratio I_3/I_1 remained, within the error of measurement, effectively constant, although the data are scattered. These results indicate that pyrene was unable to report on changes in the internal environment during the period of daily buffer exchanges, contradicting the results from entrapped 7AI. Between days 10 and 55, the vibronic ratio for each composition increased to 1.00 or greater. Such a shift is indicative of the internal environment becoming somewhat

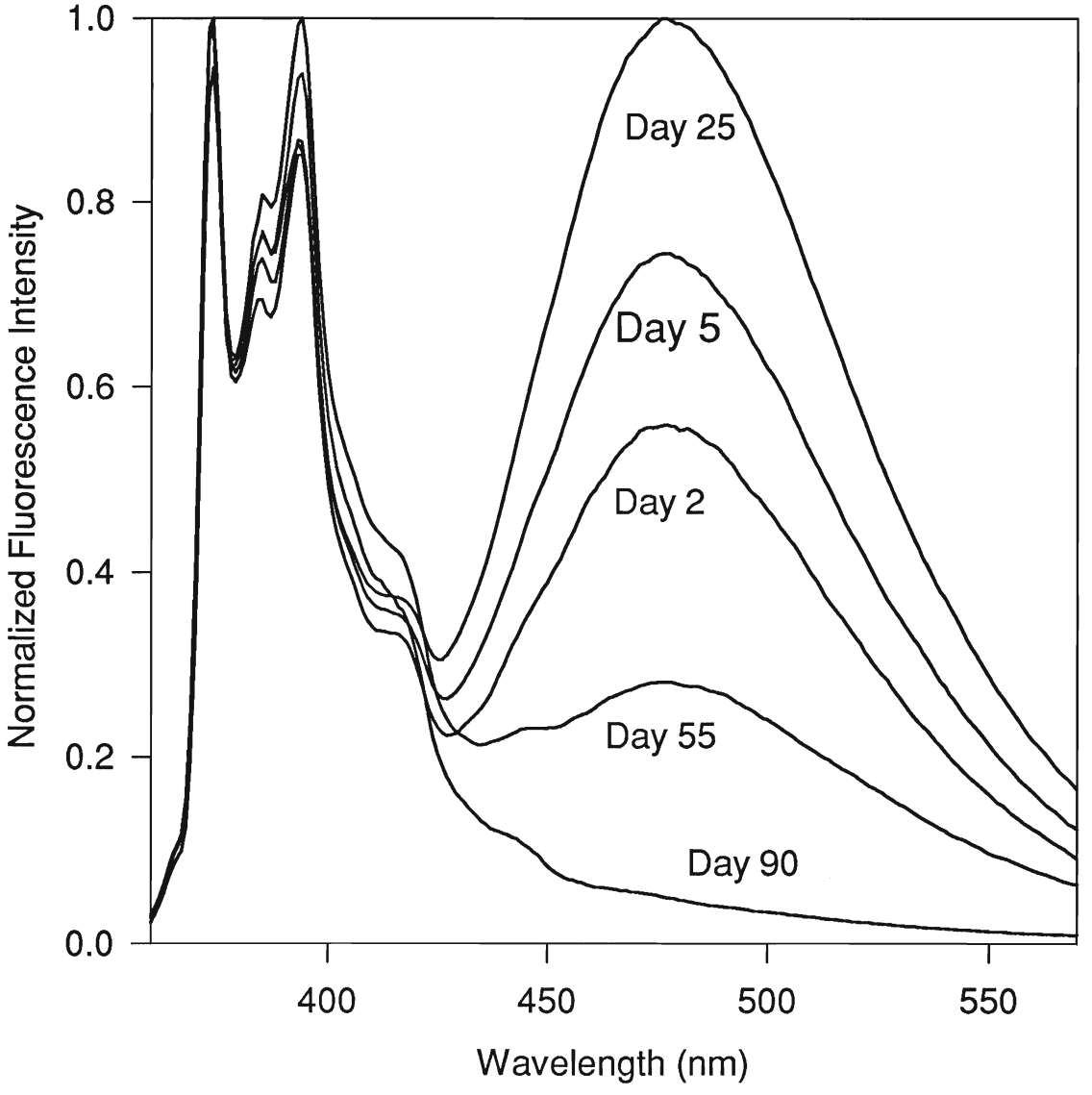

Figure 2.7. Fluorescence spectra of pyrene collected at various times during wet-aging of TEOS derived monoliths prepared with a 3:1 TEOS:buffer ratio for gelation. The intensity has been normalized to the value of the I_1 band except for the spectrum for day 55, which is normalized to the I_3 band.

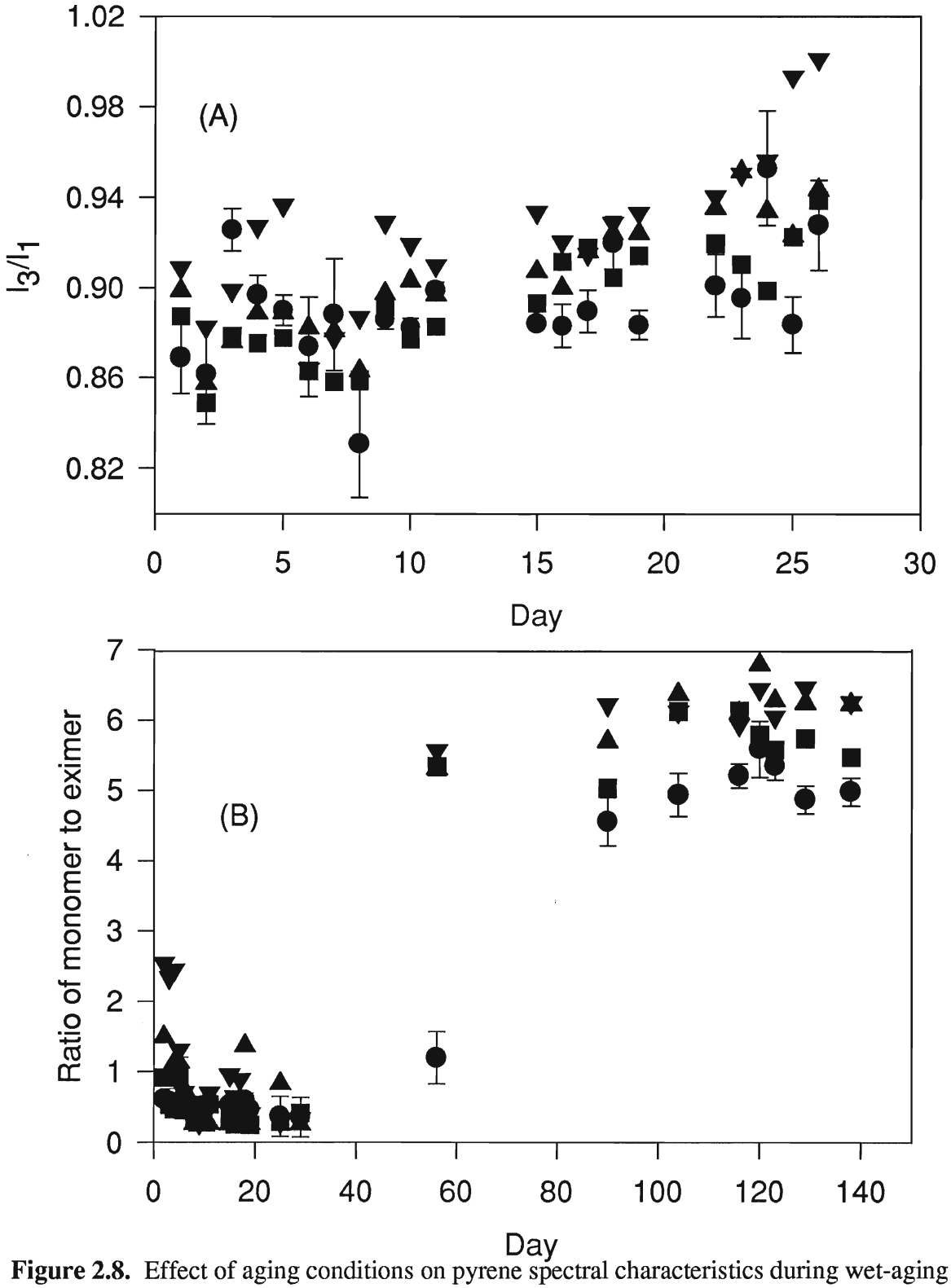

Figure 2.8. Effect of aging conditions on pyrene spectral characteristics during wet-aging of TEOS derived monoliths prepared with different TEOS:buffer ratios for gelation. (A) change in I_3/I_1 vibronic band ratio during wet-aging. (λ) 1:1 TEOS:buffer, (■) 2:1 TEOS:buffer, (▲) 3:1 TEOS:buffer, (▼) 4:1 TEOS:buffer. (B) change in monomer/excimer band ratio during wet-aging. (λ) 1:1 TEOS:buffer, (■) 2:1 TEOS:buffer, (▲) 3:1 TEOS:buffer, (▼) 4:1 TEOS:buffer.

less polar with time due to dehydration of the internal environment. [2,41] Between days 55 and 104 the vibronic ratio decreases slightly and then remains relatively constant. This correlates with the blue-shift and spectral broadening observed for entrapped 7AI. Given the small range of the changes in the amplitude ratios and the scatter in the data, it is apparent that the emission of pyrene provides less information that was obtained from 7AI, indicating that 7AI is a superior probe for monitoring the internal environment of wet-aged sol-gel derived silicates.

A second feature of Figure 2.7 is the excimer emission centered around 470 nm. The excimer emission increases until about day 25, and then decreases in intensity as aging progresses until no excimer was detected. Based on the 7AI results and the calculated ratios of ethanol-to-water, it is expected that the amount of entrapped water increases at the expense of ethanol over the first several days. As ethanol is replaced with water, the solubility of pyrene will decrease, favoring further excimer formation during the early stages of aging. The decrease in the intensity of the excimer band over time beyond day 25 (shown in Figure 2.8b) is the result of a shift in equilibrium from excimer to monomer forms of the probe. Such a phenomenon has been reported previously, [2] and is caused by two processes. The first is adsorption of pyrene onto the surface of silica as aging proceeds. The second process is entrapment of monomers in the nanometer-scale pores. [2] Both processes result in a lower concentration of free monomer, and thus shift the equilibrium from the excimer form to the monomer form. This interpretation is supported by spectra which were collected from pyrene that was adsorbed onto quartz slides by allowing evaporation of an aqueous solution of pyrene which had been deposited onto the slide using a microsyringe. Initial spectra

showed the excimer band; however, this band decreased in amplitude over time as the solvent evaporated, resulting in only monomer emission after solvent evaporation was complete.

2.3.5 Fluorescence Measurements on Dry-Aged Monoliths

The other aging method studied was aging in the absence of added buffer. This aging procedure is similar to that used by most groups who use sol-gel derived materials for bioencapsulation. [10-18] Representative spectra of 7AI in the 1:1 TEOS:buffer system are shown in Figure 2.9. Spectral characteristics at different times for all ratios studied are shown in Table 2.3. Comparison of different ratios showed that the initial polarity was similar in all systems, and was identical to the initial polarity obtained for the wet-aged monoliths even though no additional water was added to the dry-aged systems. Figure 2.10 shows the changes in the emission wavelength for 7AI in monoliths prepared with the four different ratios of TEOS:buffer. In all cases the spectra red-shifted over the first 6 days, with the emission maxima shifting by ~ 5 nm for each system over this time and ending up between 375 nm and 380 nm. This wavelength shift is consistent with the preferential loss of ethanol from the matrix. [4]

Between days 6 and 10, the emission of 7AI in each system showed a broadening of the spectral contour and a shift in the emission wavelength maximum. Several aspects of these changes warrant special attention. First, the spectral change occurred for the 4:1 system first, and the 1:1 system last. This trend indicates that the lower amount of water at the initial stages of monolith formation caused the wavelength shift to occur earlier, consistent with the shorter drying time expected for systems with lower amounts of solvent. Second, the emission wavelength of 7AI in all monoliths was equal to or greater than 400 nm

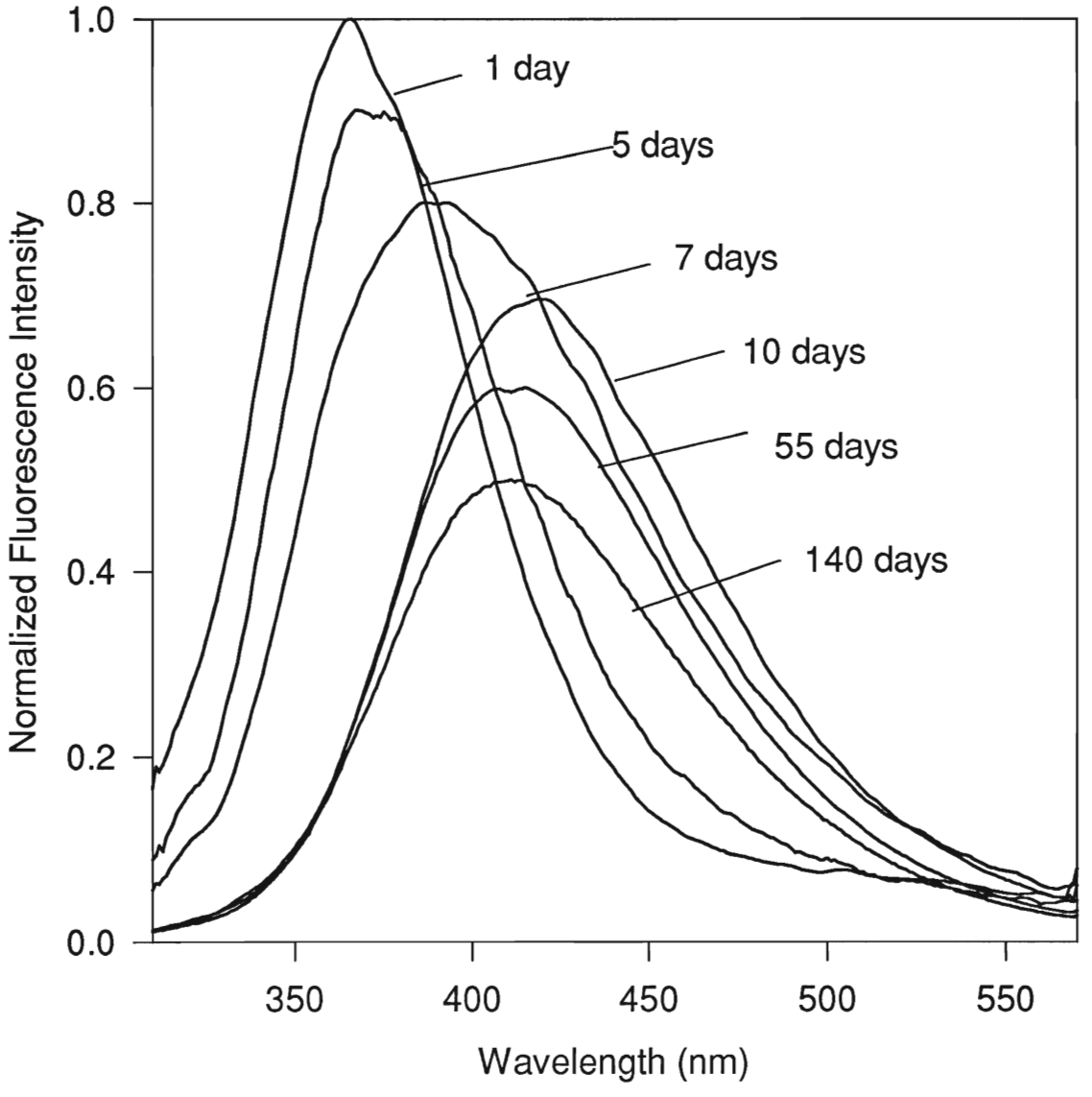

Figure 2.9. Fluorescence spectra of 7AI collected at various times during dry-aging of TEOS derived monoliths prepared with a 3:1 TEOS:buffer ratio for gelation. The intensity values have been scaled to allow easier visualization of the differences between the spectra.

Table 2.3. Fluorescence characteristics of dry-aged TEOS derived monoliths containing 20 μM 7-azaindole or pyrene as a function of drying time.

Probe	Aging time	Wavelength or amplitude ratio 1:1[a,b]	Wavelength or amplitude ratio 2:1	Wavelength or amplitude ratio 3:1	Wavelength or amplitude ratio 4:1
7-azaindole	Initial nm	371 (71)[c]	368 (73)	369 (71)	368 (75)
	10 days	399 (104)	409 (104)	419 (100)	420 (102)
	25 days	408 (96)	410 (94)	416 (90)	418 (95)
	55 days	405 (96)	407 (98)	412 (97)	416 (97)
	90 days	404 (88)	405 (99)	410 (86)	416 (95)
	104 days	404 (89)	405 (100)	410 (97)	415 (96)
	116 days	403 (95)	404 (99)	410 (96)	415 (95)
	126 days	403 (99)	409 (98)	408 (98)	414 (96)
	140 days	402 (96)	405 (98)	410 (99)	413 (96)
Pyrene	Initial I_3/I_1	0.86	0.88	0.88	0.89
	10 days	0.82	0.91	0.93	0.94
	25 days	0.87	0.94	0.92	0.97
	55 days	0.95	0.92	0.92	0.96
	90 days	0.88	0.89	0.90	0.91
	104 days	0.91	0.87	0.88	0.90
	116 days	0.93	0.86	0.91	0.91
	126 days	0.85	0.99	0.89	0.88
	140 days	0.88	0.89	0.89	0.87

a) all values represent the average emission wavelength maximum and spectral full-width-at-half-maximum (FWHM) values from three different samples of identical composition, b) typical errors in emission maxima for 7AI are ± 1 nm or less, typical errors in FWHM for 7AI are ± 3 nm or less, typical errors in the amplitude ratio for pyrene are ± 0.02 or less, c) the number in brackets is the FWHM, in nanometers,

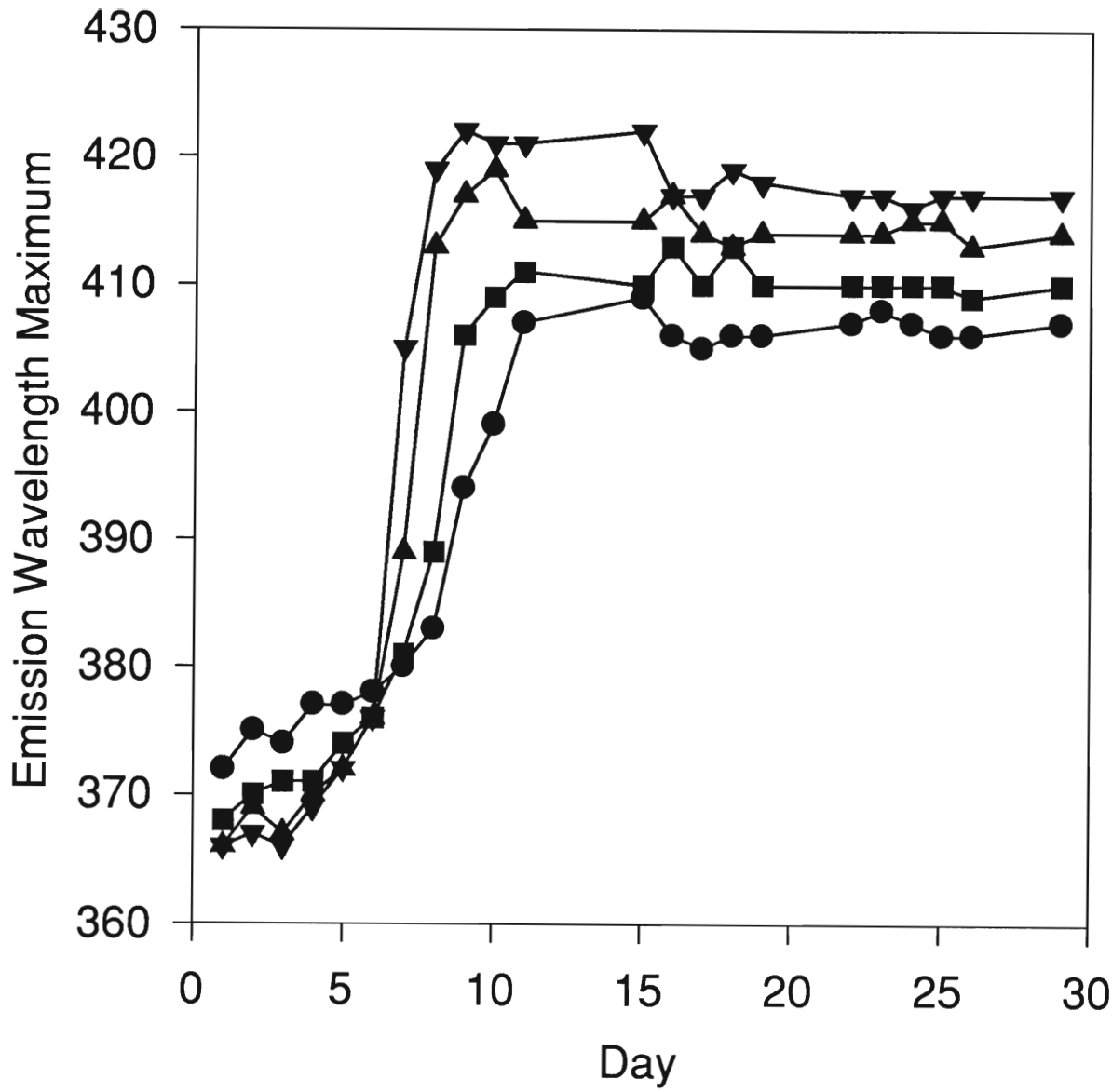

Figure 2.10. Effect of aging conditions on 7AI emission wavelength during the first 25 days of dry-aging for TEOS derived monoliths prepared with different TEOS:buffer ratios for gelation. (●)1:1 TEOS:buffer, (■) 2:1 TEOS:buffer, (▲) 3:1 TEOS:buffer, (▼) 4:1 TEOS:buffer. Representative error bars have been included for the 1:1 TEOS:buffer system. Similar error values are obtained for all other ratios.

by day 10, with the FWHM values being *ca.* 25-30 nm broader than was obtained in water. To examine whether this wavelength shift was due to a shift to acidic pH values, the emission of the pH sensitive probe seminaptharhodafluor-1 (SNARF-1) was examined in TEOS matrices which were prepared with the various TEOS:buffer ratios. The SNARF-1 emission corresponded to a pH value between 6 and 6.5 (results not shown), thus a pH-based wavelength shift was ruled out. Hence, the wavelength shift for entrapped 7AI indicated that adsorption of the probe onto surface silanol groups was occurring.[3] Third, the emission wavelength of 7AI at the completion of the wavelength shift (i.e., day 25) was longer for systems which had a lower water content. For example, 7AI in the 4:1 TEOS:buffer system had an emission wavelength at 418 nm while the emission maximum of 7AI in the 1:1 system was 408 nm. These results indicated that the proportion of silanol groups available for interaction with 7AI decreased as the amount of water used for gelation increased, in agreement with the infrared absorbance studies on dry systems.

Between days 10 and 140, the emission maximum of 7AI shifted to shorter wavelengths and in most cases the spectra became more narrow. In all cases the spectra ended up at a wavelength maximum greater than 400 nm. This blue shift is consistent with the loss of entrapped water[4] and may also indicate a condensation of silanol groups to produce siloxane bonds. This broadening and narrowing trend during aging indicates that the probe moves through a distribution of environments during drying (perhaps indicating uneven drying), but ends up with a much narrower distribution upon fully drying. It must be noted that even after prolonged aging the FWHM values for all systems are 20-25 nm broader than the spectral FWHM obtained in water.

At day 140, there is a substantial fraction of probe which is adsorbed (emission maximum > 400 nm), and the proportion increases as the ratio of TEOS:buffer used for gelation increased. While there is a narrower FWHM than in wet-aged monoliths, the larger width compared to that in water indicates that the emission wavelengths are a combination of probe environments which are polar yet solvated (385-400 nm) and adsorbed (~ 415-420 nm). The differences in the final emission wavelengths likely reflect differences in the total amount of silanol groups present for adsorption. This is consistent with the lower amount of silanol groups, and the concomitantly shorter emission maxima, obtained from wet-aged systems.

To further examine the dry-aged systems, the emission of entrapped pyrene was studied for the various TEOS:buffer ratios. The spectra (not shown) for pyrene in the dry-aged monoliths were similar to those for wet-aged monoliths except for the absence of an excimer band. The spectral data for all systems is given in Table 2.3. Pyrene spectra for all systems had an initial I_3/I_1 ratio of between 0.86 and 0.89, which is similar to the values obtained from the wet-aged samples, indicating that all samples began with similar internal environments. As the matrices aged the I_3/I_1 ratio initially remained constant within the measurement error for most samples, but decreased slightly for the sample containing the most water (1:1 TEOS:buffer). This is consistent with the lower initial concentration of ethanol in this system, and with the preferential expulsion of ethanol, and is qualitatively similar to the behaviour of the 7AI probe over the first 5 days.

Between days 7 and 25 the I_3/I_1 ratio remained constant or increased slightly, suggesting that there were no major changes in the polarity of the internal environment during this period. This result is extremely important since it provides a clear indication that

the changes in 7AI emission during the first 25 days in the dry-aged systems are *not* simply due to changes in solvent composition. This result thus confirms that 7AI reports on differences in the silane composition, providing compelling evidence that the 7AI probe is able to give unique information regarding sol-gel derived materials.

It is of interest to compare the fluorescence results from 7AI to the IR spectra and physical properties for both aging methods. Fluorescence investigations of the dried materials indicated that 7AI was affected by the specific chemical composition of sol-gel derived materials, and that the composition was dependent on the amount of water available for aging, as would be expected based on the effects of water on the properties of sol-gel derived materials, described in section 3.1. For example, the final properties of the wet-aged monoliths were all similar after drying was complete (i.e., IR spectra, pore-size, rehydration stability, hardness and transparency). In this case, the 7AI probe indicated that the internal environments were similar for all samples measured, in excellent agreement with the physical properties. For the dry-aged systems, the different TEOS:buffer ratios resulted in different physical properties when testing was done on day 140, as shown in Table 2.1. In this case, the 7AI probe clearly showed that the final environment within the monoliths was different (in agreement with IR results), and that the evolution toward the final environment was different for each of the four systems studied.

2.4. Conclusions

The studies presented herein show that both the silane:water ratio used for gelation and the aging method employed for preparation of sol-gel derived monoliths affected the physical properties and internal environment of the dry matrix. Several important conclusions can be made. With regard to the fluorescence studies, the results clearly show the 7-azaindole provides unique information about the internal environment of sol-gel derived materials which correlates well with both physical properties and IR spectral data. With regard to protein encapsulation studies, several conclusions can be drawn. First, wet-aged monoliths required roughly two days for complete removal of alcohol from the monoliths, as shown by pyranine, indicating that frequent buffer exchanges should be done to minimize the affects of alcohol upon encapsulated proteins. Second, increasing the ratio of TEOS:buffer in dry-aged monoliths decreased the drying time, but also produced smaller pores, a larger silanol content, and decreased rehydration stability. Third, wet-aging resulted in large pores (which is useful for reducing response times for analyte-protein interactions) and excellent resistance to cracking during rehydration; however, leaching of small proteins may limit the application of such materials for protein encapsulation. Overall, the results indicate that wet-aging should be done if at all possible. In cases where dry-aging is necessary (i.e., when leachable proteins are entrapped), encapsulation should be done with the largest amount of water possible for gelation since this will provide the best overall properties for the dry material.

2.5 References for Chapter 2

1)Brinker, C. J.; Scherer, G. W. *Sol-Gel Science*; Academic Press: San Diego, 1990.

2)Matsui, K.; Tominaga, M.; Arai, Y.; Satoh, H.; Kyoto, M. *J. Non-Cryst. Solids* **1994**, *169*, 295.

3)Matsui, K.; Matsuzuka, T.; Fuijita, H. *J. Phys. Chem.* **1989**, *93*, 4991.

4)Narang, U.; Jordan, J. D.; Bright, F. V.; Prasad, P. N. *J. Phys. Chem.* **1994**, *98*, 8101.

5)McKiernan, J.; Pouxviel, J. C.; Dunn, B.; Zink, J. I. *J. Phys. Chem.* **1989**, *93*, 2129.

6)Klein, L. C. *Ann. Rev. Mater. Sci.* **1985**, *15*, 22.

7)Sakka, S.; Kamiya, K. *J. Non-Cryst. Solids* **1982**, *48*, 31.

8)Scherer, G. W. *J. Non-Cryst. Solids* **1988**, *108*, 18.

9)Miller, J. M.; Dunn, B.; Valentine, J. S.; Zink, J. I. *J. Non-Cryst. Solids* **1996**, *220*, 279.

10)Braun, S.; Rappoport, S.; Zusman, R.; Avnir, D.; Ottolenghi, M. *Mater. Lett.* **1990**, *10*, 1.

11)Jordan, J. D.; Dunbar, R. A.; Bright, F. V. *Anal. Chem.* **1995**, *67*, 2436.

12)Yamanaka, S. A.; Dunn, B.; Valentine, J. S.; Zink, J. I. *J. Am. Chem. Soc.* **1995**, *117*, 9095.

13)Lundgren, J. S.; Bright, F. V. *Anal. Chem.* **1996**, *68*, 3377.

14)Wang; Narang, U.; Prasad, P. N.; Bright, F. V. *Anal. Chem.* **1993**, *65*, 2671.

15)Dave, B. C.; Soyez, H.; Miller, J. M.; Dunn, B.; Valentine, J. S.; Zink, J. I. *Chem. Mater.* **1995**, *7*, 1431.

16)Yamanaka, S. A.; Nishida, F.; Ellerby, L. M.; Nishida, C. R.; Dunn, B.; Valentine, J. S.; Zink, J. I. *Chem. Mater.* **1992**, *4*, 495.

17)Braun, S.; Shtelzer, S.; Rappoport, S.; Avnir, D.; Ottolenghi, M. *J. Non-Cryst. Solids* **1992**, *147*, 739.

18)Dave, B. C.; Dunn, B.; Valentine, J. S.; Zink, J. I. *Anal. Chem.* **1994**, *66*, 1120A.

19)Avnir, D.; Braun, S.; Lev, O.; Ottolenghi, M. *Chem. Mater.* **1994**, *6*, 1605.

20)Edmiston, P. L.; Wambolt, C. L.; Smith, M. K.; Saavedra, S. S. *J. Coll. Int. Sci.* **1994**, *163*, 395.

21)Narang, U.; Prasad, P. N.; Bright, F. V.; Ramanathan, K.; Kumar, N. D.; Malhotra, B. D.; Kamalasanan, M. N.; Chandra, S. *Anal. Chem.* **1994**, *66*, 3139.

22)Ellerby, L. M.; Nishida, C. R.; Nishida, F.; Yamanaka, S. A.; Dunn, B.; Valentine, J. S.; Zink, J. I. *Science* **1992**, *225*, 1113.

23)Hench, L. L.; West, J. K. *Chem. Rev.* **1990**, *90*, 33.

24)Hench, L. *Science of Ceramic Chemical Processing*; Wiley: New York, 1986.

25)Zarzycki, J.; Prassas, M.; Phalippou, J. *J. Mater. Sci.* **1982**, *17*, 3371.

26)Esquivias, L.; Zarzycki, J. *Ultrastructure Processing of Advanced Ceramics*; Wiley: New York, 1988.

27)Nishida, F.; McKiernan, J. M.; Dunn, B.; Zink, J. I.; Brinker, C. J.; Hurd, A. J. *J. Amer. Ceram. Soc.* **1995**, *78*, 1640.

28)Fujii, T.; Mabuchi, T.; Mitsui, I. *Chem. Phys. Lett.* **1990**, *168*, 5.

29)Matsui, K.; Nakazawa, T. *Bull. Chem. Soc. Jpn.* **1990**, *63*, 11.

30)Fujii, T.; Toriumi, K. J. *Chem. Soc. Faraday Trans.* **1993**, *89*, 3437.

31)Negishi, N.; Fujino, M.; Yamashita, H.; Fox, M. A.; Anpo, M. *Langmuir* **1994**, *10*, 1772.

32)Narang, U.; Bright, F. V.; Prasad, P. N. *Appl. Spec.* **1993**, *47*, 229.

33)Badini, w. E.; Grattan, K. T. V.; Tseung, A. C. C. *Analyst* **1995**, *120*, 1025.

34)Kaufman, V. R.; Avnir, D.; Pines-Rojanski, P.; Huppert, D. *J. Non-Cryst. Solids* **1988**, *99*, 379.

35)Matsui, K. *Langmuir* **1992**, *8*, 673.

36)Minquan, W.; Guodong, Q.; Mang, W.; Xianping, F.; Zhanglain, H. *Mater. Sci. and Eng.* **1996**, *B40*, 67.

37)Ilharco, L. M.; Santos, A. M.; Silva, M. J.; Martinho, J. M. G. *J. Sol-Gel. Sci. Tech.* **1997**, *8*, 877.

38)Negrerie, M.; Gai, F.; Bellefeuille, S. M.; Petrich, J. W. *J. Phys Chem.* **1991**, *95*, 8663.

39)Chen, Y.; Rich, R. L.; Gai, F.; Petrich, J. W. *J. Phys. Chem.* **1993**, *97*, 1770.

40)Chapman, C. F.; Maroncelli, M. *J. Phys Chem.* **1992**, *96*, 8430.

41)Chen, Y.; Gai, F.; Petrich, J. W. *J. Phys. Chem.* **1994**, *98*, 2203.

42)Avouris, P.; Yang, L. L.; El-Bayoumi, M. A. *Photochem. Photobiol.* **1976**, *24*, 211.

43)Ingham, K. C.; El-Bayoumi, M. A. *J. Amer. Chem. Soc.* **1974**, *96*, 1674.

44)Dunn, B.; Zink, J. I. *Chem. Mat.* **1997**, *9*, 2280.

45)Zheng, L.; Brennan, J. D. *Analyst* , In press.

46)Zheng, L.; Reid, W. R.; Brennan, J. D. *Anal. Chem.* **1997**, *69*, 3940.

47)Fyfe, C. A.; Aroca, P. P. *Chem. Mater.* **1995**, *7*, 1800.

48)Barrett, E. P.; Joyner, L. G.; Halenda, P. H. *J. Amer. Chem. Soc.* **1951**, *73*, 373.

49)Iler, R. K. *The Chemistry of Silica*; Wiley: New York, 1979.

50)Brinker, C. J.; Scherer, G. W. *J. Non-Cryst. Solids* **1985**, *70*, 301.

51)Shoup, R. D. *Colloid and Interface Science*; Academic Press: New York, 1976; Vol. 3.

52)Bertoluzza, A.; Fagnano, C.; Morelli, M. A.; Gottardi, V.; Guglielmi, M. *J. Non-Cryst. Solids* **1982**, *48*, 117.

Chapter 3: Fluorimetric Sensing of Ca^{2+} Based on an Induced Change in the Conformation of Sol-Gel Entrapped Parvalbumin

3.1 Introduction

In Chapter 2, different protocols for the encapsulation of biomolecules into TEOS based sol-gel derived matrices were investigated by monitoring physical characteristics such as pore size, rehydration/hydration stability, hardness and clarity as well as investigating the interior environment by the use of two polarity sensitive probes, 7-Azaindole and pyrene. It was determined that TEOS-derived sol-gels should be composed of a TEOS:H_2O ratio of 1:1 to obtain matrices which are optically clear, free of cracks, large enough pores to host biomolecules and also have a sufficient rehydration stabiltiy. It is optimal to conduct washing steps to dilute the ethanol byproducts from the sol-gel, although this poses a problem for proteins small is size, such as Cod III parvalbumin (Cod III parv). In this project, the fluorescent probe tryptophan will be used to investigate the environment surrounding the free and entrapped protein.

Numerous studies have been reported regarding the function, [1-12] structure, [13,14] dynamics, [15] accessibility, [13,14,16] reaction kinetics[17] initial stability[18-22] and long-term stability[1-10,23-29] of entrapped proteins. These studies have established that, in many cases, entrapped biological molecules retain their characteristic biochemical functionality and remain stable over periods of months. The majority of these studies involved enzymes, antibodies or O_2-binding proteins, such as cytochrome *c* and myoglobin, which do not undergo substantial conformational changes on binding of ligands. However, in many cases, the binding of an analyte to a protein requires that the protein be able to undergo conformational changes, and in certain cases, the conformational change itself is transduced into the optical signal which

provides information on analyte concentration. Examples of this strategy include the use of fluorescein labelled calmodulin to detect Ca^{2+},[30] and the development of maltose[31] and glucose[32] sensors based on fluorescent allosteric signal transduction (FAST) proteins. In each case, binding of the analyte results in a conformational change in the protein which produces a change in the environment and hence the emission characteristics of the protein-bound fluorophore.

An important question arises regarding how entrapment within a sol-gel derived matrix affects the conformational mobility of proteins which rely on such changes to develop optical signals. Previous studies have examined the conformational motions and rotational mobility of entrapped proteins using absorbance, [33] fluorescence[13-15] and ac impedance[12] measurements. These studies have indicated that the conformational motions of large proteins, such as hemoglobin[33] and BSA, [14,15] can be substantially restricted in sol-gel media. On the other hand, small proteins, such as cytochrome *c*, [12] appear to be only moderately affected by entrapment. The study involving BSA[14] was interesting since it showed that changes in the intrinsic fluorescence from the tryptophan (Trp) residues could be used to probe conformational changes that were induced by alterations of pH. This indicated that intrinsically fluorescent proteins could, in principle, be considered as models of the FAST proteins described above.

A particularly useful protein for examining the effects of entrapment on FAST proteins is isotype III of the calcium binding protein parvalbumin which is isolated from Codfish (Cod III parvalbumin, parv). The protein is small, (108 amino acids, MW ~12,000) and contains two calcium binding loops. The protein also contains a single Trp residue at position 102, which is in the middle of the terminal F-helix, away from the Ca^{2+}-binding sites.

The metal-free form of the protein is loosely packed. In this form, the quantum yield of the Trp is 0.09 ± 0.01 and the emission wavelength maximum is 335 nm. [34,35] Upon binding of Ca^{2+}, the structure becomes much more compact. In this case, the quantum yield increases to 0.14 ± 0.01 and the emission wavelength maximum shifts to 315 nm. [34] The fluorescence changes on Ca^{2+} binding should, therefore, make Ca^{2+} sensing possible.

In this study, we have utilized Trp fluorescence to examine the changes in the conformational motions of Cod III parvalbumin when the protein was entrapped in sol-gel derived matrices formed from tetraethylorthosilicate (TEOS). Changes in conformation were induced both by binding of Ca^{2+} as well as by thermal and chemical denaturation methods. The effects of aging and storage conditions on the stability and metal-ion-binding capability of the entrapped protein was investigated, and preliminary Ca^{2+}-sensing studies were done.

3.2 Experimental

3.2.1 Chemicals

Tetraethylorthosilicate (TEOS, 99.999 +%) was purchased from Sigma (St. Louis, MO). Anhydrous calcium chloride (99.9%) and magnesium chloride (99%) were supplied by Fisher scientific (Toronto, ON). Acrylamide (99%) was supplied by Aldrich (Milwaukee, WS). Hydrated strontium chloride (99%) and cadmium chloride (99%) were purchased from BDH Chemicals Ltd. (Toronto, ON). Urea (>99.5%) was purchased from Fluka BioChemika. The Sephadex G-25 fine powder was supplied by Pharmacia Biotech (Uppsala, Sweden). Chelex® grade 100 cation exchange resin (sodium form) was purchased from Biorad (Toronto, ON). All water was distilled and deionized using an Elga water purification system. All other chemicals were of analytical grade and were used as received.

3.2.2 Isolation and Purification of Protein

The Cod III parvalbumin was isolated from President's Choice™ Pacific Codfish and purified using the methods described by Hutnik[34] and Horrocks, [36] with no major modifications. The purified protein was dissolved in 10 mM PIPES, 100 mM KCl, pH 7.2. Metal-free proteins were prepared by precipitation with trichloroacetic acid (TCA), followed by resuspension and passage through a Ca^{2+}-free Chelex® cation exchange column, as described elsewhere. [37] Protein concentration was determined from UV-Vis spectroscopy using $\varepsilon_{280} = 7180\ M^{-1}cm^{-1}$. [34]

3.2.3 Preparation of Protein-Doped Monoliths

Sols were prepared by sonicating a mixture of 4.5 mL of TEOS, 1.4 mL of water and 100 μL of 0.1 N HCl for one hour at ambient temperature until the mixture became monophasic. The solution was then stored at -20°C for 7-10 days before use. [13] A volume of 300 μL of the hydrolyzed TEOS solution was mixed with an equal volume of PIPES buffer (10 mM, pH 7.2, with 100 mM KCl, with or without 7 μM protein). The buffer either contained no metal ions, or had; Ca^{2+} added in 10-fold increments from 10-fold to 50-fold (molar ratio of Ca^{2+}:protein), a 2.5:1 molar ratio of Tb^{3+} to protein, or a 50-fold molar excess of Mg^{2+}, Sr^{2+} or Cd^{2+} compared to the concentration of protein. After adding the protein solution to the hydrolyzed TEOS solution, the mixture was quickly vortexed and was immediately placed into a disposable cuvette which was then sealed with Parafilm and placed on its side until gelation occurred (generally 3 to 5 minutes). The monoliths were aged in air at 4°C for 20 days (unless otherwise stated) and were then rehydrated by adding 2.0 mL of

PIPES buffer dropwise, either with or without metal-ions present, over a period of several minutes.

3.2.4 Fluorescence Spectroscopy

Fluorescence measurements were done using equipment which is described elsewhere.[13] Fluorescence spectra of proteins in solution were obtained using samples containing 2 μM protein. Spectra of dry monoliths and rehydrated monoliths (present in 2.0 mL of buffer) used samples which were carefully mounted in quartz cuvettes at an angle of 45° with respect to the excitation path such that the excitation radiation was reflected away from the emission monochromator and PMT. [13] In all cases, the samples were excited at 285 nm and emission was collected from 295 nm to 450 nm in 1 nm increments using a 4 nm bandpass and an integration time of 0.3 s per point. Appropriate "no protein" blanks were subtracted from each sample and the spectra were corrected for deviations in emission monochromator throughput and PMT response.

3.2.5 Ca^{2+}-Binding and Detection Experiments

The holo protein was entrapped with different levels of excess Ca^{2+} present in the gelation buffer (0-fold to 50-fold molar excess). Fluorescence spectra were collected from aged monoliths before and at several times after addition of 2.0 mL of Ca^{2+}-free buffer to test the effects of entrapment on the ability of the protein to bind Ca^{2+}, and to test the reversibility of binding. Monoliths were also prepared and aged with a 2.5 molar excess of Tb^{3+} or a 50-fold molar excess of Mg^{2+}, Sr^{2+} or Cd^{2+} present in the gelation buffer. The aged monoliths were rehydrated with 1.5 mL of a buffer solution containing either a 2.5 molar excess of Tb^{3+}

or a 50-fold molar excess of Mg^{2+}, Sr^{2+} or Cd^{2+}, depending on the metal-ion present during entrapment. In each case, the fluorescence spectrum of the protein was obtained before and at several times after the addition of 1.5 mL of a 10.0 mM Ca^{2+} solution to test the level of interference imposed by the secondary ions.

The affinity of Ca^{2+}-binding for the entrapped proteins was examined by first making the protein metal-free by incubation in Ca^{2+}-free PIPES buffer. The apo protein was then titrated by adding 10 μL aliquots of a 30 mM stock solution of Ca^{2+} in PIPES buffer and collecting a spectrum at each point until no further spectral changes were observed. The spectra were integrated over the entire emission band and the intensity was converted to a percent signal enhancement. The percent enhancement was plotted against Ca^{2+} concentration to generate Ca^{2+} binding curves.

Scatchard analysis of Ca^{2+} binding was also done to obtain dissociation constants. In this case, the fluorescence intensity was first converted to the fraction of binding sites filled (*f*) according to the equation:

$$f = \frac{F - F_{min}}{F_{max} - F_{min}} \qquad (28)$$

where F is the measured fluorescence at a given concentration of Ca^{2+}, F_{min} in the fluorescence intensity in the absence of Ca^{2+}, and F_{max} is the maximum fluorescence intensity obtained in the presence of excess Ca^{2+}. The fraction of sites filled was multiplied by the protein concentration to determine the amount of Ca^{2+} bound, and this value was in turn used to calculate the free concentration of Ca^{2+} at each point during the titration. The concentration of Ca^{2+} bound was divided by the protein concentration to obtain the average

number of Ca^{2+} ions bound per macromolecule (ν). Finally, $\nu/[A]_{free}$ was plotted against ν and the dissociation constants (K_d) were obtained from the Scatchard equation:

$$\frac{\nu}{[A]} = -K_d\nu + K_dN \qquad (29)$$

where N is the number of binding sites.

3.2.6 Quenching Studies

The rehydrated monolith containing either metal-loaded (holo) or metal-free (apo) protein was mounted into a quartz cuvette with a total of 2.0 mL of buffer present. Samples were titrated with 8.0 M acrylamide in PIPES buffer. A fluorescence spectrum was collected from the sample and an appropriate blank after each addition. The spectra were integrated over the entire emission band and the intensity data was analyzed using the modified version of the Stern-Volmer equation which accounts for both dynamic and static quenching of Trp fluorescence which is Equation 18.

3.2.7 Thermal Denaturation Studies

The thermal stability was examined for free and entrapped holo parvalbumin with no excess Ca^{2+} present and with a 50-fold molar excess of Ca^{2+} present with respect to protein concentration to examine the effects of Ca^{2+} and entrapment on stability. For solution studies, a total of 2.0 mL of solution was used. For monoliths, a total of 2.0 mL of buffer solution was placed into the cuvettes containing the monolith. In all cases, the solution was purged with nitrogen for 15 minutes and the cuvette was immediately capped to minimize the amount of dissolved oxygen. The temperature was raised in *ca.* 5°C increments starting at

20°C and going to 90°C, then lowered to 20°C to check reversibility. The temperature of the solution in a second cuvette which was also present in the 4 sample turret was measured directly using a thermistor probe (Hanna Instruments model 9043A) to account for loss of heat through the tygon tubing connecting the sample holder and the water bath. The samples were allowed to equilibrate for at least ten minutes at each temperature, at which point a fluorescence spectrum was collected from the sample and from an appropriate "no protein" blank. The corrected emission spectra were integrated over the entire emission band. The integrated intensity was normalized to the intensity at the starting temperature (20°C) and was plotted against temperature to generate the unfolding curve.

The unfolding enthalpy change (ΔH^0_{un}) and entropy change (ΔS^0_{un}) were calculated by fitting the unfolding curve to Equation 22 and 23.

3.2.8 Chemical Unfolding Studies

Chemical stability was examined for free and entrapped holo parvalbumin at the same Ca^{2+} levels used for thermal denaturation studies. For monolith studies, the rehydrated monolith was mounted into a quartz cuvette with a total of 1.50 mL of buffer present. For solution-based studies, a volume of 1.50 mL of protein in buffer was used. In both cases, the proteins were denatured by titrating with 10.0 M urea in PIPES buffer. The solution was constantly stirred and a minimum of 20 minutes was allowed for equilibration after each addition. A fluorescence spectrum was collected at each point for both the sample and a blank containing an identical concentration of urea. Solution-based spectra were corrected for dilution factors. No dilution correction was necessary for monoliths containing protein. The unfolding curves for these experiments were obtained by manipulating the spectra as

described for the thermal denaturation experiments, with integrated intensity plotted against denaturant concentration. The unfolding curves were fit using Equation 24.

3.3 Results and Discussion

3.3.1 Ca^{2+} Binding and Fluorimetric Detection

Initially, the holo protein was entrapped with different levels of Ca^{2+} present in the gelation buffer, ranging from no excess Ca^{2+} to a 50-fold molar excess. In all cases, the spectra of the dry monoliths (before addition of buffer) were similar, with an emission maximum at 315 nm and a FWHM of 42 ± 1 nm. Thus it was possible to entrap the protein with Ca^{2+} bound, indicating that the negatively charged matrix did not extract Ca^{2+} from the protein. Addition of Ca^{2+}-free buffer caused the emission maxima to shift from 315 nm to 334 ± 2 nm and the FWHM to increase to 64 ± 1 nm for all samples, with the time required for the shift increasing from 30 minutes with no excess Ca^{2+} to greater than 3 hours as the molar excess Ca^{2+} increased to 50-fold. For comparison, the apo form of the protein in solution has an emission maximum at 337 nm and a full width at half maximum (FWHM) of 66 ± 1 nm. The similarity in the emission maximum values for the free and entrapped apo-proteins suggested that the entrapped protein was able to fully undergo Ca^{2+}-induced conformational changes. The removal of Ca^{2+} from the matrix could be stopped by storing the aged monolith in a buffer which contained a 50-fold molar excess of Ca^{2+}-to-protein, even when low levels of Ca^{2+} were used in the gelation buffer. Using these storage conditions, no changes in spectral appearance were observed over a period of at least eight weeks, indicating that the entrapped protein could be stored in a functional form over long time periods.

Entrapped proteins which were made apo by exchange with Ca^{2+}-free buffer were immersed into a solution containing 3.0 mM $CaCl_2$. For all samples, the presence of Ca^{2+} caused the intensity to increase and the wavelength to slowly shift to 315 nm over a period of approximately 2 hours, while the FWHM decreased by 23 ± 1 nm, approaching the values obtained for the holo protein before removal of Ca^{2+}, as shown in Figure 3.1. The spectral changes indicated that the entrapped apo-protein was able to bind Ca^{2+} and undergo induced conformational changes. The slow kinetics for the reaction are consistent with literature reports which suggest that positively charged analytes are hindered in their movement though negatively charged silicate matrices.[13,17]

To further examine the conformational changes of the entrapped protein on binding of Ca^{2+}, acrylamide quenching was done for the apo and holo forms of the entrapped protein using acrylamide, which is a neutral quencher. Figure 3.2 shows the Stern-Volmer plots for the quenching of the holo- and apo-forms of the entrapped protein. Fitting of the curves to equation 18 indicated that the holo form of the protein had a K_{SV} value of 3.2 ± 0.2 M^{-1} with a V value of 1.0 ± 0.1 M, while the apo form of the protein had a K_{SV} value of 6.5 ± 0.3 M^{-1} and a V value of 0.5 ± 0.1 M. The increase in the K_{SV} value may be due to either an increase in the unquenched fluorescence lifetime (τ_0), or an increase in the bimolecular quenching rate constant (k_q). If it is assumed that the fluorescence lifetimes of entrapped holo- and apo-Cod III parvalbumin are similar to the values in solution, then the τ_0 value of the holo protein is 3.3 ns, while the τ_0 value for the apo protein is 3.4 ns. [34] These lifetime values result in k_q values of (9.7 ± 0.6) x 10^8 $M^{-1}.s^{-1}$ for the holo protein and (1.9 ± 0.1) x 10^9 $M^{-1}.s^{-1}$ for the apo protein, indicating that rate constant for quenching doubles on removal of Ca^{2+}. The increase in k_q indicates a greater exposure of the Trp residue to solvent upon removal of Ca^{2+}.[38] Thus,

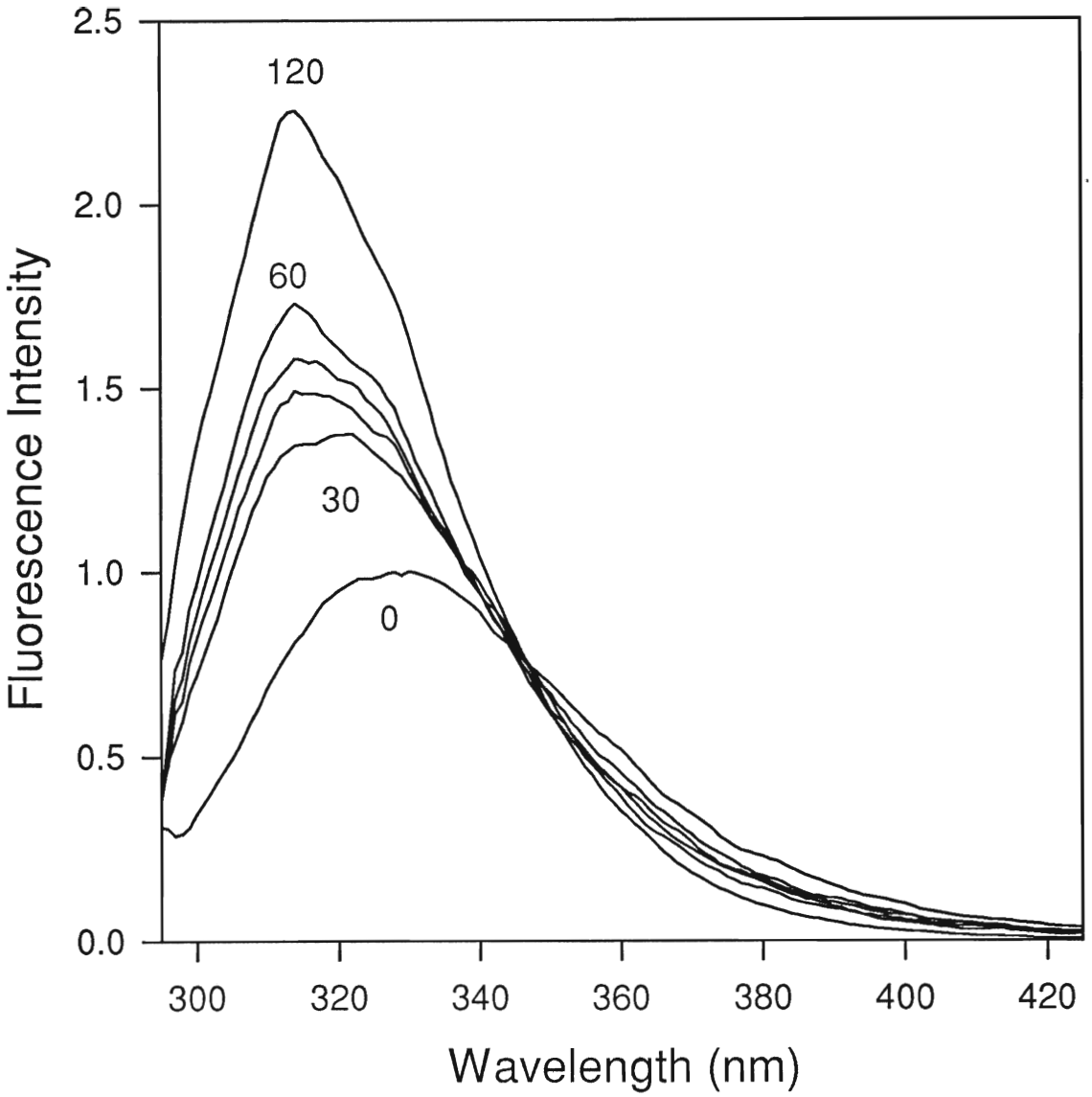

Figure 3.1. Changes in the fluorescence spectrum for entrapped Cod III parvalbumin with time after the addition of a 3.0 mM solution of Ca^{2+}. Excitation was done at 285 nm. The spectra are corrected background signals and for instrumental distortions. The intensity has been normalized to the maximum intensity of the spectrum obtained before the addition of Ca^{2+}. The values shown on the plot are the times in minutes after addition of Ca^{2+}.

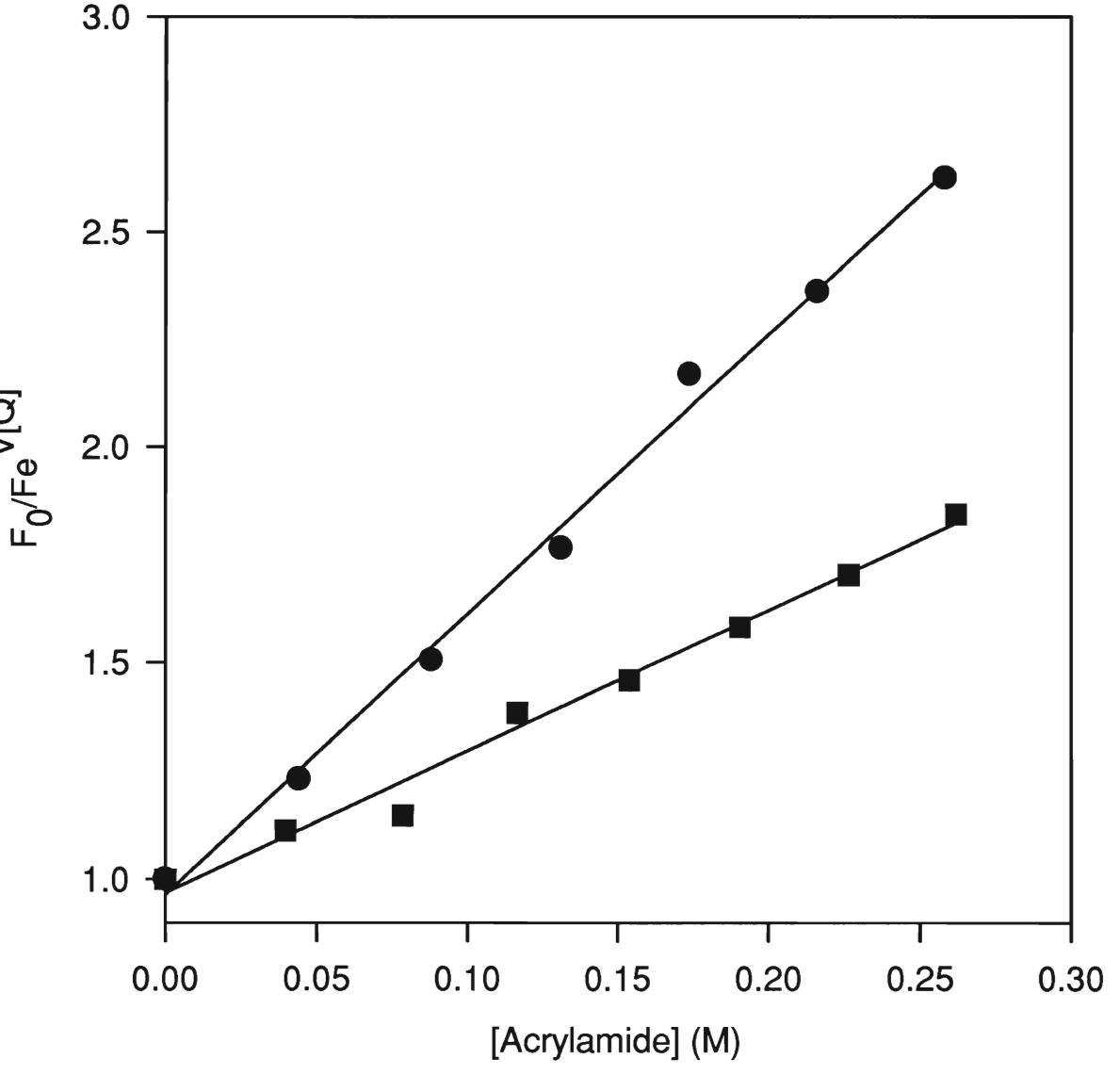

Figure 3.2. Stern-Volmer plots for acrylamide quenching of entrapped Cod III parvalbumin in the absence of Ca^{2+} (●), and in the presence of 3.0 mM Ca^{2+} (■). The data was plotted according to equation 18, and the fitting values are given in the text. r^2 for apo-protein was 0.995, r^2 for holo-protein was 0.986.

the protein is indeed able to undergo significant Ca^{2+}-dependent conformational changes, even when entrapped in a silicate matrix.

The ability to remove Ca^{2+} from the entrapped protein using a simple buffer exchange method, as described above, was not expected, since the removal of Ca^{2+} from parvalbumin in solution requires addition of [Ethylenebis(oxyethlyenenitrilo)]tetraacetic acid (EGTA) or precipitation with trichloroacetic acid (TCA). [34] This finding indicated that the binding affinity of parvalbumin was likely lowered upon entrapment. To quantitatively assess the changes in binding affinity, and to test the overall effectiveness of induced conformational changes as a quantitative method for Ca^{2+} sensing, Ca^{2+} binding curves were generated for entrapped apo-proteins which were prepared by incubation of monoliths in Ca^{2+}-free buffer. The binding curves obtained at two different aging times are shown in Figure 3.3. Several aspects of these curves merit further attention. First, the range of Ca^{2+} concentrations over which the fluorescence signal changes becomes larger as the monolith ages in air for a longer period of time. Secondly, the binding curves suggest a lower affinity for Ca^{2+} as aging in air continues. [5,29] Lastly, the sensitivity of the response curves and the limit-of-detection (LOD) change significantly with aging time. For example, 20 day old monoliths have an analytical range of ~600 μM, a maximum sensitivity of 5.0% change in fluorescence intensity per 10 μM change in Ca^{2+} concentration (compared to the full range being 100%), and a LOD of 3 μM (at a signal-to-noise level of 3). In contrast, the 30 day old monoliths show an analytical range of *ca.* 2 mM, with a sensitivity of 1.4% change in signal per 10 μM change in Ca^{2+} concentration and a LOD of 10 μM. The performance of the entrapped protein was retained by 75% over three cycles of Ca^{2+} removal and addition. Samples which were stored in Ca^{2+}-loaded buffer after an initial aging period of 20 days showed almost no change in binding

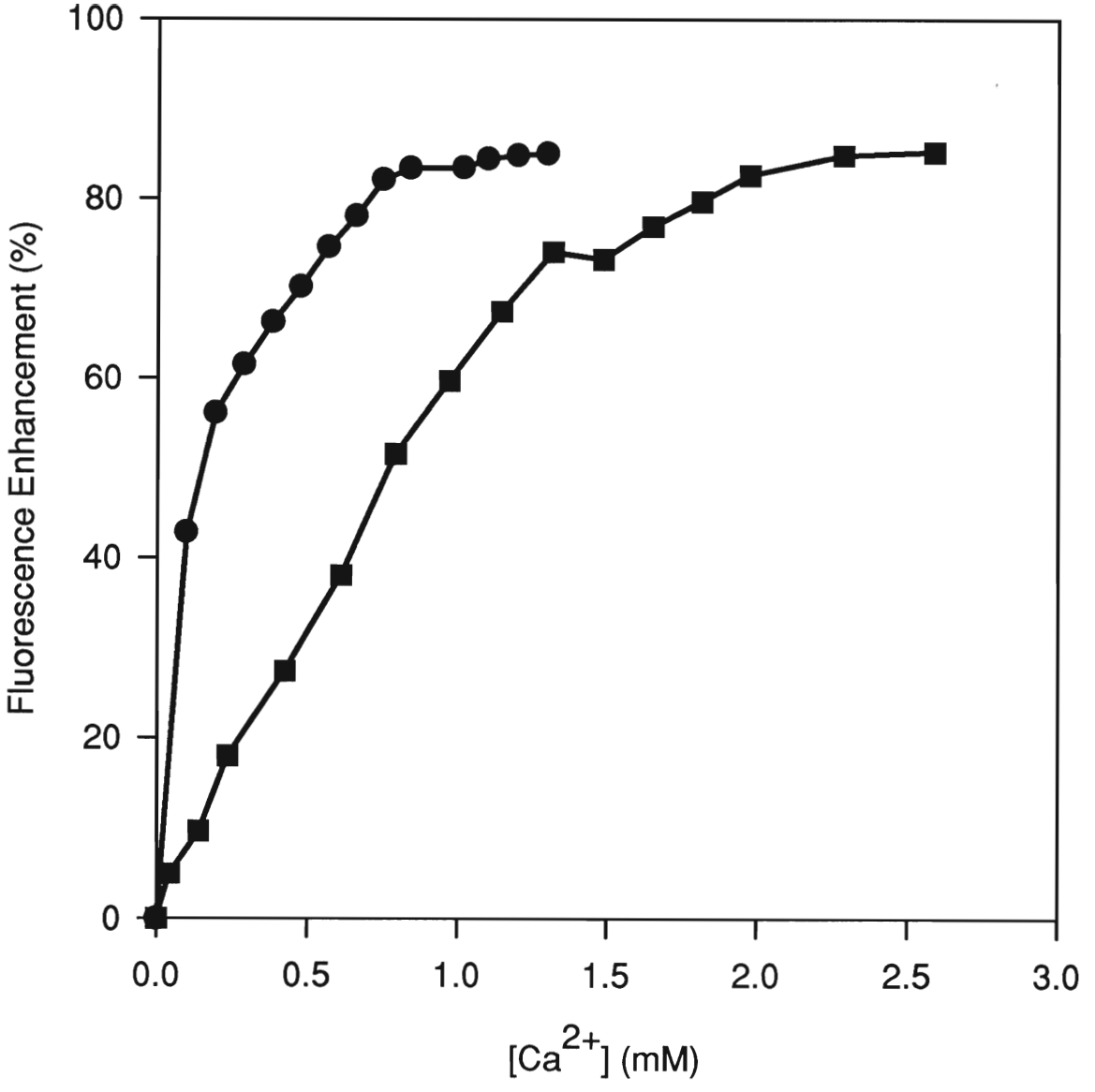

Figure 3.3. Changes in integrated fluorescence intensity during the addition of Ca^{2+} to entrapped Cod III parvalbumin. Monoliths were aged for 20 days (●), or 30 days (■). The data is presented as percent signal enhancement using the integrated intensity of the apo protein as the initial point.

affinity over at least eight weeks, indicating that storage in Ca^{2+}-loaded buffer maintains the binding ability of the entrapped protein.

The broad concentration range over which Ca^{2+} bound suggested that the binding affinity of the protein was lowered substantially upon entrapment. To obtain dissociation constants for the entrapped proteins, Scatchard analysis was done. It was first necessary to determine the concentration of protein within the pores of the aged monoliths. This required that the volume change on aging be determined, hence it was necessary to determine the volume of solution within the aged monolith. Pore-size analysis of fully dried monoliths, done using cryogenic nitrogen desorption experiments, suggested a pore volume of 63.5 ± 1.5 μL. [13] This value indicated that there was approximately a 5-fold increase in the protein concentration on aging (i.e., the initial volume of solution containing protein was 300 μL, the final volume was ~ 60 μL). Hence, a protein concentration of 35 μM was used in the Scatchard analysis. Using this value, and correcting the total Ca^{2+} concentration by accounting for the volume of solution inside the monolith, it was possible to obtain Scatchard plots for the 20 day old and 30 day old samples as shown in Figure 3.4. For both samples, the plots showed two linear regions with a distinct break between them, indicative of two sites with different K_d values. Analysis of each portion of the curve provided K_d values of $(3.8 \pm 0.5) \times 10^3$ M^{-1} and $(6.4 \pm 1.1) \times 10^3$ M^{-1} for the 20 day old sample, and $(1.2 \pm 0.3) \times 10^3$ M^{-1} and $(5.2 \pm 1.5) \times 10^2$ M^{-1} for the 30 day old sample. For comparison, the K_d values for Ca^{2+} binding to parvalbumin in solution are ~10^8 - 10^9 M^{-1}, [34] with the EF-loop having a somewhat higher affinity for Ca^{2+}.[34] The binding data clearly show that the binding affinity drops by several orders of magnitude on entrapment. This is in qualitative agreement with results obtained for entrapped antibodies, where a drop of 100-fold in the affinity constant

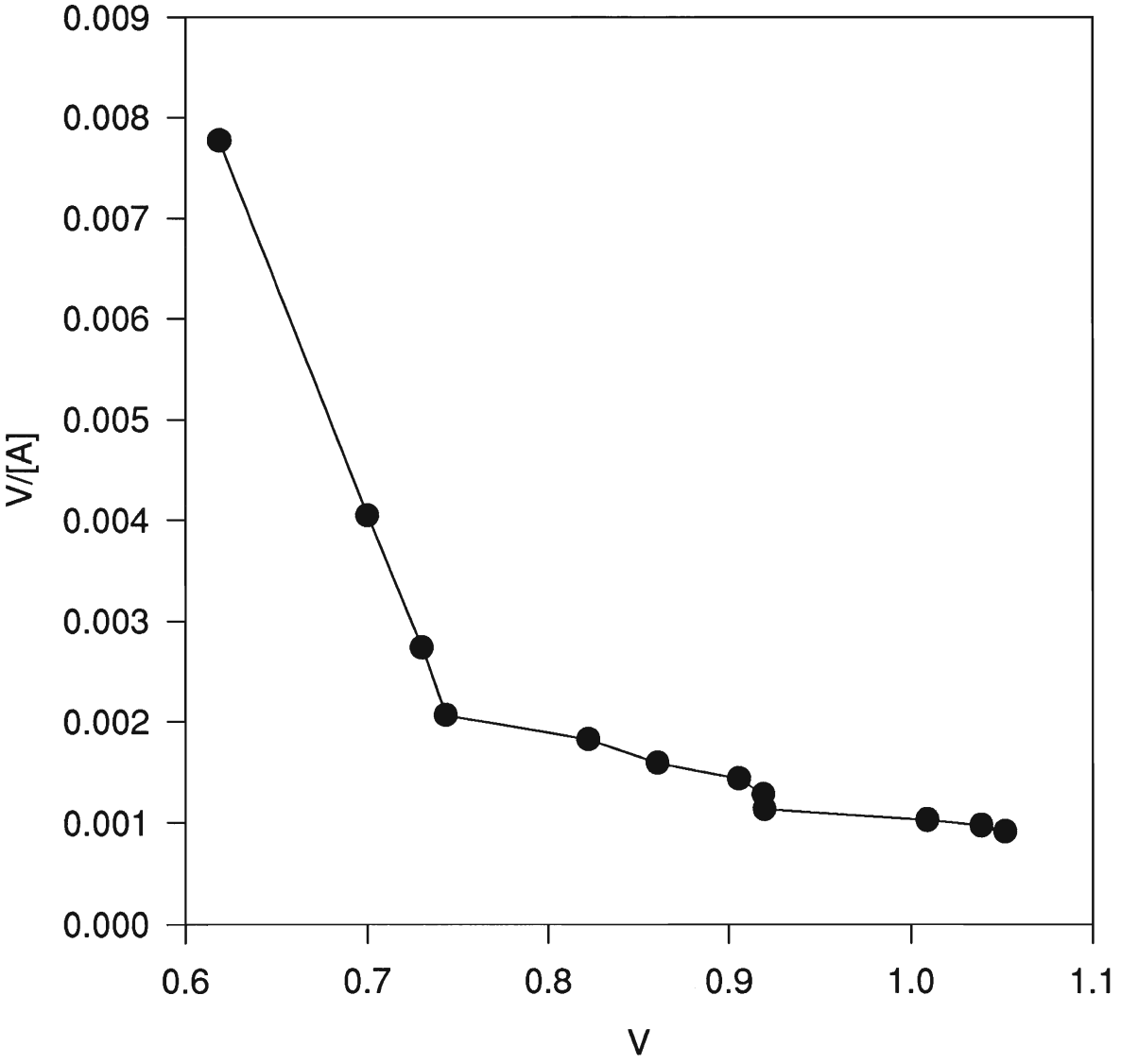

Figure 3.4 Scathchard Plot of Ca^{2+} binding to encapsulated Cod III parvalbumin with a 20 day old sample (●).

was observed on entrapment. [39] The basis of the lower K_d values is not fully understood, but is likely due to a combination of factors, including partial denaturation of a fraction of the protein, and electrostatic interactions between the negatively charged silicate matrix and the negatively charged groups in the binding loops of the protein. Although the basis for the change in affinity constant is not known, the lower binding constants may have a beneficial effect in that they extend the range of Ca^{2+} detection to the mM level, providing a much larger range than is found for common Ca^{2+} indicator dyes, such as indo-1 and fura-2, which have analytical ranges in the low micromolar range. [38]

To evaluate the interferences posed by other divalent ions, the protein was entrapped with different metal ions present in the gelation buffer and the aged monoliths were rehydrated with 2.0 mL of a buffer solution containing Mg^{2+}, Sr^{2+}, Cd^{2+} or Tb^{3+}, depending on the metal-ion present during entrapment. In each case, the fluorescence spectrum of the protein was obtained before and at several times after the addition of 1.0 mL of a 10.0 mM Ca^{2+} solution. With the exception of Tb^{3+}, the protein maintained spectral characteristics which were indicative of the apo state if no Ca^{2+} was present. The presence of Tb^{3+}, however, resulted in the protein emission spectrum shifting to 318 nm, indicative of holo characteristics. This spectral shift reflects the high affinity of lanthanide ions for Ca^{2+} binding proteins. [30,40] The addition of Ca^{2+} to monoliths containing Mg^{2+}, Sr^{2+}, Cd^{2+} caused the spectral characteristics of each protein to shift to the characteristic holo-form, indicating that Ca^{2+} could selectively bind to the protein, even in the presence of an excess of other divalent ions. The Ca^{2+} binding selectivity is in agreement with previous studies of Cod III parvalbumin in solution. [34] The addition of metal-ion-free buffer to the holo protein in the presence of any of the divalent ions caused a reversible transition to the apo form of the

protein, consistent with the results obtained when Ca^{2+} was bound in the absence of other metal ions. These results indicated that the use of entrapped Cod III parvalbumin provided a reliable method for sensing of Ca^{2+} based on a Ca^{2+} selective induced conformational change.

3.3.2 Thermally Induced Unfolding and Stability

To further examine both the ability of the entrapped protein to undergo conformational changes, and the overall stability of the entrapped protein as compared to the free protein, denaturation experiments were done. Table 3.1 lists the changes in spectral characteristics which occurred upon thermal denaturation of the free and entrapped proteins at different Ca^{2+} levels. Upon heating, the emission wavelength of the free proteins in solution shifted to between 340 nm and 342 nm, regardless of the level of Ca^{2+} present. However, the emission maximum of the entrapped proteins did not shift beyond 328 nm in any case, and the Ca^{2+}-loaded protein did not shift from 315 nm, even upon increasing the temperature to 90 °C (the upper limit for our instrument). Furthermore, the full-width-at-half-maximum (FWHM) for the emission spectrum of the entrapped protein broadened by only 7-10 nm at a temperature of *ca.* 90 °C, compared to 18 ± 1 nm for the spectrum obtained from the protein in solution. Finally, the intensity of the denatured protein in the sol-gel derived matrix decreased by a slightly smaller amount compared to the protein in solution. Put together, these results indicate that the entrapped protein could undergo conformational motions when entrapped , but was not able to fully unfold at 90 °C, providing evidence of enhanced stability for entrapped proteins.

Table 3.1. Fluorescence spectral data for thermal denaturation of free and entrapped parvalbumin.

Conditions Used	Intensity Decrease (± 2%)[a]	λ_{max} unfolded[b] (nm)	λ_{max} change (nm)[a]	FWHM unfolded[a,b,c] (nm)	FWHM change[a,c] (nm)
Solution with no excess Ca^{2+}	77%	340 ± 1	26 ± 1	57 ± 1	17 ± 1
Solution with 50-fold excess Ca^{2+}	77%	342 ± 2	28 ± 2	58 ± 1	18 ± 1
Entrapped with no excess Ca^{2+}	75%	328 ± 1	13 ± 1	50 ± 1	10 ± 1
Entrapped with 50-fold excess Ca^{2+}	71%	315 ± 1	0	47 ± 1	7 ± 1

a) Changes reported refer to a change in temperature from 20°C to 90°C for Cod III parvalbumin in solution or entrapped in monoliths, b) these values were obtained at 90°C, although the unfolding curves did not appear to have reached a final baseline value, suggesting incomplete unfolding (see text), c) FWHM is full-width-at-half-maximum.

The intensity-based unfolding curves for the free and entrapped protein at the two Ca^{2+} levels are shown in Figure 3.5. In all cases, an unfolding transition can be clearly seen for both free and entrapped proteins. In comparing the unfolding curves from the entrapped protein to those obtained in solution two features are immediately apparent. Firstly, the unfolding transitions of the entrapped protein (at similar levels of Ca^{2+}) occur at higher temperatures. Secondly, the unfolding transition always occurs as a single step, although the transitions are generally broader for the entrapped protein compared to the protein in solution. The broadening may indicate a distribution of environments for the entrapped protein, in agreement with previous reports for entrapped proteins. [13]

The results of the thermodynamic analysis of the unfolding curves using equation 22 are listed in Table 3.2. Several aspects of the stability data merit special attention. First,

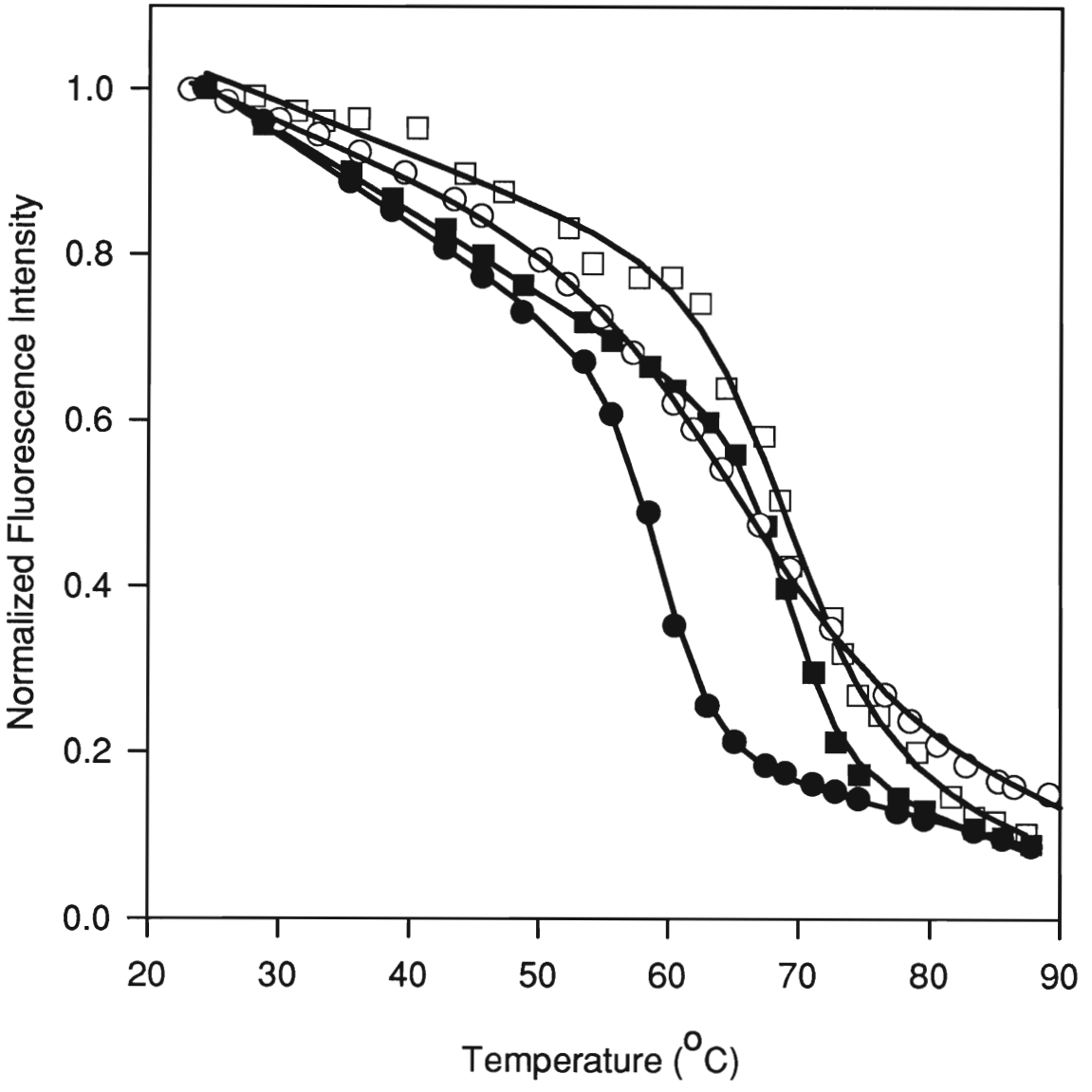

Figure 3.5. Changes in integrated fluorescence intensity for cod III parvalbumin as a function of temperature in solution with no excess Ca^{2+} (●) and with 50-fold excess Ca^{2+} (■); and for the entrapped protein with no excess Ca^{2+} (○) and with 50-fold excess Ca^{2+} (□). The symbols are the experimentally derived data points. The solid lines are the lines-of-best-fit as determined by fitting to equation 22.

increased levels of Ca^{2+} lead to improvements in stability for both free and entrapped proteins, based on increases in both the thermodynamic parameters and the T_{un} values. Such a finding has been previously reported for Cod III parvalbumin in solution. [41,42] The improved stability of the entrapped protein in the presence of excess Ca^{2+} suggests that long-term storage should be done in the presence of excess Ca^{2+}, in agreement with the results obtained from the Ca^{2+}-binding experiments. Second, the T_{un} values for the entrapped protein are similar or higher than those obtained for the protein in solution at similar levels of Ca^{2+}. This indicates that entrapment does not have a deleterious effect on protein stability, and may in fact improve stability. Third, the changes in ΔH^0_{un} and ΔS^0_{un} were in all cases smaller for the entrapped protein compared to the protein in solution. The lower values of the thermophysical parameters for the entrapped protein, compared to the free protein, is partly due to the broadening of the unfolding transition, but may also be partially due to incomplete unfolding of the entrapped protein. Comparing the spectra of the folded and denatured protein in solution to those for the entrapped with a 50-fold molar excess of Ca^{2+} present, it can be concluded that the smaller changes in the thermophysical parameters were most likely due to different final states for the unfolded protein in solution and in sol-gel matrices, indicating that the entrapped protein was not able to fully unfold under thermal denaturation conditions.

The effects of storage conditions and aging time on protein stability were also investigated to further examine the most appropriate storage method. The stability of the entrapped protein was found to be dependent on the method used for storage and on the aging/storage time. Unfolding curves obtained from protein which was entrapped with a 50-fold molar excess of Ca^{2+} and aged for 20 days or 30 days show a single unfolding transition

at the earlier time (as in Figure 3.5), but show at least two distinct stages in the unfolding curve at later times and a lower overall stability (data not shown). The multi-step unfolding profile is indicative of a broad distribution of environments for the entrapped protein, each with a different thermodynamic stability, and may be indicative of uneven drying rates throughout the monolith. The decreased stability at longer aging times indicates that the monolith should be aged for shorter times (20 days at most) to avoid an irreversible loss of function. Aging in a Ca^{2+}-loaded buffer solution after 20 days of aging in air led to no significant changes in the thermal unfolding curves over a period of several weeks, indicating such storage conditions provided long-term stability to the protein.

Table 3.2. Thermodynamic parameters for thermal unfolding of free and entrapped Cod III parvalbumin.

Conditions Used	ΔH^0_{un} (kJ.mol^{-1})[a,b]	ΔS^0_{un} (J.K^{-1}.mol^{-1})[a,b]	T_{un} (°C)[c]
Solution with no excess Ca^{2+}	414 ± 28	1246 ± 62	60 ± 3
Solution with 50-fold excess Ca^{2+}	442 ± 37	1291 ± 106	69 ± 5
Entrapped with no excess Ca^{2+}	149 ± 10	439 ± 22	66 ± 3
Entrapped with 50-fold excess Ca^{2+}	263 ± 25	768 ± 55	69 ± 6

a) determined from non-linear curve fitting to equation 22 using SigmaPlot 1.02 for Windows,

b) fitting parameters were as follows:

Holo Solution: $F_{0N} = 1.260$, $F_{0U} = 0.450$, $s_N = -0.011$, $s_U = -0.004$;

50x excess Ca^{2+} in solution : $F_{0N} = 1.242$, $F_{0U} = 0.609$, $s_N = -0.010$, $s_U = -0.005$;

Holo in sol-gel matrix: $F_{0N} = 1.160$, $F_{0U} = 0.598$, $s_N = -0.006$, $s_U = -0.005$;

50x excess Ca^{2+} in sol-gel matrix: $F_{0N} = 1.169$, $F_{0U} = 0.489$, $s_N = -0.006$, $s_U = -0.006$.

c) calculated from $\Delta H^0_{un} / \Delta S^0_{un}$

3.3.3 Chemically Induced Unfolding

Chemical denaturation was also conducted to examine chemically induced conformational changes for the free and entrapped protein. Initial experiments showed that the positively charged denaturant guanidine hydrochloride was preconcentrated by the negatively charged sol-gel matrix, making stability measurements of entrapped proteins difficult to interpret. Therefore, all chemical denaturation experiments were done with the neutral denaturant urea. The urea-induced unfolding curves for the free and entrapped holo protein in presence no excess Ca^{2+} and 50-fold excess Ca^{2+} are shown in Figure 3.6, while the spectroscopic parameters obtained during denaturation are shown in Table 3.3. For both free and entrapped proteins, the unfolding curves showing a definite unfolding transition and a post-unfolding baseline. As shown in Table 3.3, the intensity of the free protein decreased by ~23% with the presence of 5.0 M urea and the wavelength shifted to 344 ± 1 nm, indicative of complete unfolding. There were slightly larger decreases in intensity for the entrapped proteins, although these changes required the addition of 6.0 M to 7.5 M urea. However, the wavelength shifted to only *ca.* 336 nm for the entrapped proteins. These wavelength shifts are much greater than those obtained during thermal denaturation of entrapped proteins, suggesting larger changes in conformation occurred. However, the changes in emission maximum for the entrapped protein are still somewhat less than the values obtained in solution. It must be noted that the emission of N-acetyltryptophanamide in sol-gel derived monoliths aged for 30 days has been reported to be 335 ± 1 nm, [13] indicating that entrapped proteins are not likely to be able to emit at wavelengths beyond this value. Hence, the emission maximum of the entrapped protein is likely indicative of complete unfolding.

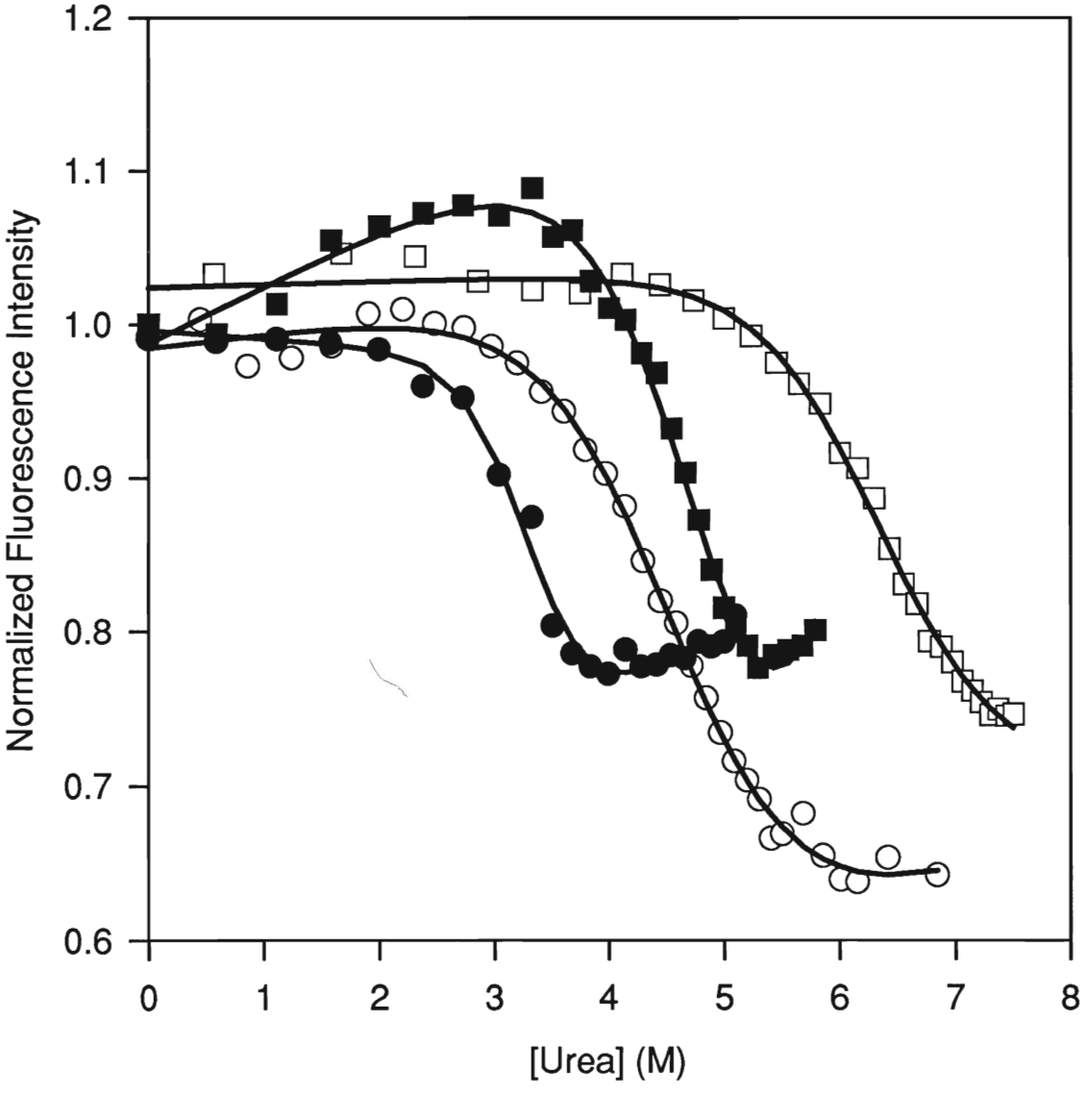

Figure 3.6. Changes in integrated fluorescence intensity for Cod III parvalbumin as a function of urea concentration in solution with no excess Ca^{2+} (●) and with 50-fold excess Ca^{2+} (■); and for the entrapped protein with no excess Ca^{2+} (○) and with 50-fold excess Ca^{2+} (□). The symbols are the experimentally derived data points. The solid lines are the lines-of-best-fit as determined by fitting using equation 24.

Table 3.3. Fluorescence spectral data for chemical denaturation of free and entrapped parvalbumin.

Conditions Used	Intensity Decrease (± 1%)[a]	λ_{max} unfolded (nm)	λ_{max} change (nm)[a,b]	FWHM unfolded[a,c] (nm)	FWHM change[a,c] (nm)
Solution with no excess Ca^{2+}	23%	344	30	61	21
Solution with 50-fold excess Ca^{2+}	22%	343	29	60	20
Entrapped with no excess Ca^{2+}	34%	337	23	66	18
Entrapped with 50-fold excess $Ca^{2+(d)}$	25%	335	21	63	20

a) Changes reported refer to a change in urea concentration from 0 M to 7.5 M for Cod III parvalbumin in solution or entrapped in monoliths, b) the error is each value is ±1 nm, c) FWHM is full-width-at-half-maximum, d) these values were obtained at 7.5 M urea, although the unfolding curves did not appear to have reached a final baseline value, suggesting incomplete unfolding (see text).

Thermodynamic analysis of the unfolding curves was done using equation 24. The results are given in Table 3.4. Two main points deserve further attention. Firstly, higher levels of Ca^{2+} result in improvements in the stability of both the free and entrapped protein (based on $D_{1/2}$ values), confirming that Ca^{2+} has a beneficial effect on the stability of the protein, even when it is entrapped in a sol-gel derived matrix. Secondly, at both levels of Ca^{2+}, the entrapped protein required a much higher concentration of denaturant than the free protein in order to unfold. For example, the $D_{1/2}$ of entrapped parvalbumin was more than 1 M greater than in solution at both Ca^{2+} levels. This confirms that a significant increase in stability occurs upon entrapment. It is important to note that the major unfolding transitions generally occur over a much larger range (approximately 3 M) of denaturant in the sol-gel, compared to ~1.5 M - 2.0 M in solution. The broader transition in the monolith is indicative of a distribution of

protein environments, in qualitative agreement with thermal denaturation studies. The breadth of the transition was similar for different rates of addition of denaturant spanning 6 minute intervals out to 1 hour intervals. This indicates that the broader transition was not the result of insufficient time for equilibration of denaturant with the entrapped protein.

Table 3.4. Thermodynamic parameters for the urea induced unfolding of free and entrapped Cod III parvalbumin.

Conditions	ΔG_{un} (kJ.mol^{-1})[a,b]	$-m_G$ (kJ.L.mol^{-2})[a,b]	$D_{1/2}$ (M)[c]
Solution with no excess Ca^{2+}	28.0 ± 0.6	8.7 ± 0.5	3.2 ± 0.1
Solution with 50-fold excess Ca^{2+}	29.2 ± 0.6	6.4 ± 0.3	4.6 ± 0.2
Entrapped with no excess Ca^{2+}	21.6 ± 1.5	4.9 ± 0.3	4.4 ± 0.3
Entrapped with 50-fold excess Ca^{2+}	29.4 ± 2.6	4.7 ± 0.4	6.3 ± 0.6

a) determined from non-linear curve fitting to equation 24 using SigmaPlot 1.02 for Windows.

b) fitting parameters were as follows: **Holo Solution:** $F_N = 0.996$, $F_U = 0.587$, $m_N = -0.005$, $m_U = 0.042$; **50x excess Ca^{2+} in solution :** $F_N = 0.994$, $F_U = 0.510$, $m_N = 0.028$, $m_U = 0.046$;
Holo in sol-gel matrix: $F_N = 0.987$, $F_U = 0.670$, $m_N = 0.005$, $m_U = -0.005$;
50x excess Ca^{2+} in sol-gel matrix: $F_N = 1.024$, $F_U = 0.706$, $m_N = 0.002$, $m_U = 0.00$

c) this value was obtained by dividing ΔG_{un} by $-m_G$.

Overall, the chemical denaturation results show that the protein is able to undergo substantial conformational changes upon addition of denaturant, confirming that external species could enter the matrix and could cause conformational changes in the protein. The results also provided evidence that both entrapment and elevated levels of Ca^{2+} had a stabilizing effect on the protein. These results, combined with the results obtained from Ca^{2+} binding studies and thermal denaturation studies, indicate that storage of monoliths in an

aqueous buffer solution containing millimolar levels of Ca^{2+} provides excellent resistance against protein denaturation, making sol-gel entrapped parvalbumin a useful candidate for the development of a Ca^{2+} sensor.

3.3.4 Quenching Studies of Entrapped Protein

The solvent accessibility of the Trp within the entrapped protein was examined at various stages of denaturation using both the neutral quencher acrylamide and the negatively charged quencher iodide. Denaturation was done with urea to avoid complications arising from charge-charge interactions between the denaturant and the quencher and/or matrix. The quenching data was analyzed using Equation 18 and the results for solution are shown in Table 3.5. The Stern Volmer quenching constant (K_{SV}) and V values were found to increase as a function of increasing denaturant, as expected. Thus, the Trp residue becomes more solvent exposed as a function of chemical denaturation which correlates to the red shift seen in spectra during chemical denaturation.

The experiments were repeated for C3P entrapped in a sol-gel derived matrix. The Ksv and the V value for native protein in the monolith was found to be higher in both cases using acrylamide as the quencher. The K_{sv} was found to be 3.2 with a V of 1. These values fall between the solution values containing 0-1M GdHCl, indicating that perhaps some of the protein is denatured or that it is not fully holo. This could explain the distribution of environments which exist. If some of the protein is denatured, then it would appear that we do not have a 100% native, accessible fraction which would also indicate that the amount of Ca^{2+} present is greater than a 1.5:1 Ca^{2+}: protein ratio. The increase in K_{sv} may be due to changes in k_q or τ_o.

Table 3.5: Stern-Volmer analysis of acrylamide quenching for native and partially denatured Cod III parvalbumin in solution.

[GdHCl] (M)	K_{SV} (M^{-1})	V (M^{-1})	constant	r^2
0	2.4	0.75	1.00	0.99
0.19	2.7	1.2	0.99	0.96
0.96	3.8	2.4	1.00	0.99
1.28	4.0	2.7	0.96	0.99
1.75	8.8	2.8	1.00	1.00
2.55	10.1	3.3	1.00	1.00
in monolith	3.2	1	0.98	0.98

3.4 Conclusions

It has been shown that Cod III parvalbumin can successfully be encapsulated into a TEOS derived sol-gel matrix with retention of its structure, stability, conformational flexibility and ability to bind Ca^{2+}. The binding and removal of Ca^{2+} was reversible, and could be repeated over multiple cycles. A particularly important finding is that the development of an analytical signal based on a fluorescent allosteric signal transduction mechanism is feasible when using sol-gel entrapped Cod III parvalbumin. However, caution must be exercised with regard to the aging and drying conditions, since longer drying times were found to have deleterious effects on the performance and stability of the entrapped protein. Denaturation studies showed that aging for 20 days followed by storage in a Ca^{2+}-loaded buffer solution was the optimal method for maintaining the entrapped protein in a functional state.

The current detection strategy has two obvious drawbacks in terms of sensor development. The first is the need for UV excitation, which is not conveniently obtained from inexpensive laser sources. The second is the lack of remote sensing capabilities. Both of these issues are addressed in the following chapter.

3.5 References for Chapter 3

1)Braun, S.; Shtelzer, S.; Rappoport, S.; Avnir, D.; Ottolenghi, M. *J. Non-Cryst. Solids* **1992**, *147*, 739.

2)Ellerby, L. M.; Nishida, C. R.; Nishida, F.; Yamanaka, S. A.; Dunn, B.; Selverstone Valentine, J.; Zink, J. I. *Science* **1992**, *255*, 1113.

3)Yamanaka, S. A.; Nishida, F.; Ellerby, L. M.; Nishida, C. R.; Dunn, B.; Valentine, J. S.; Zink, J. I. *Chem. Mater.* **1992**, *4*, 495.

4)Wu, S.; Ellerby, L. M.; Cohan, J. S.; Dunn, B.; El-Sayed, M. A.; Valentine, J. S.; Zink, J. I. *Chem. Mater.* **1993**, *5*, 115.

5)Narang, U.; Prasad, P. N.; Bright, F. V.; Kumar, K.; Kumar, N. D.; Malhotra, B. D.; Kamalasanan, M. N.; Chandra, S. *Chem. Mater.* **1994**, *6*, 1596.

6)Yamanaka, S. A.; Dunn, B.; Valentine, J. S.; Zink, J. I. *J. Am. Chem. Soc.* **1995**, *117*, 9095.

7)Blyth, D. J.; Aylott, J. W.; Richardson, D. J.; Russell, D. A. *Analyst* **1995**, *120*, 2725.

8)Lundgren, J. S.; Bright, F. V. *Anal. Chem.* **1996**, *68*, 3377.

9)Aylott, J. W.; Richardson, D. J.; Russell, D. A. *Analyst* **1997**, *122*, 77.

10)Akbarian, F. L., A.; Dunn, B.; Valentine, J.S.; Zink, J.I. *J. Sol-Gel Sci. Technol.* **1997**, *8*, 1067.

11)Nishida, F.; McKiernan, J. M.; Dunn, B.; Zink, J. I.; Brinker, C. J.; Hurd, A. J. *J. Am. Ceram. Soc.* **1995**, *78*, 1640.

12)Dave, B. C.; Soyez, H.; Miller, J. M.; Dunn, B.; Valentine, J. S.; Zink, J. I. *Chem. Mater.* **1995**, *7*, 1431.

13)Zheng, L.; Reid, W. R.; Brennan, J. D. *Anal. Chem.* **1997**, *69*, 3940.

14)Edmiston, P. L.; Wambolt, C. L.; Smith, M. K.; Saavedra, S. S. *J. Coll. Int. Sci.* **1994**, *163*, 395.

15)Jordan, J. D.; Dunbar, R. A.; Bright, F. V. *Anal. Chem.* **1995**, *67*, 2436.

16)Wambolt, C. L.; Saavedra, S. S. *J. Sol-Gel Sci. Tech.* **1996**, *7*, 53.

17)Shen, C.; Kostic, N. M. *J. Amer. Chem. Soc.* **1997**, *119*, 1304.

18)Heichal-Segal, O.; Rappoport, S.; Braun, S. *Biotechnology* **1995**, *13*, 798.

19)Reetz, M. T.; Zonta, A.; Simpelkamp, J. *Biotechnol. Bioengin.* **1996**, *49*, 527.

20)Miller, J. M.; Dunn, B.; Valentine, J. S.; Zink, J. I. *J. Non-Cryst. Solids* **1996**, *220*, 279.

21)Chen, Z.; Kaplan, D. L.; Yang, K.; Kumar, J.; Marx, K. A.; Tripathy, S. K. *J. Sol-Gel Sci. Technol.* **1996**, *7*, 99.

22)Dave, B. C.; Miller, J. M.; Dunn, B.; Valentine, J. S.; Zink, J. I. *J. Sol-Gel Sci. Technol.* **1997**, *8*, 629.

23)Tatsu, Y.; Yamashita, K.; Yamaguchi, M.; Yamamura, S.; Yamamoto, H.; Yoshikawa, S. *Chem. Lett.* **1992**, *missing*, 1615.

24)Audebert, P.; Demaille, C.; Sanchez, C. *Chem. Mater.* **1993**, *5*, 911.

25)Pankratov, I.; Lev, O. *J. Electroanal. Chem.* **1995**, *393*, 35.

26)Sampath, S.; Lev, O. *Anal. Chem.* **1996**, *68*, 2015.

27)Choche-Guerente, L.; Cosnier, S.; Labbe, P. *Chem. Mater.* **1997**, *9*, 1348.

28)Lev, O.; Wu, Z.; Bharathi, S.; Glezer, V.; Modestov, A.; Gun, J.; Rabinovich, L.; Sampath, S. *Chem. Mater.* **1997**, *9*, 2354.

29)Narang, U.; Prasad, P. N.; Bright, F. V.; Ramanathan, K.; Kumar, N. D.; Malhotra, B. D.; Kamalasanan, M. N.; Chandra, S. *Anal. Chem.* **1994**, 3139-3144.

30)Blair, T. L.; Yang, S. T.; Smith-Palmer, T.; Bachas, L. G. *Anal. Chem.* **1994**, *66*, 300.

31)Marvin, J. S.; Corcoran, E. E.; Hattandadi, N. A.; Zhang, J. V.; Gere, S. A.; Hellinga, H. W. *Proc. Natl. Acad. Sci. U.S.A.* **1997**, *269*, 4266.

32)Marvin, J. S.; Hellinga, H. W. *J. Amer. Chem. Soc.* **1998**, *120*, 7.

33)Shibayama, N.; Saigo, S. *J. Mol. Biol.* **1995**, *251*, 203.

34)Hutnik, C. M. L.; MacManus, J. P.; Szabo, A. G. *Biochemistry* **1990**, *29*, 7318.

35)Hutnik, C. M. L.; MacManus, J. P.; Banville, D.; Szabo, A. G. *J. Biol. Chem.* **1990**, *265*, 11456.

36)Horrocks, W. D., Jr.; Collier, W. E. *J. Am. Chem. Soc.* **1981**, *103*, 2856.

37)Haeich, J.; Klee, C. B.; Demaille, J. G. *Biochemistry* **1981**, *20*, 3890.

38)Haugland, R. P. *Handbook of Fluorescent Probes and Research Chemicals*; 6 ed.; Molecular Probes Inc.: Eugene:, 1996; Vol. Chapter 22.

39)Wang, R.; Narang, U.; Prasad, P. N.; Bright, F. V. *Anal. Chem.* **1993**, *65*, 2671.

40)Zheng, L.; Hogue, C. W. V.; Brennan, J. D. *Biophys. Chem.* **1998**, *71*, 157.

41)Sudhakar, K.; Philips, C. M.; Owen, C. S.; Vanderkooi, J. M. *Biochemistry* **1995**, *34*, 1355.

42)Laberge, M.; Wright, W.; Sudhhkar, K.; Liebman, P. A.; Vanderkooi, J. M. *Biochemistry* **1997**, *36*, 5363.

Chapter 4: Development of a Fiber-Optic Ca^{2+} Sensor based on Fluorescently Labelled Cod III Parvalbumin

4.1 Introduction

Cod III parvalbumin (C3P) is a particularly useful biomolecule for the development of a biosensor for detection of Ca^{2+}, as demonstrated in Chapter 3. The protein is able to give distinctive fluorescence signals in the presence and absence of Ca^{2+}, with no interference from Mg^{2+}, even at a 5000-fold excess. In addition, sufficient conformational motion remained to do Ca^{2+} sensing when C3P was encapsulated in a sol-gel derived matrix. Given such exceptional characteristics, this protein is ideal for investigation of further sensing applications.

Sol-gel processed monoliths containing C3P provided a matrix that was amenable to Ca^{2+} detection utilizing Trp fluorescence. However, obstacles such as slow diffusion of analytes into the matrix, the potential for photobleaching using UV excitation, the lack of inexpensive UV excitation sources, and the changes in K_d values with drying/aging time diminish the applicability of sensors based on this format. To overcome these barriers it is necessary to label the protein with a probe that can be excited in the visible region, and entrap the labelled protein in thin sol-gel derived films with retention of structure, stability and conformational motions.

The single sulfhydryl group in C3P (Cys-18) can be labelled with a fluorescent probe, which can be excited in the visible region. Ideally, the probe used to label the protein should show large changes in quantum yield or maximum wavelength emission for small changes in environment, as occurs with conformational change of C3P upon binding Ca^{2+}. The probe should also be small and uncharged to avoid probe interference with conformational changes.

Given these constraints, appropriate probes for labelling of C3P are iodoacetoxy-nitrobenzoxadiazole (IANBD) and acrylodan (Ac). The structures of these probes are shown in Figure 4.1.

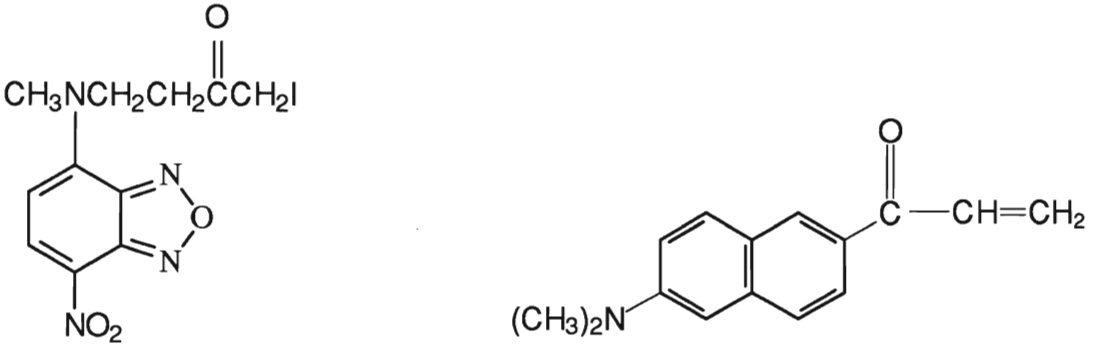

Figure 4.1 Structure of IANBD and Acrylodan

NBD was chosen since it can be excited at 442 nm with a He-Cd laser or at 460 nm using an inexpensive blue light emitting diode (LED) source. This probe is very sensitive to changes in local polarity[1] as well as local concentration. NBD labelled proteins have also been used to examine protein conformational changes based on changes in energy transfer,[2] or on binding of glucose[3] or maltose.[4] In the present work, Cod III parvalbumin was labelled with NBD in order to monitor the conformational changes of the protein by directly exciting NBD instead of Trp to determine whether a Ca^{2+} dependent FAST mechanism[3,4] was obtained. Acrylodan was also used to label Cod III parvalbumin. This probe was chosen for these studies because it is sensitive to the local environmental dipolarity. This probe has the advantage that it will selectively bind the free sulfhydryl group, in the case of C3P, resulting in one probe per protein. The acrylodan probe has also been used previously by others to study the structure and dynamics of proteins (HSA-Ac),[5-8] and to examine FAST processes in glucose binding proteins.[3]

Currently work is being performed in our research group to find optimal dipcasting protocols for entrapment of biomolecules into thin films. The work in this chapter is the preliminary work required for the characterization of the labelled proteins, which will be used in future studies involving thin films. The preliminary work done in this chapter involved the investigation of the stability and Ca^{2+} binding behavior of both free and encapsulated C3P-NBD and free C3P-Ac. These studies were done both in a standard spectrofluorimeter and at the end of an optical fiber via distal end sensing. The main questions addressed in this chapter are; Is it possible to label the Cys-18 on Cod III parvalbumin with the probes chosen? Does the label effect the stability of the protein or the ability of the protein to bind Ca^{2+}? Can the probes, when directly excited, monitor the conformational changes induced upon binding Ca^{2+}? Can the in-house fiber optic system be used to excite the label in order to obtain useful information (ie. Ca^{2+} binding curves, unfolding curves), thereby allowing extensions to thin films studies? These questions need to be addressed before the proteins can be analyzed in thin films.

4.2 Experimental

4.2.1 Chemicals

The chemicals used were the same as those listed in Chapter 3, except for 6-acryloyl-2-(dimethylamino)naphthalene (acrylodan, Ac) and iodoacetoxynitrobenzoxadiazole (IANBD) which were obtained from Molecular Probes (Eugene, OR). Ethylenebis(oxyethlyenenitrilo)]-tetraacetic acid (EGTA) was purchased from Fisher Scientific (New Jersey). All other chemicals were of analytical grade and were used as received.

4.2.2. Instrumentation-- Optical Fiber based Fluorimeter

A schematic of the fiber optic laser system is shown in Figure 4.2. The excitation source was a Liconix 4200 NB He-Cd laser operating at 28.5 mW CW output at 441.6 nm. The laser light was passed through a 441.6 nm interference filter (3nm FWHM) to eliminate extraneous plasma discharge. The light was then passed through a 1.5 O.D. neutral density filter to reduce intensity followed by passage through the rear of an UV-enhanced perforated mirror. The excitation light was then passed through a fused silica lens (50 mm diameter, 50 mm focal length) and focused into a fused silica optical fiber (400μm core, 100μm cladding, 0.4 μm numerical aperture (NA), Fiberguide Industries SPC-400/500R) which was located on a X-Y-Z micrometer controlled translation stage. The light was passed through the optical fiber, exciting the fluorescent sample located at the distal tip of the fiber. Fluorescence emission originating at the end of the fiber was captured by the fiber and the fluorescence exiting the fiber was collimated by passage through the fused silica lens to produce a spot of ~1cm diameter which was reflected from the front side of the UV enhanced mirror through a 475 nm long pass filter. The spot was then focused onto the entrance slit of the monochromator using a second lens (60 mm focal length and 30 mm diameter), which produced a spot of 1.2 mm in diameter on the entrance slit. Emission spectra were obtained using a Sciencetech 9010 Monochromator (F/3.5, 200 mm focal length, 4 nm/mm dispersion) coupled to a Sciencetech photomultiplier tube (R928 tube in PMM-02 analog housing) normally operated at 950 V. The manufacturer supplied the monochromator and PMT control software (SciSpec version 2.0 for Windows).

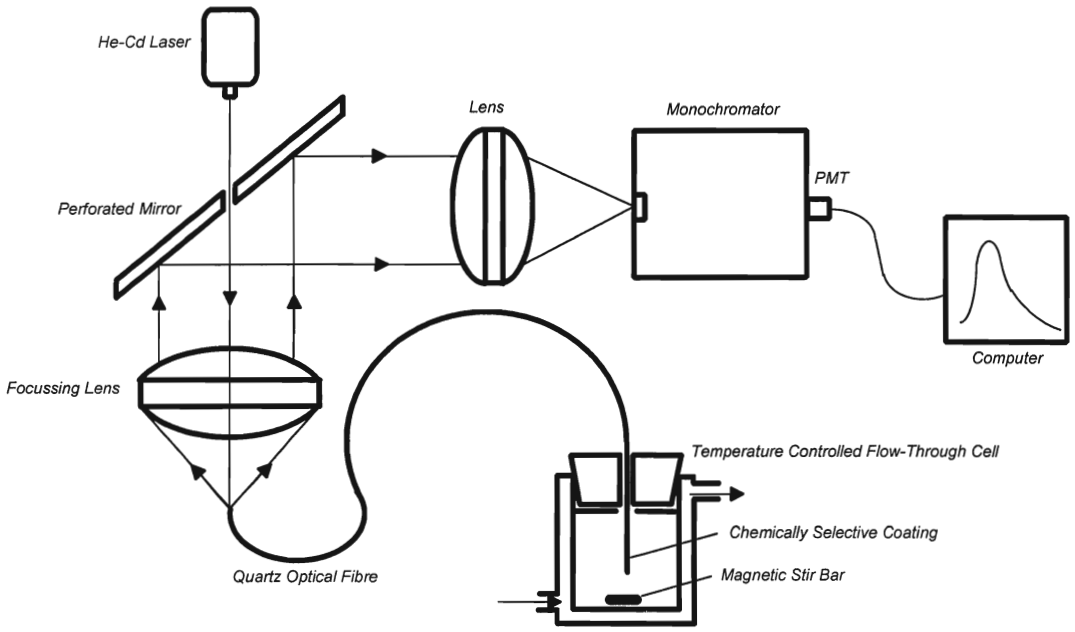

Figure 4.2 Schematic of the Fiber Optic System

4.3 Procedures

4.3.1 Labelling of Cod III Parvalbumin

Cod III parvalbumin was extracted and purified as described in chapter 3. In order to label this protein, it first must be made apo by the addition of EGTA, since the sulfhydryl group is more exposed in the apo state relative to the holo state.[9] Ac and NBD were added at 3 times molar excess with respect to the protein and let stir overnight at 4°C. The protein solution was then dialyzed against PIPES buffer with at least 2 exchanges every 12 hours. The labelled protein was then purified using a G-25 Sephadex column to dislodge any unreacted label.

NBD does not absorb at 280 nm, where the Trp absorbs, thus its labelling efficiency was found by comparing the relative absorbance of NBD (ε_{max}= 23000 $M^{-1}\cdot cm^{-1}$ at 472 nm) and C3P (ε_{max}= 7180 $M^{-1}\cdot cm^{-1}$ at 280 nm). The calculation of efficiency was more difficult for C3P-Ac since Ac absorbs at 280 nm as well as 370 nm. The concentration of labelled protein in this case was found using ε_{278} = 8700 $M^{-1}cm^{-1}$ and ε_{365} = 12800 $M^{-1}cm^{-1}$ for acrylodan [10] and ε_{280} = 7180 $M^{-1}cm^{-1}$ for C3P.

4.3.2 Stability Studies (Thermal Denaturation)

Thermal denaturation studies were carried out as described in Chapter 3 using excitation at 285 nm for monitoring Trp fluorescence. For C3P-NBD, the protein was excited at 442 nm with emission collected from 480 nm to 650 nm. C3P-Ac was excited at 360 nm with emission collected from 400 nm to 600 nm. For both C3P-Ac and C3P-NBD, the entire spectrum was integrated and the intensity was plotted against temperature to generate unfolding curves. All curves were analyzed as described in Chapter 3.

4.3.3 Entrapment and Aging

C3P-NBD was entrapped in its apo state using the protocol described in chapter 3. The monoliths containing the entrapped protein were aged in air at 4°C for 16 days before experimentation.

For entrapment of C3P-NBD to the end of the fiber, the labelled protein (1.5 μM in 10 mM PIPES, 100 mM KCl, pH 7.2) and hydrolyzed TEOS solutions were mixed in a 1:1 volumetric ratio in an eppendorf tube to give a total volume of 50μl. The end of the optical fiber was set into the mixture and the matrix was left to dry around the distal tip for 12 hours. The tip was then rehydrated by placement in a 100% humidity environment for 30 hours. The entrapped protein matrix was taken out of the eppendorf tube and the sample had dried into the shape of a drop at the end of the fiber (about 1 mm total width). Prior to experimentation, the sample was slowly immersed into 100μl of a PIPES buffer solution for 2 hours to fully rehydrate. This solution was used to test for leaching of the protein by monitoring for NBD emission from the solution after removal of the optical fiber.

4.3.4 Detection of Ca^{2+}

In solution work, the labelled proteins were simply made holo by adding excess Ca^{2+} in order to determine whether or not they were functional. Fluorescence scans were collected as described above for thermal denaturation studies, both before and after the addition of Ca^{2+}.

For optical fiber based studies of the labelled proteins in solution, the fiber was placed into 100μl of the protein solution which was in a small volume quartz cuvette. For entrapped C3P-NBD, all testing of samples was done in air after soaking in Ca^{2+}-loaded or Ca^{2+}-free

PIPES buffer solutions for approximately 3 minutes, and then leaving the sample in air for a few minutes prior to testing. Photobleaching was first tested by recording the decrease in intensity at the emission maximum over a period of 120-200s. Fluorescence spectra were then collected before and after the addition of excess Ca^{2+} using a 110 ms dwell time, at 900-950 V and with a time constant of 100 ms and a gain of 100x. All spectra had appropriate blanks subtracted, but were not corrected for monochromator throughput or PMT response. Intensity values were corrected for photobleaching if the percentage of bleaching was greater than the PMT noise.

4.4 Results and Discussion

4.4.1 Efficiency of Labelling of Cod III parvalbumin

In order to label this protein it was first necessary to make it apo via EGTA addition. Unfortunately, the labelling efficiency did not exceed 40% regardless of which of the two probes was used. The efficiency of labelling was 20%±1% for C3P-NBD and 40%±2% for C3P-Ac, for the samples used in experimentation. The low labelling efficiency may be due to inability to make all of the protein apo or perhaps due to inefficiency of the reaction. For this reason, all of the stability studies done used direct excitation of the probe and not the Trp residue, since a large proportion of unlabelled protein was present. The absorbance spectra of labelled proteins are shown in Figure 4.3.

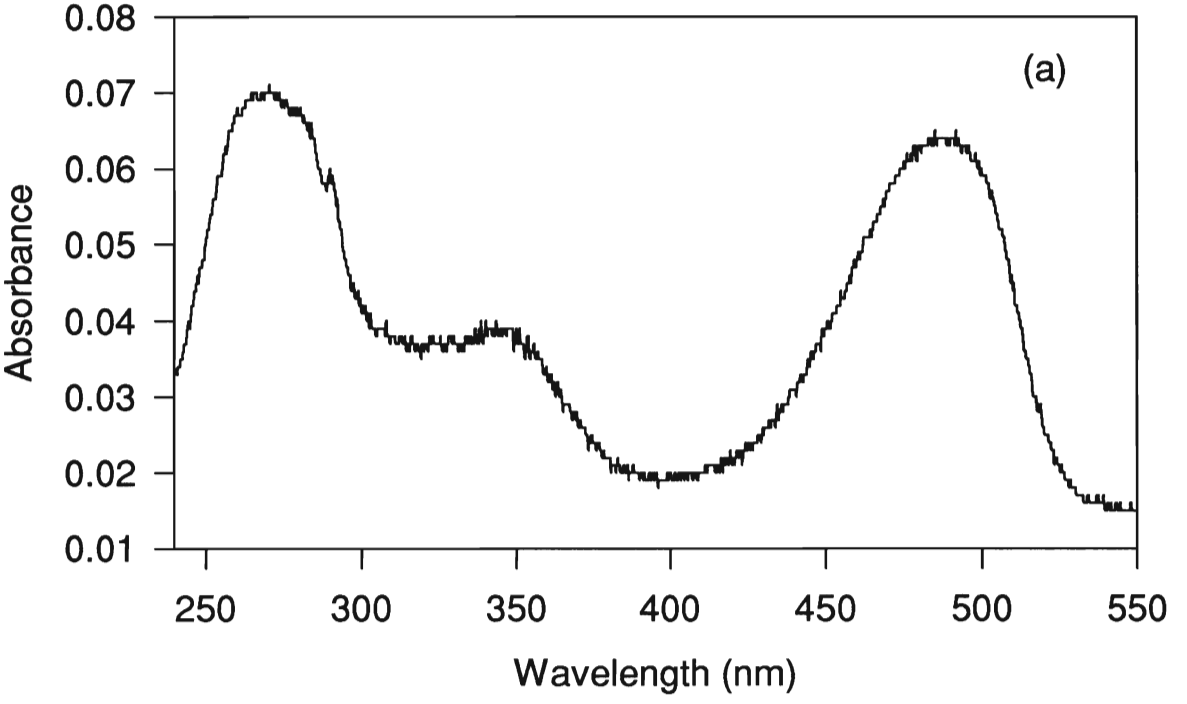

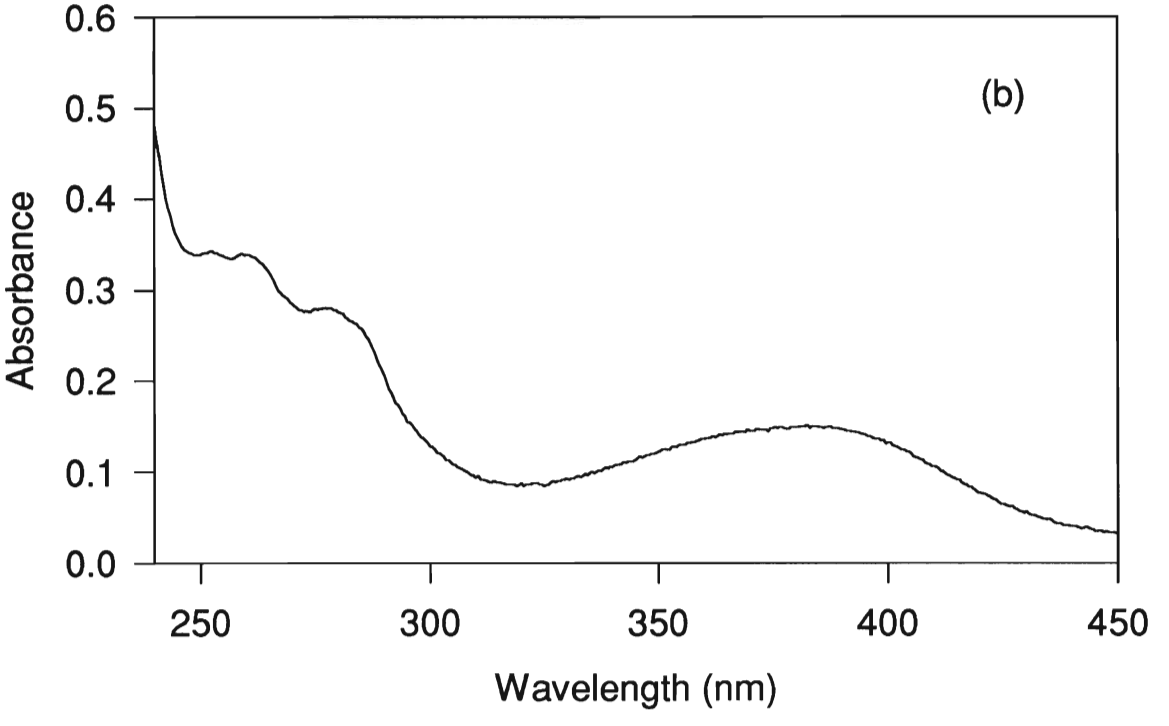

Figure 4.3 UV-absorbance spectra of (a) C3P-NBD and (b) C3P-Ac.

4.4.2 Detection of Ca^{2+}

It was important to determine whether the labelled proteins could bind Ca^{2+} and undergo a conformational change, which could alter the fluorescence signal from the label. Figure 4.4a shows the fluorimetric response obtained by adding Ca^{2+} to C3P-Ac, with excitation at 285 nm. As Ca^{2+} is added, the Trp signal blue shifts to 315 nm and increases in intensity, as expected. However, the change in Trp emission intensity was much smaller than for unlabelled C3P (see Figure 3.1). Thus, the Ac-labelled protein was not able to undergo its full Ca^{2+} induced conformational change, suggesting that the probe sterically restricted the complete refolding of the holo protein. The Ac signal, excited at 285 nm, decreases in intensity by 20%.

Figure 4.4b shows the emission of the Ac moiety in the apo and holo protein with direct excitation at 442 nm. Direct excitation also results in roughly 15% decrease in emission intensity upon Ca^{2+} addition. However, the Ac residue also undergoes a slight red-shift in its emission wavelength upon binding of Ca^{2+}. The decrease in intensity, coupled with the red-shift in λ_{max}, indicate that the Ac moiety becomes more solvent exposed as a result of the Ca^{2+}-induced conformational change. Unfortunately, the small magnitude of the intensity change makes C3P-Ac a poor candidate for further development into a Ca^{2+} sensor.

Binding of Ca^{2+} to C3P-NBD was also investigated, as shown in Figures 4.5a and b. In Figure 4.5a, the emission spectra of the holo and apo C3P-NBD were collected using excitation at 285 nm. In this case, the Trp residue increases in intensity and the label decreases in intensity. The intensity change for the Trp residue is the same for labelled and unlabelled protein in this case, a 2.3-fold increase. This indicates that the protein is able to refold completely in the presence of NBD. It is important to remember that 80% of the

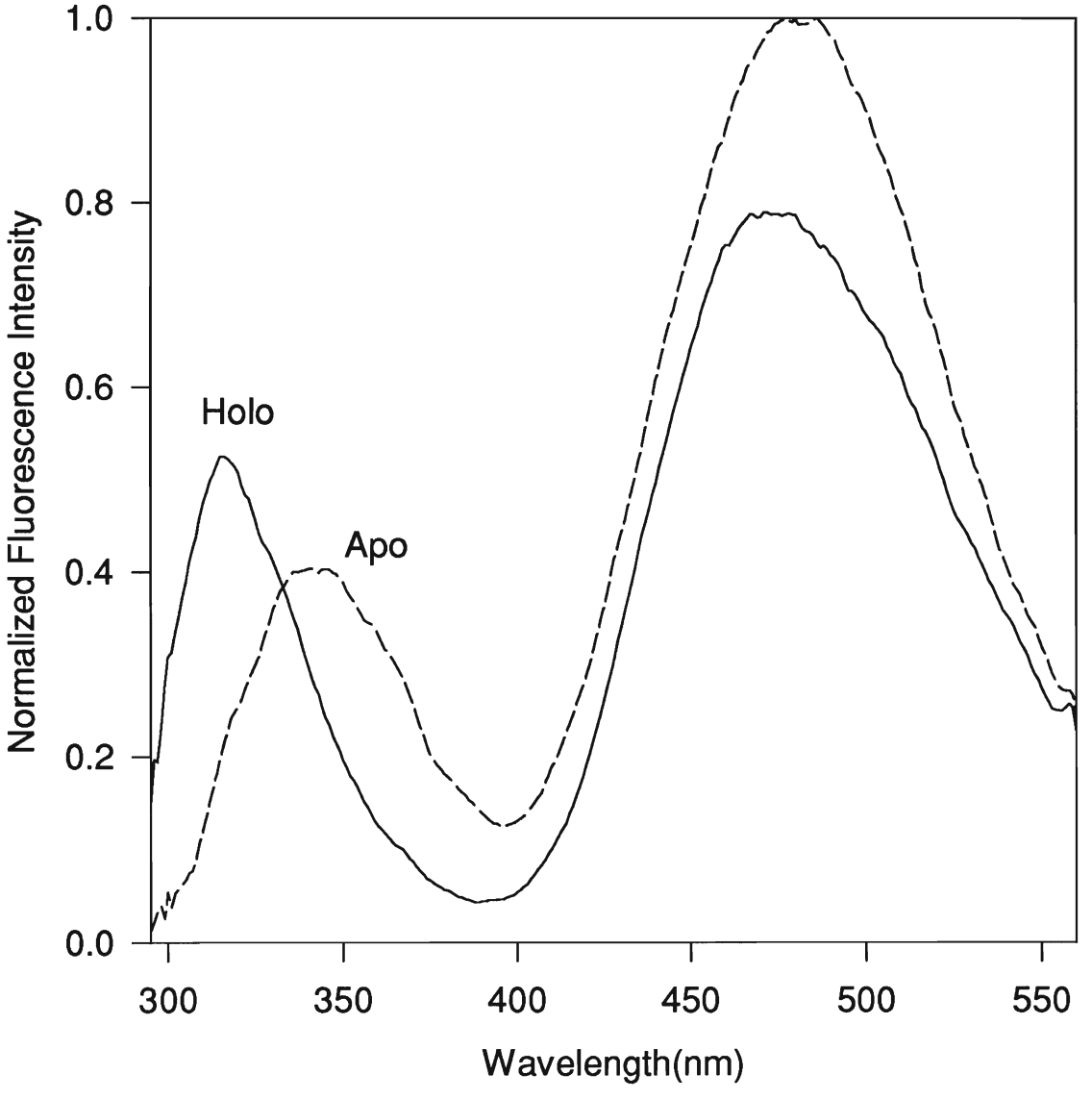

Figure 4.4a Monitoring changes in Trp intensity during Ca^{2+} addition to C3P-Ac, via excitation at 285 nm.

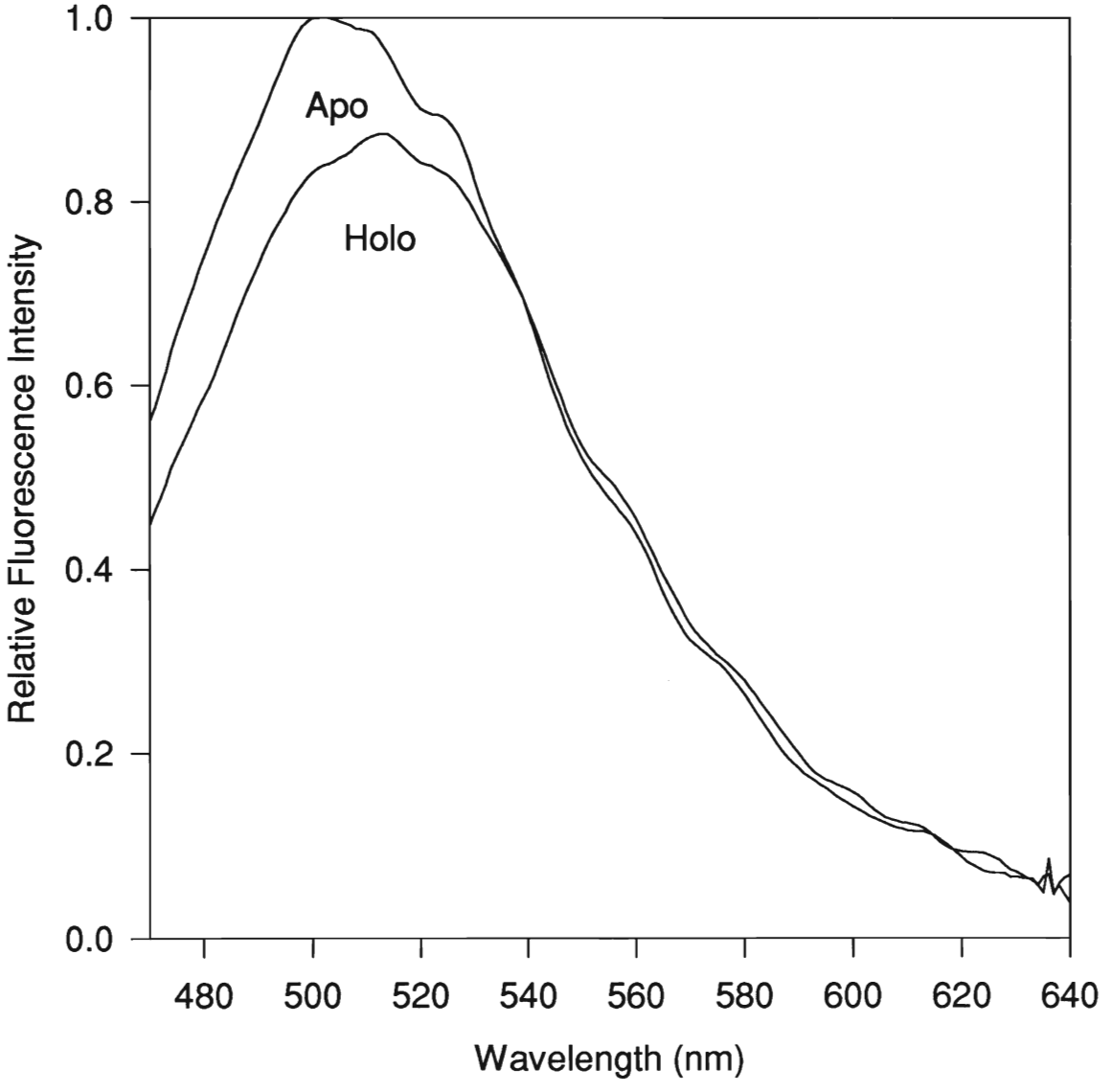

Figure 4.4b Monitoring of Ca^{2+} addition to C3P-Ac, via excitation at 442 nm.

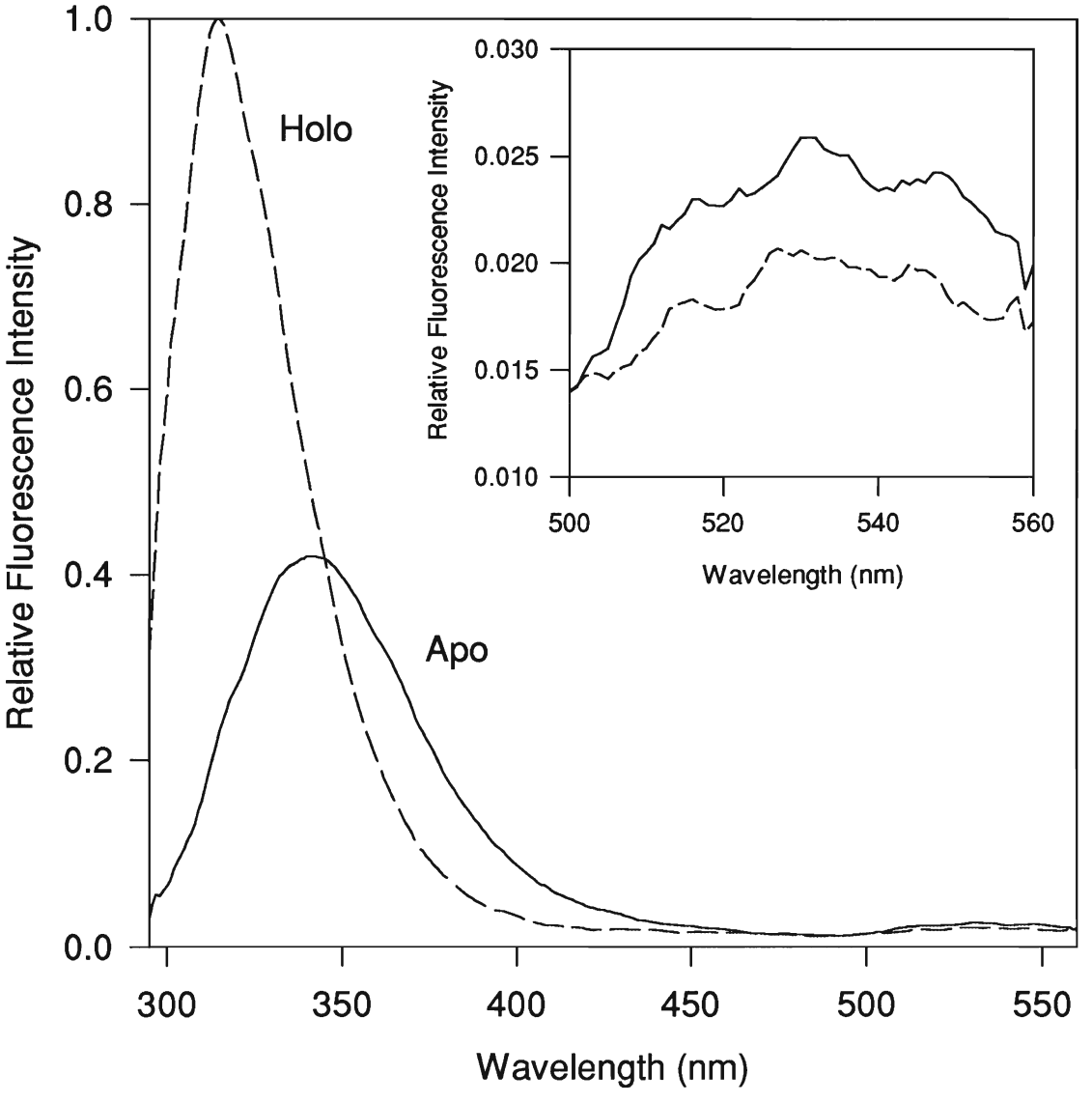

Figure 4.5a Monitoring changes in Trp intensity during Ca^{2+} addition to C3P-NBD, via excitation at 285 nm.

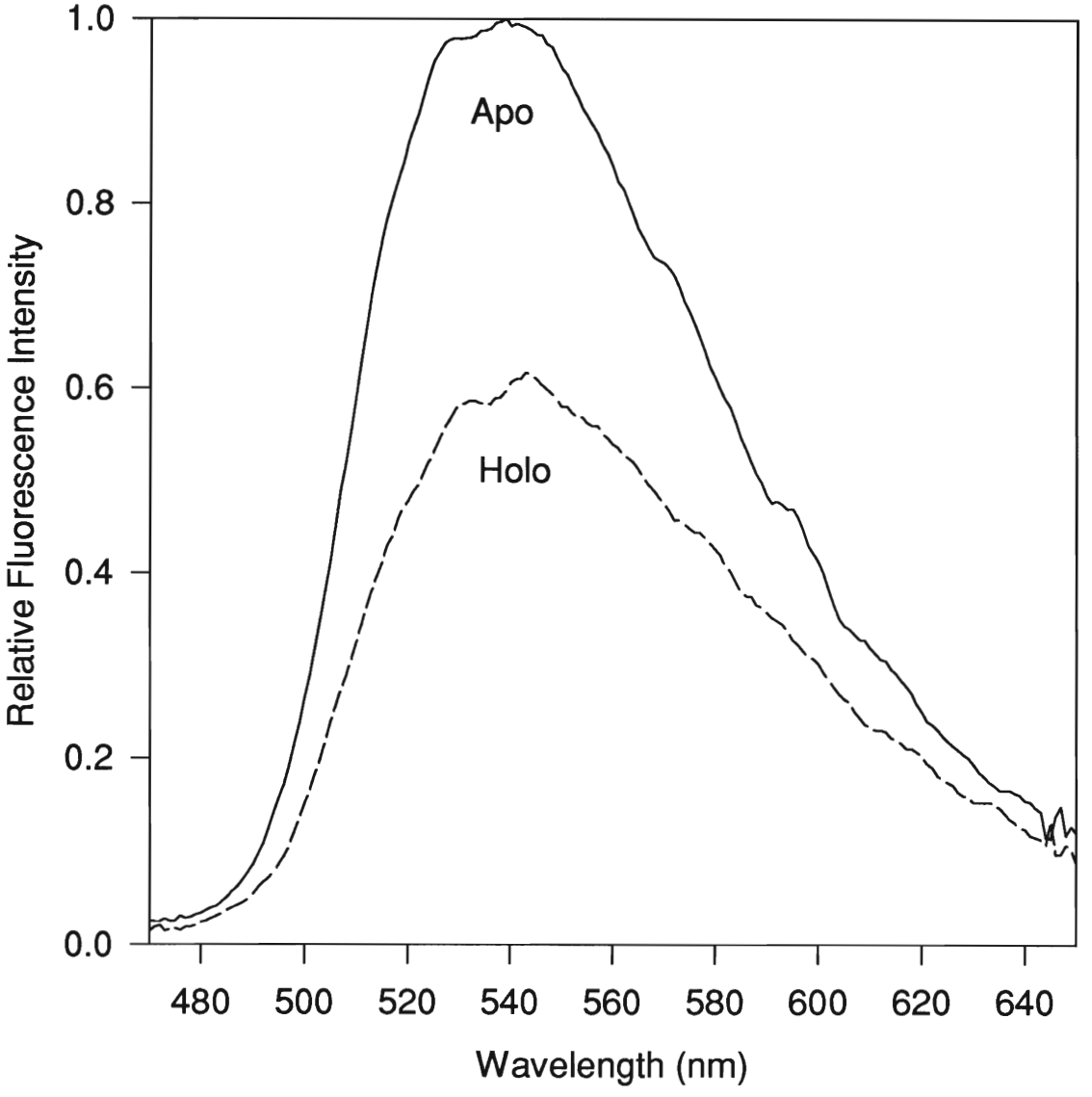

Figure 4.5b Monitoring of Ca^{2+} addition to C3P-NBD, via excitation at 442 nm.

protein is unlabelled, thus the Trp signal will be mostly influenced by the unlabelled protein. However, since the Trp residue was able to fully recover in intensity, it shows that the NBD label does not interfere with the refolding of the protein. This is in contrast with the much smaller increase in Trp intensity for C3P-Ac (1.3-fold) even though 60% of the protein was unlabelled. Thus, NBD does not interfere with the refolding of the protein.

The probes chosen for labelling Cys-18 were not as efficient as Trp at monitoring the conformational changes which occur for binding Ca^{2+} in solution. This may be due to a smaller overall change in the local environment in the region of the Cys-18. Unfortunately, no other mutants are available with the Cys residue in different locations to test this hypothesis, or to improve the fluorescence response

C3P-NBD proved to be the better protein system for monitoring the binding of Ca^{2+}. The fact that a change in intensity of 40% occurs upon Ca^{2+} binding, via excitation at 442 nm, is a crucial criterion for sensor development. Direct excitation of the label is able to detect the conformational change taking place upon binding. This is very important, as now this model system can be used to develop a Ca^{2+} sensor with the fiber optic system. The large change in intensity should allow for slight changes in concentrations of Ca^{2+} to be detected. Based on these results, all fiber optic work was done with C3P-NBD.

4.4.3 Thermal Stability Studies of Labelled Cod III Parvalbumin

In order to investigate the stability of the labelled proteins, thermal denaturation experiments were done on C3P-Ac and C3P-NBD to see whether or not the probes could monitor the denaturation of the protein, and to see whether the probes effect stability.

Figure 4.6 (solid circles) shows the thermal denaturation of C3P-NBD excited at 442

nm. The unfolding curve is sigmoidal and occurs as a one step unfolding. This shows that the thermal denaturation of Cod III parvalbumin can be monitored through excitation of the labelled moiety and thus can be monitored using the fiber optic laser system. The intensity of the label decreased 90% in the holo state. The emission spectra did not shift in wavelength with unfolding, consistent with its location in a solvent exposed region. The post transition region did not come to a linear baseline, therefore thermodynamic parameters could not be obtained. However, a T_{un} value of about 70°C can be estimated from the unfolding curve, which is consistent with the value obtained for unlabelled Cod III parvalbumin with excess Ca^{2+}.

C3P-NBD was also encapsulated within a sol-gel derived matrix to examine the effects of entrapment on the unfolding curve. Figure 4.6 (solid squares) shows the unfolding curve generated for the entrapped protein during thermal denaturation. In this case the intensity only dropped a fraction of what it did in solution, 30% for the entrapped protein versus 90% for the free protein. The basis for the smaller change in intensity is not known. However, one reason for this could be a decrease in thermally induced quenching for the entrapped protein due to fewer solvent collisions. A second possibility is that the addition of Ca^{2+} prior to thermal denaturation may have resulted in a conformational change which caused quenching of the folded protein (~ 40%). A final possibility is incomplete unfolding, however this is unlikely when the results for unlabelled C3P are considered.

Figure 4.7a shows thermal denaturation of C3P-Ac in solution, excited at 360 nm. Figure 4.7b shows the thermal denaturation of the same sample obtained by examining the Trp fluorescence with by excitation at 285 nm. It can be seen in both figures that the protein starts to unfold immediately, showing an apparent two-stage unfolding profile with T_{un} values

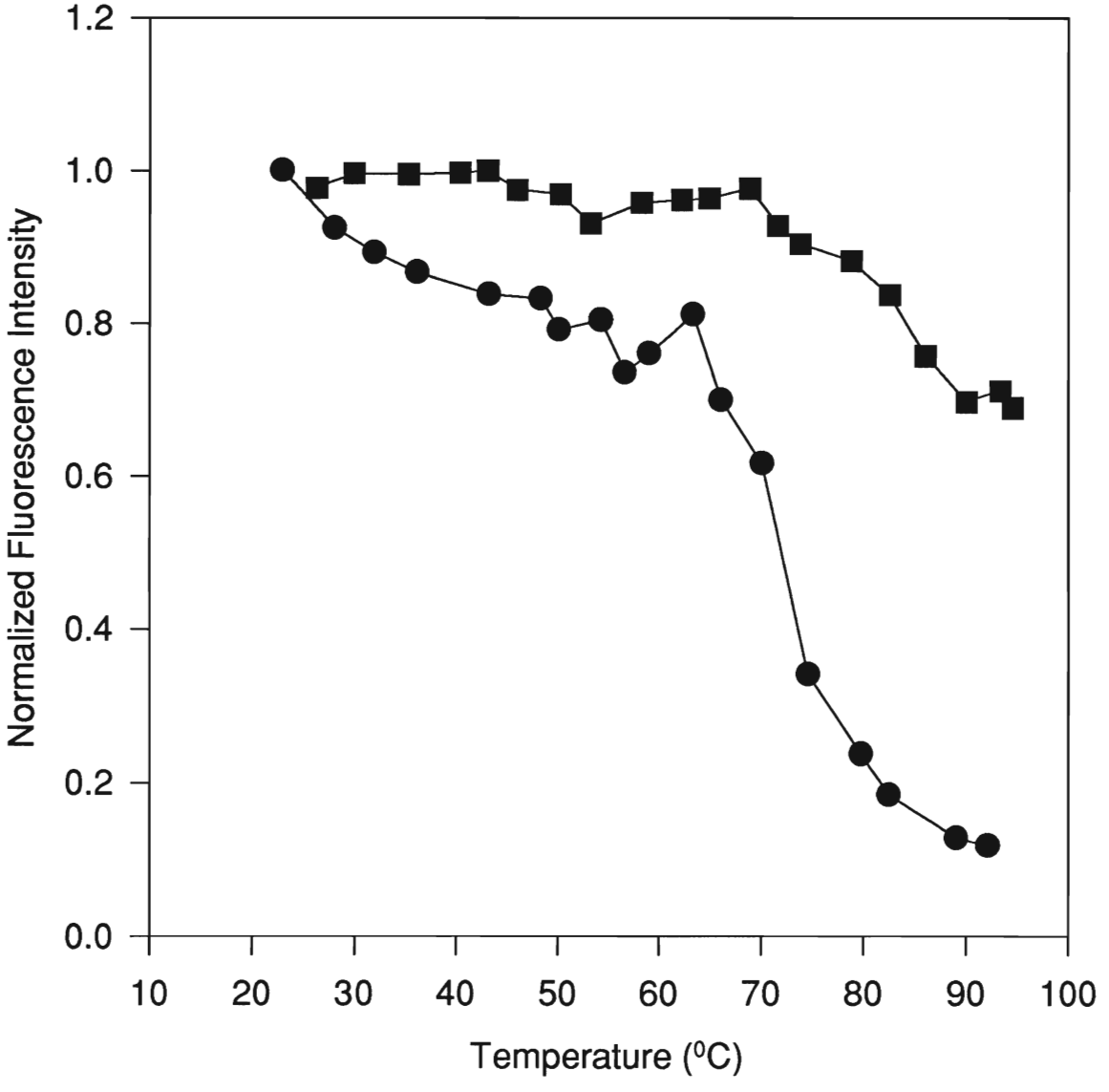

Figure 4.6 Unfolding Curve of free (●) and entrapped (■) C3P-NBD during thermal denaturation, excited at 442 nm.

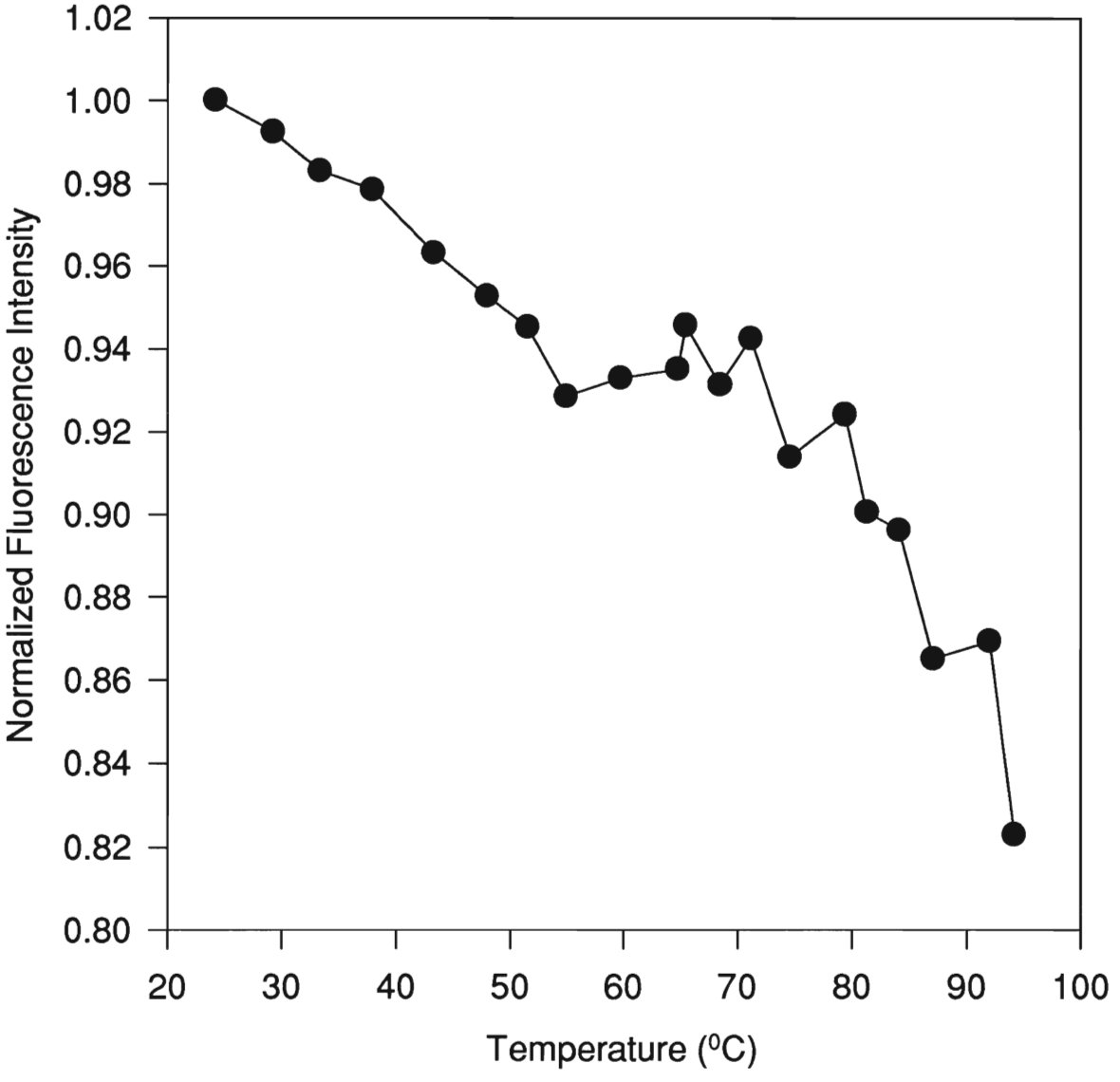

Figure 4.7a Unfolding profile of C3P-Ac during thermal denaturation, excited at 360 nm.

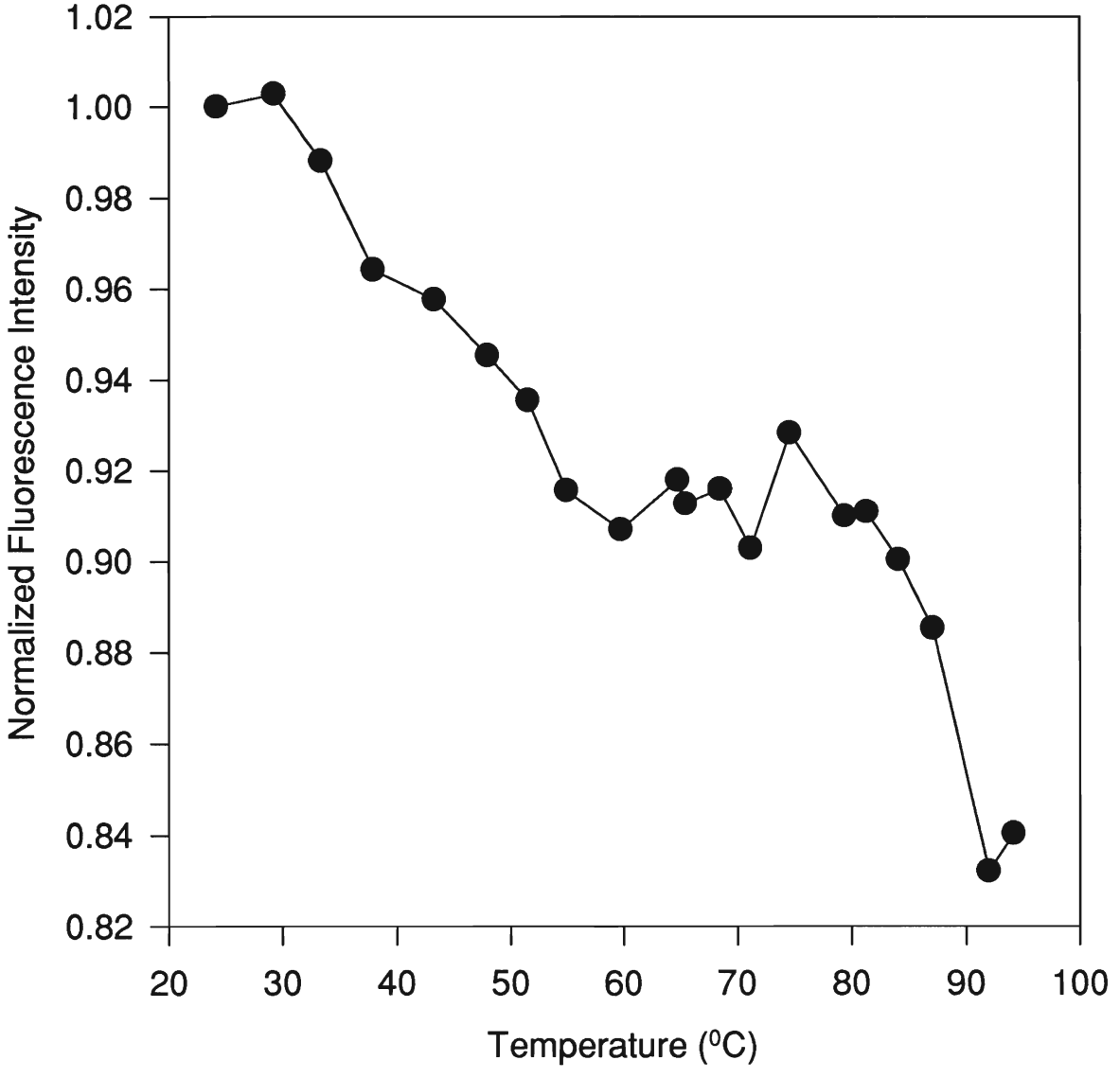

Figure 4.7b Unfolding profile of Trp in C3P-AC from thermal denaturation, excited at 285 nm.

of approximately 40°C and 80°C. There are two possibilities; (1) the protein begins to unfold immediately and what is seen beyond 75°C is photobleaching taking place or (2) a fraction of the protein was not completely folded to begin with (the labelled portion) and that is what is seen unfolding immediately followed by the unfolding of the unlabelled C3P, which follows since it is folded and thus more stable. The latter explanation seems more plausible when exciation is done at 295 nm, since the binding efficiency was calculated to be 40%. This means that 60% native C3P still exists in the sample. In Figure 4.7a with the direct excitation of Ac, only the labelled portion is detected, hence the transition after 75°C may be due to the presence of a distribution of environments. It is also possible that there exists two independent conformational changes at Cys-18, or that we are seeing the unfolding of holo vs. apo or apo vs. unfolded or holo vs. unfolded in the two stages. This experiment again proved that all of the protein is not folded completely and that the stability of the protein decreases upon labelling with Ac. This again indicates that Ac is not an appropriate probe for labelling C3P.

4.4.4 Fiber Optic Sensing with Free C3P-NBD

Given the superior characteristics of C3P-NBD as compared to C3P-Ac, the NBD labelled protein was chosen for preliminary testing of fiber optic Ca^{2+} sensing. One anticipated problem with the use of laser excitation was photobleaching of the protein. Figure 4.8 shows that photobleaching was indeed a problem, with the intensity decreasing by 7% over 200 seconds. This experiment was done with a 1.0 O.D. neutral density filter, which was capable of blocking out 90% of the laser light. A similar degree of photobleaching was obtained for C3P-Ac (5% over 120 seconds). Spectral acquisition parameters were chosen

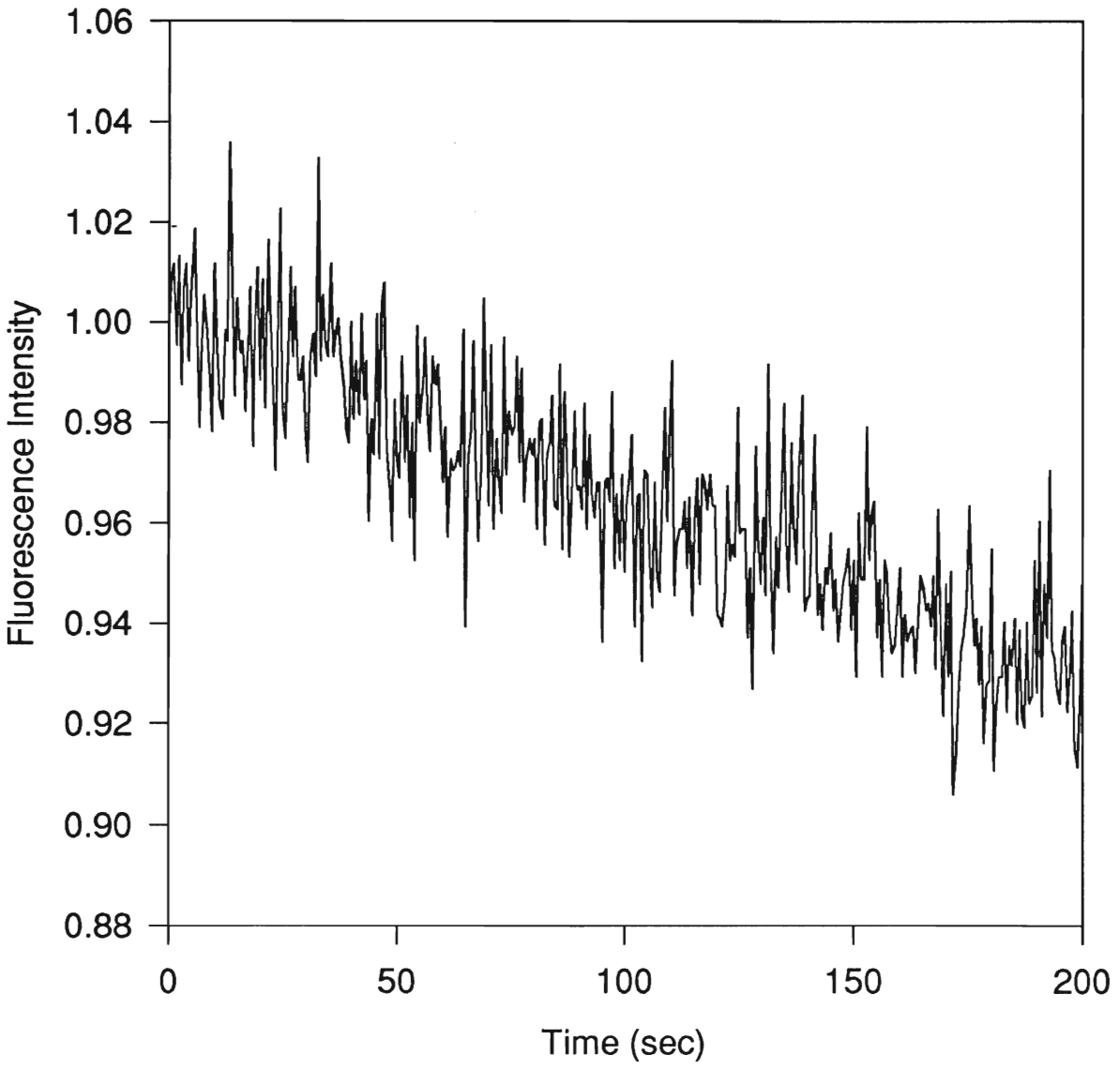

Figure 4.8 Photobleaching of 0.5 μM C3P-NBD at the end of the optical fiber with a 1.0 OD neutral density filter.

to allow a spectrum to be collected under 15 seconds, and 1.5 O.D. neutral density filters were used to minimize this problem.

Figure 4.9 shows the comparison of the NBD spectrum of entrapped C3P-NBD, excited at 442 nm, obtained on the SLM 8100 fluorimeter (corrected and uncorrected) and the fiber optic system (uncorrected only). It can be seen that the spectrum obtained on the fiber optic system resembles the uncorrected spectrum obtained on the SLM fluorimeter, but shows a narrower spectral FWHM in comparison to the corrected spectrum. These spectra may allow the output of the fiber optic fluorimeter to be corrected by comparison to the corrected output of the SLM fluorimeter.

Ca^{2+} sensing was also done with the fiber optic system using both labelled proteins, excited at 442 nm. The results obtained with the SLM fluorimeter were reproducible with the fiber optic system. For C3P-NBD, the intensity dropped 50% upon Ca^{2+} binding, as shown in Figure 4.10, using laser excitation through the optical fiber, in comparison to 40% using the SLM. The additional loss is likely due to photobleaching. For C3P-Ac the intensity dropped 20% when measured through the optical fiber (Figure 4.11), which is similar to the value obtained with the SLM. These results again indicated that C3P-NBD was the better probe for sensing Ca^{2+} when entrapped in a sol-gel derived matrix.

4.4.5 Fiber Optic Sensing with Entrapped C3P-NBD

Preliminary Ca^{2+} sensing was also done at the distal end of an optical fiber, using entrapped C3P-NBD, and gave promising results. The entrapped protein was first tested for leaching by monitoring the fluorescence from the buffer in which the bioglass had been rehydrated. The results showed that no leaching had occurred over a period of several hours.

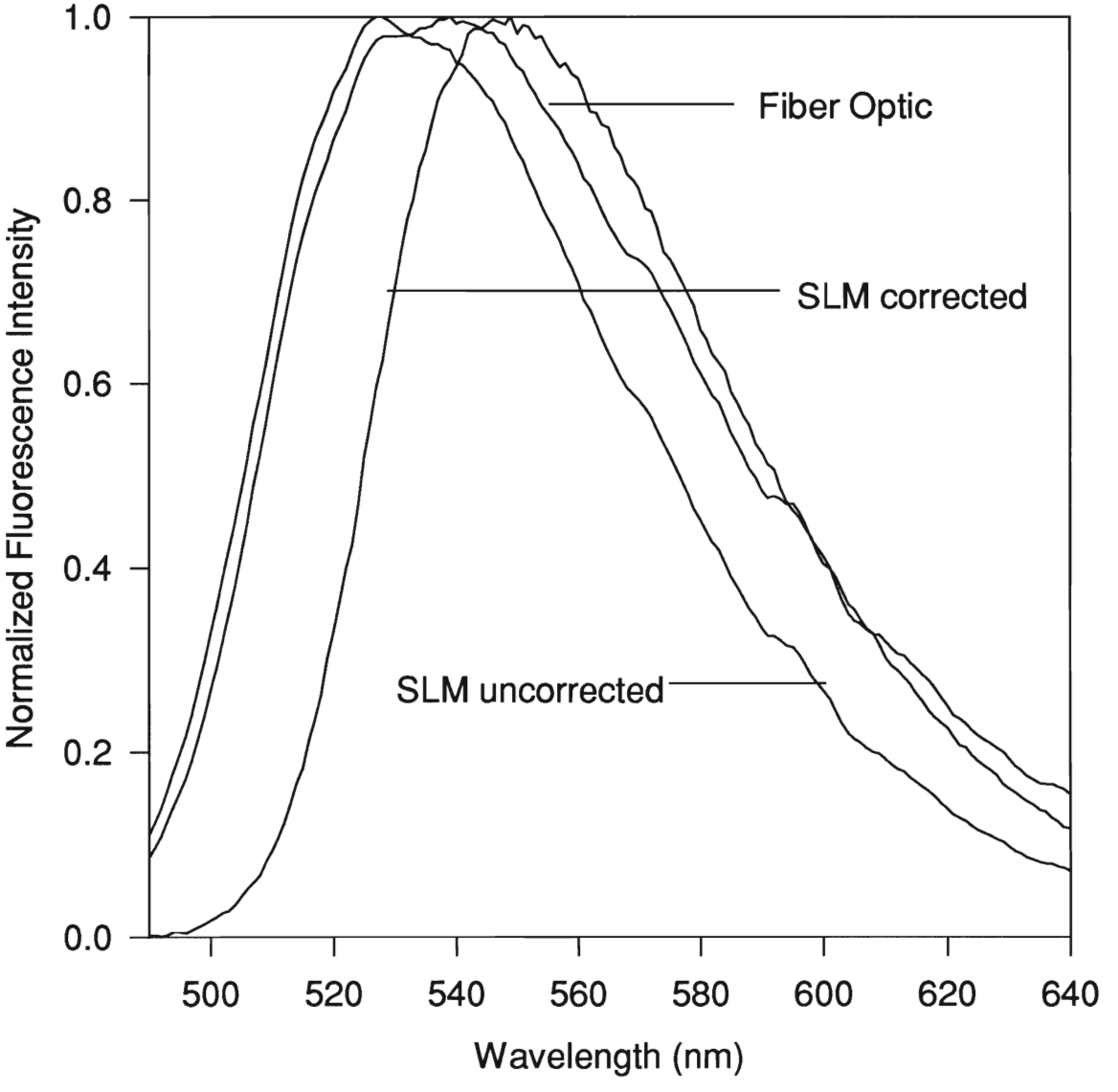

Figure 4.9 Comparison of spectra of C3P-NBD collected on the SLM-8100 and the fiber optic system.

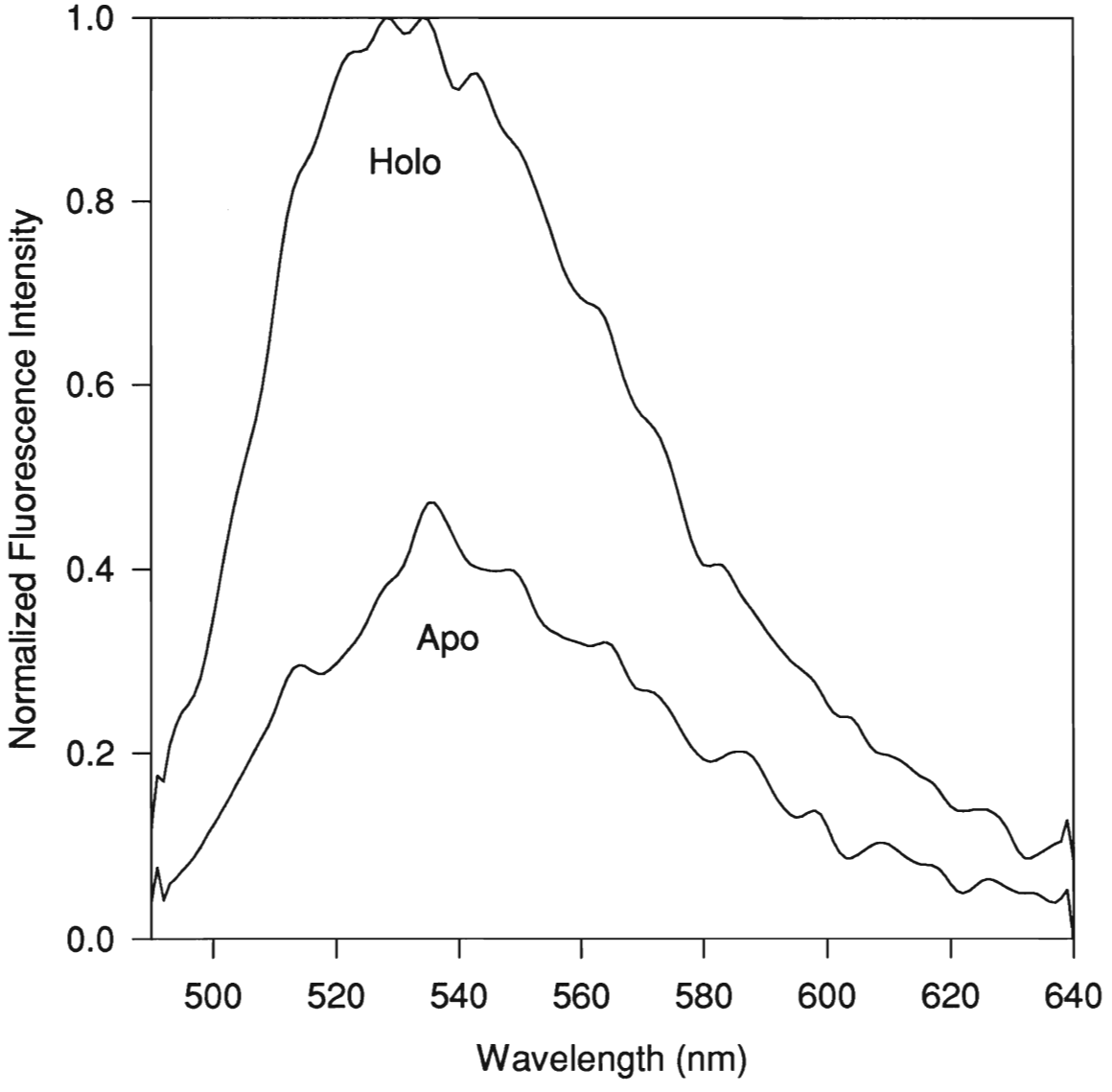

Figure 4.10 Monitoring of Ca^{2+} binding to free C3P-NBD, by 442 nm excitation on the fiber optic system.

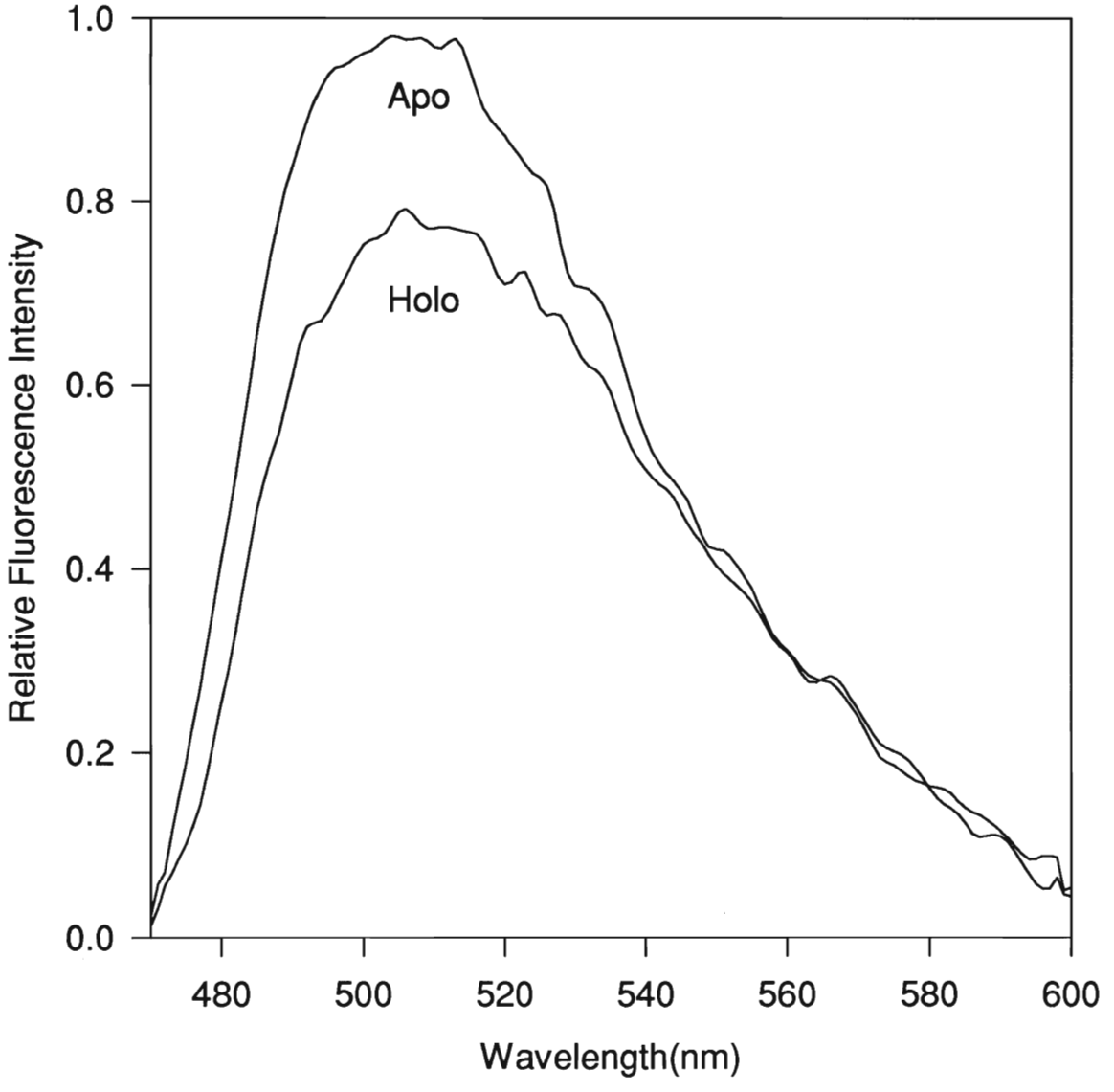

Figure 4.11 Monitoring of Ca^{2+} to free C3P-Ac, by 442 nm excitation on the fiber optic system.

Figure 4.12 shows the photobleaching which occurred for the entrapped protein when excited with the 442 nm line of the He-Cd laser (using a 1.5 OD neutral density filter), in both the apo and holo forms. This figure shows that the photobleaching is slightly greater for the protein in the apo form. The photobleaching was 1% per minute for the protein in the holo form in contrast to 7% per minute for the protein in the apo form.

Figure 4.13 showed the Ca^{2+} binding response of the entrapped protein, corrected for photobleaching. Unexpectedly, there was a 80% decrease in intensity upon immersion into a solution containing 50μM Ca^{2+}. This decrease was considerably larger than the value obtained in solution (50%), and was much larger than the response obtained for unlabelled C3P in glass monoliths. The larger change in intensity may be due to the Cys-18 residue being in an environment that causes more quenching, relative to the free form. The enhanced sensitivity as compared to the unlabelled protein in silicate monolith may be due to either the much shorter aging time for the entrapped C3P-NBD, or the smaller amount of the silicate with respect to the volume of the Ca^{2+} solution, which may reduce diffusional problems. The large intensity change on binding of Ca^{2+} makes this an excellent system for detecting Ca^{2+}.

Based on experiments where the fiber tip was rapidly dipped and removed from Ca^{2+} solutions, it was determined that the diffusion of the Ca^{2+} into the matrix was relatively rapid, but that the time required for the protein to undergo its conformational change was much longer (~ 5 minutes). Figure 4.14 shows the intensity change with time for Ca^{2+} binding to the entrapped protein. Figure 4.15 shows the increase in the signal which was obtained over time after each washing step of holo protein in Ca^{2+}-free buffer. Both figures clearly indicate response times on the order of minutes. This relatively slow response time may be overcome by encapsulating C3P-NBD into thin (<1 μm) sol-gel derived films.

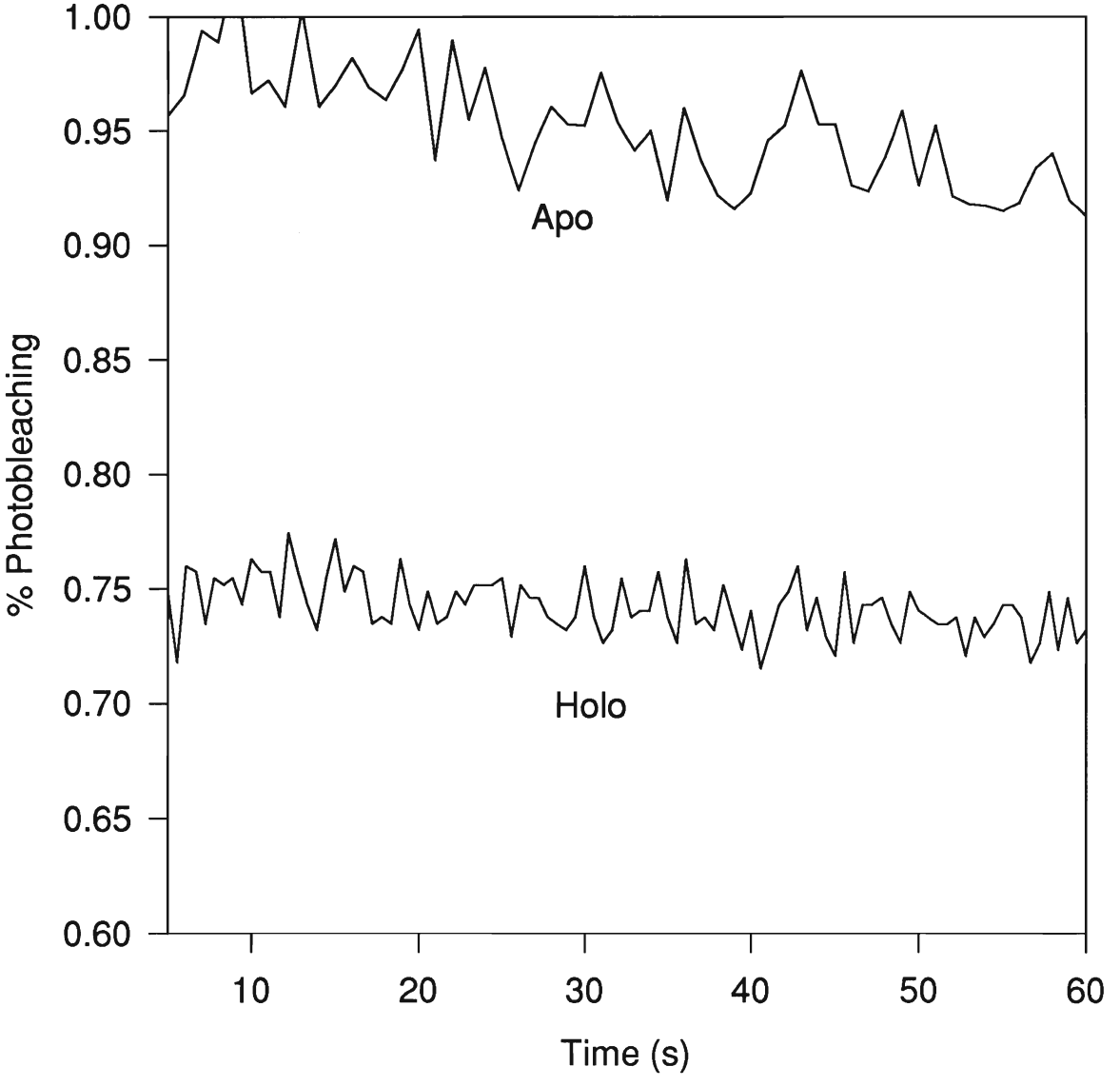

Figure 4.12 Photobleaching encountered for entrapped C3P-NBD at the end of the optical fiber.

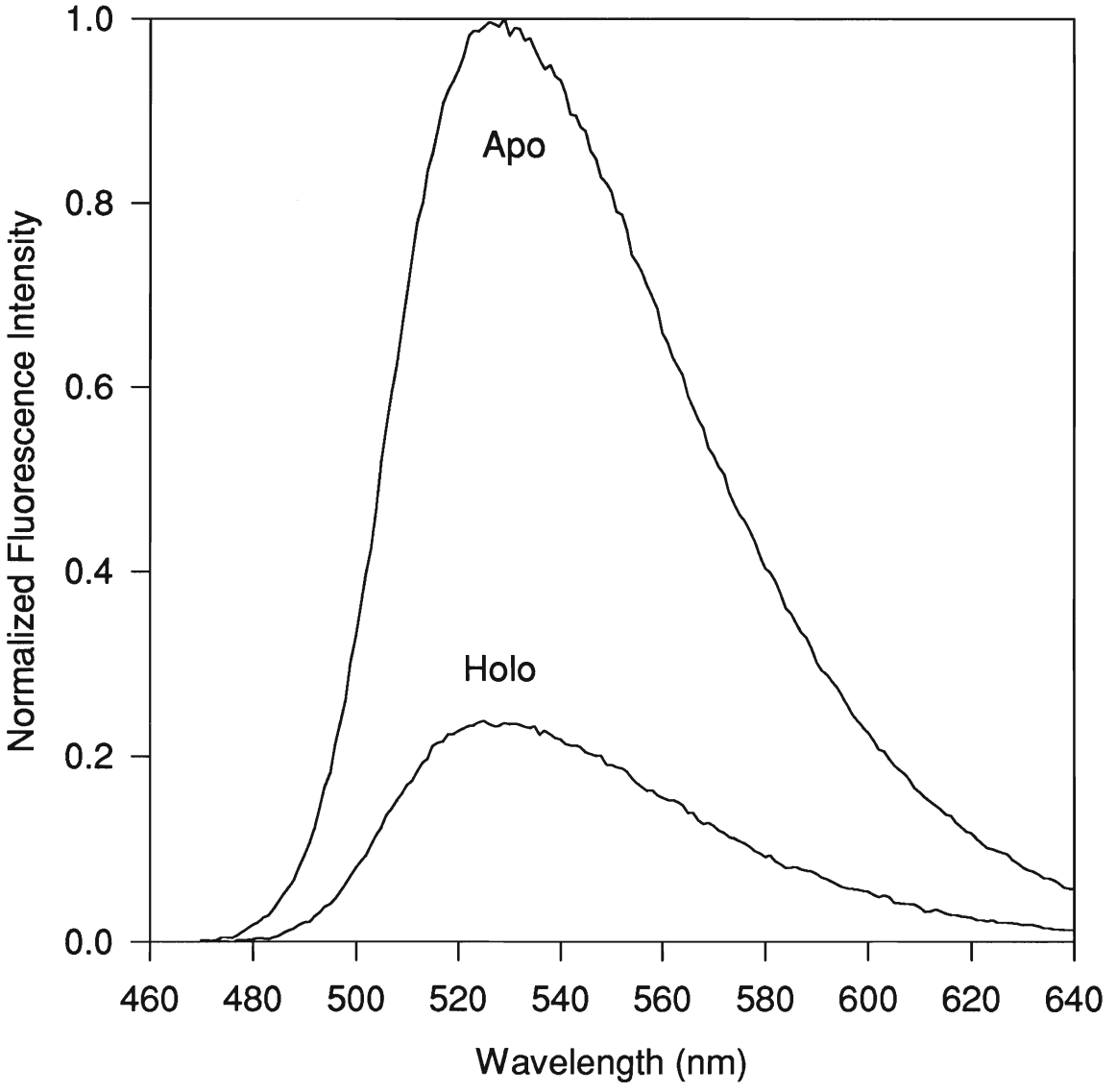

Figure 4.13 Ca^{2+} detection by entrapped C3P-NBD via excitation at 442 nm, at the end of the optical fiber.

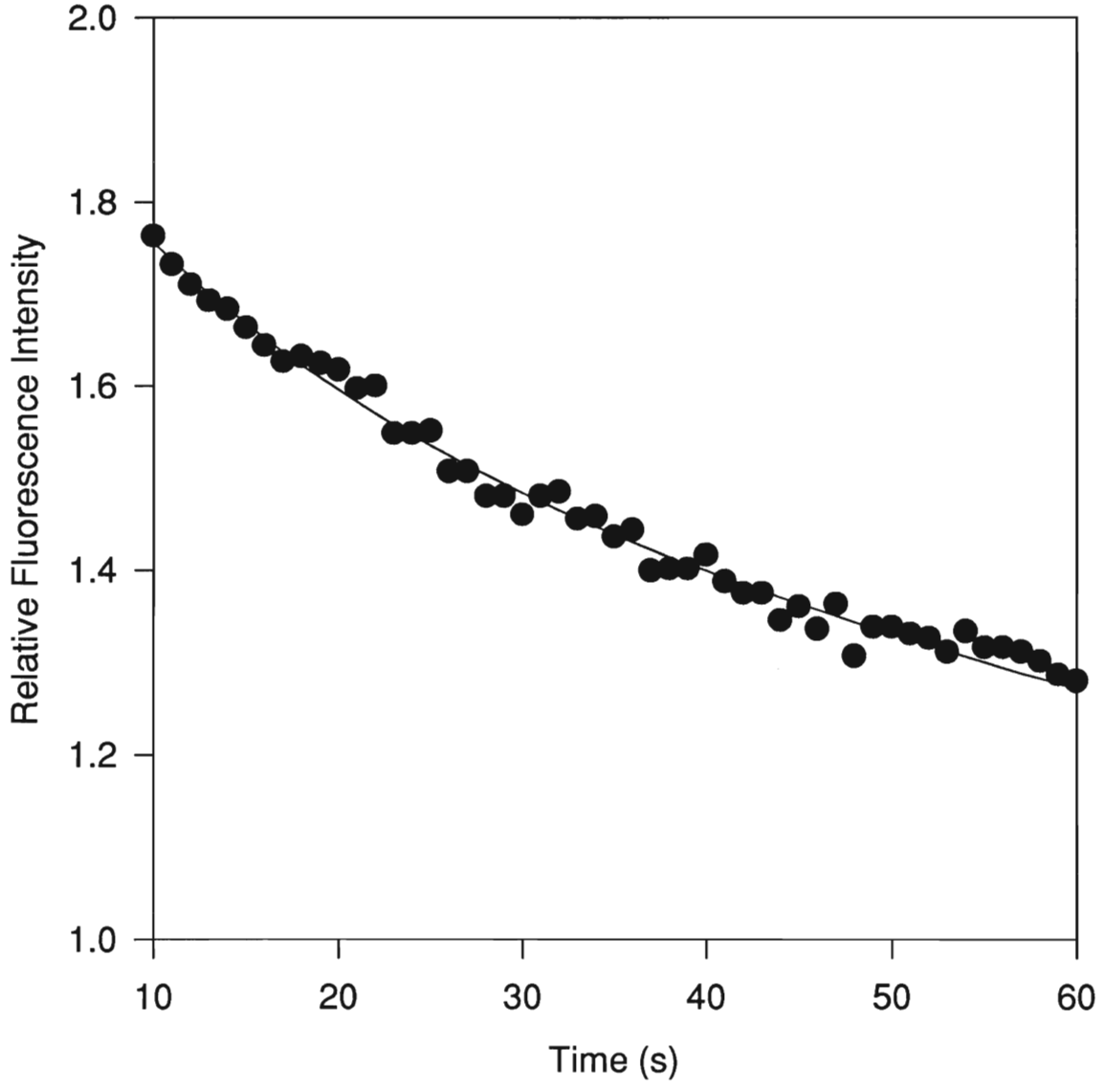

Figure 4.14 Kinetics of Ca^{2+} binding to the entrapped C3P-NBD, via excitation at 442 nm with the fiber optic system.

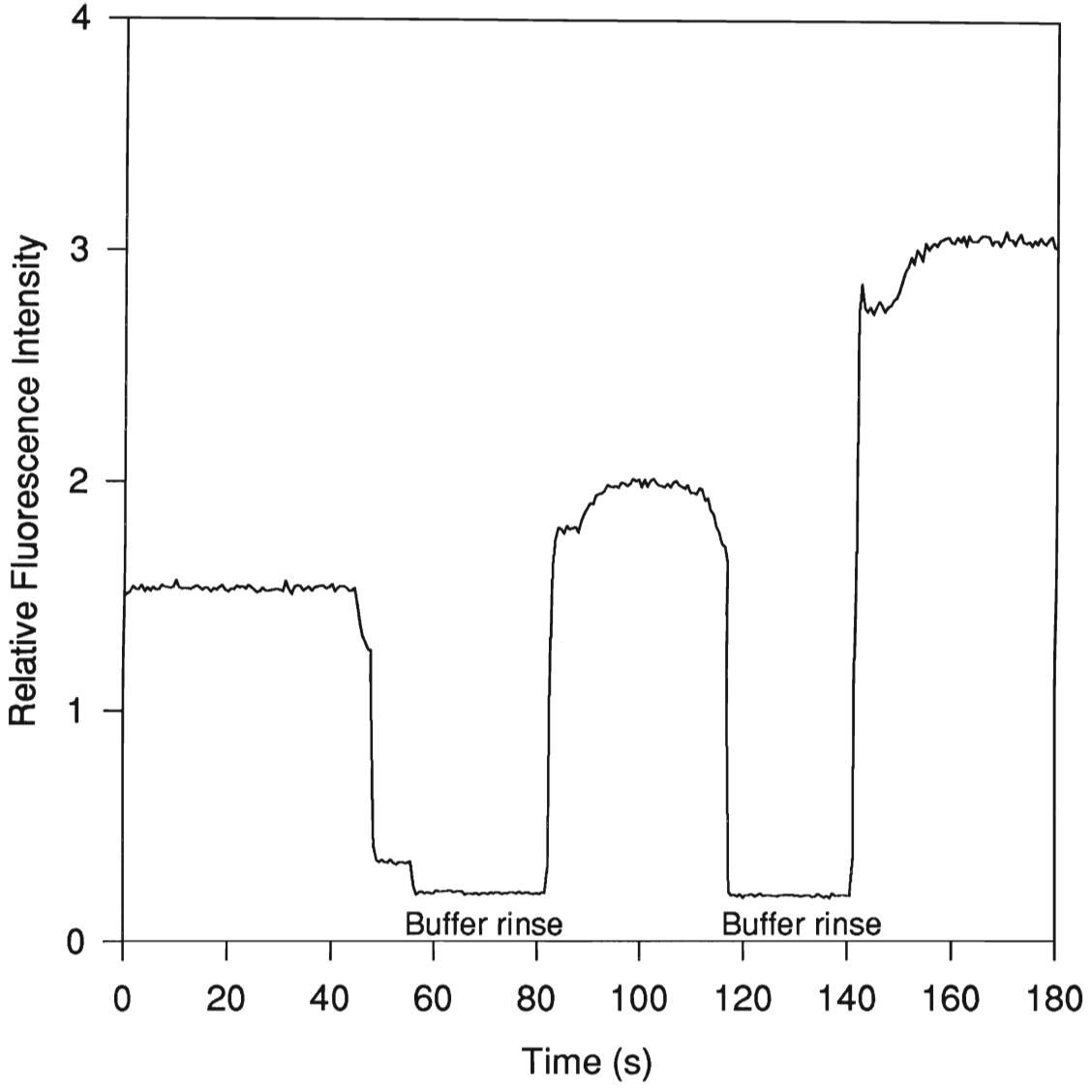

Figure 4.15 Monitoring of the signal obtained for entrapped, holo C3P-NBD after subsequent washing steps, with laser excitation at 442 nm using the fiber optic system.

The fiber-optic Ca^{2+} sensor was tested for reversibility and reproducibility by moving the fiber between a 50 μM Ca^{2+} solution and a Ca^{2+}-free solution. The results are shown in Figure 4.16. Initial testing indicated that the sensor was reversible, and that the signal obtained were reasonably reproducible if care was taken to allow equilibration to occur, and if photobleaching was accounted for. It must be noted that these were preliminary tests, and that further work is required to characterize the behaviour of this model system.

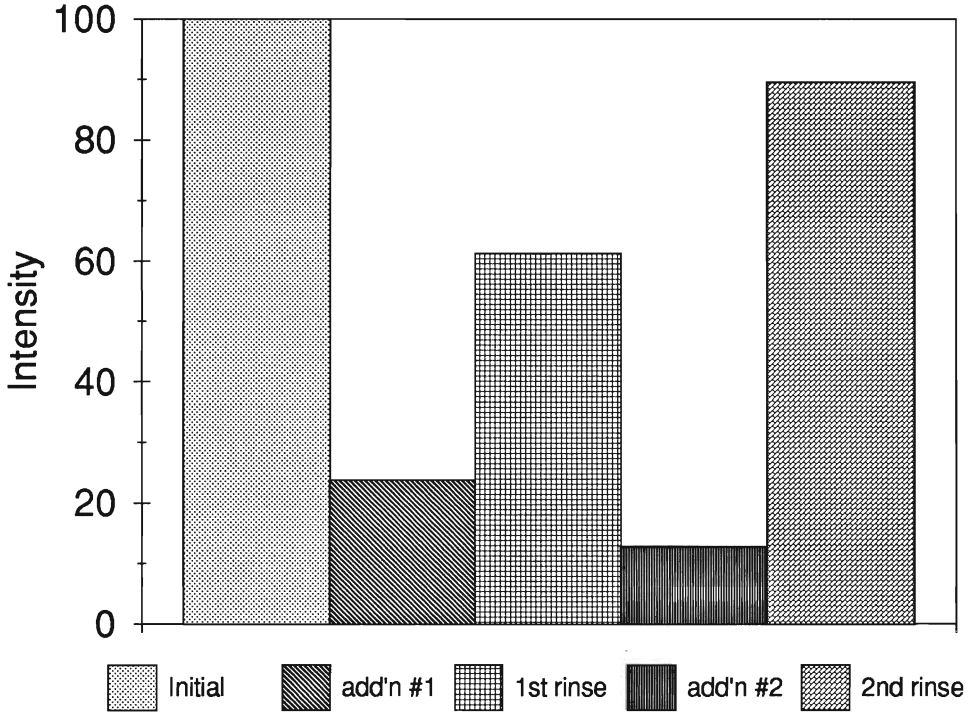

Figure 4.16 Monitoring of the signal obtained for C3P-NBD entrapped on the end of an optical fiber on cycling through Ca^{2+}-loaded and Ca^{2+}-free buffer solutions.

4.5 Conclusions

In this chapter, Cod III parvalbumin was labelled with NBD and Ac and the Ca^{2+} binding ability and thermal stability of the labelled proteins was examined. It was discovered that Ac was likely too large to allow the protein to completely undergo its conformational change upon binding of Ca^{2+}. C3P-NBD, on the other hand, was able to undergo the full conformational change that occurs upon Ca^{2+} binding. Thermal denaturation results confirmed that the NBD-labelled C3P provided less of a deleterious change in the protein structure-function relationships, compared to C3P-Ac. Thus NBD is the better probe to choose for extension of this work to thin films and fiber optic sensing.

Preliminary studies of free and entrapped C3P-NBD as a Ca^{2+} selective binding protein using the fiber optic laser system showed the feasibility of the FAST process for fluorescently labelled proteins. Difficulties with photobleaching were encountered, and need to be addressed, and the detection system needs to be optimized in future studies. However, it was shown that C3P-NBD entrapped into sol-gel derived matrix on the end of a fiber is capable of reversibly sensing Ca^{2+} with good sensitivity, and a LOD of less than 5 μM (based on sensitivity and S/N levels). Future studies will address the use of thin sol-gel derived films for entrapment of C3P-NBD, and the use of pulsed excitation sources, such as an N_2 laser, to diminish photobleaching.

4.6 References for Chapter 4

1)Chattopadhyay, A. *Chemistry and Physics of Lipids* **1990**, *53*, 1.

2)Geldwerth, D.; al., e. *Biochimica et Biophysica Acta* **1991**, *1082*, 255.

3)Marvin, J. S.; Hellinga, H. W. *J. Amer. Chem. Soc.* **1998**, *120*, 7.

4)Marvin, J. S.; Corcoran, E. E.; Hattandadi, N. A.; Zhang, J. V.; Gere, S. A.; Hellinga, H. W. *Proc. Natl. Acad. Sci. U.S.A.* **1997**, *269*, 4266.

5)Lundgren, J. S.; Heitz, M. P.; Bright, F. V. *Anal. Chem.* **1995**, *67*, 3775.

6)Prendergast, F. G.; Meyer, M.; Carlson, G. L.; Iida, S.; Potter, J. D. *J. Biol. Chem.* **1983**, *258*, 7541.

7)Ilich, P.; Prendergast, F. G. *J. Phys. Chem.* **1989**, *93*, 4441.

8)Yem, A. W.; Epps, D. E.; Matthews, W. R.; Guido, D. M.; Richard, K. A.; Staite, N. D.; M.R. Deibel, J. *J. Biol. Chem.* **1992**, *267*, 3122.

9)Permyakov, E. A.; Kalinichenko, L. P.; Derezhkov, V. Y.; Antalik, M.; Meinholtz, D. C.; Berliner., L. J. *Biophysical Chemistry* **1992**, *42*, 189.

10)Edmiston, P. L.; Wambolt, C. L.; Smith, M. K.; Saavedra, S. S. *J. Coll. Int. Sci.* **1994**, *163*, 395.

Chapter 5: Unfolding of Acrylodan Labeled Human Serum Albumin Probed by Steady-State and Time-Resolved Fluorescence Methods

5.1 Introduction

All of the work described up to this point has involved a small Ca^{2+} binding protein (Cod III parvalbumin). Fluorescence studies indicated tht the protein retained its structure, stability, function and conformational flexibility while entrapped in a sol-gel matrix. The remainder of this thesis will address the effects of encapsulation on the behaviour of human serum albumin (HSA), which is representative of larger proteins with more complex tertiary structures. Prior to investigation of encapsulated HSA, studies must be conducted to throughly characterize and understand the structure, stability and function of the protein in solution.

HSA is a large protein which is formed from a single polypeptide chain of 585 residues. [1] The structure is divided into 3 major domains, and contains a total of 17 disulfide bonds. [2] Despite the size and complexity of HSA, there is only a single Trp residue within the protein at position 214 in domain II. [1] In addition, the protein contains only one free Cys residue at position 34 in domain I. [2] The presence of the free thiol allows for site-specific labelling of the protein with chromophoric or fluorescent probes. [3-9]

HSA is the most abundant human blood protein and has the ability to bind several ligands, including small aromatic and heterocyclic carboxylic acids such as the non-steroidal anti-inflammatory drugs (NSAIDs). [10] The ability of HSA to bind multiple ligands combined with the size and complexity of the protein structure (which is in some ways reminiscent of enzymes and antibodies) has resulted in the protein becoming a popular model system for studies of immobilized or entrapped biorecognition elements which are employed in biosensor

devices. [5-9] Both unlabelled HSA and HSA which was labelled with the fluorescent probe acrylodan at Cys-34 have been examined in solution and when immobilized to inorganic surfaces. [5-9] Figure 5.1 illustrates the structure of Ac which binds to Cys-34 on HSA via the Michael Addition. The acrylodan probe was chosen for these studies because it is sensitive to the local environmental dipolarity and dynamics within the binding pocket surrounding Cys-34. [9,11-14] The acrylodan probe allowed the structure and dynamics of acrylodan labelled HSA (HSA-Ac) to be examined, and also allowed factors such as the accessibility of the reporter group to be monitored. [3-6]

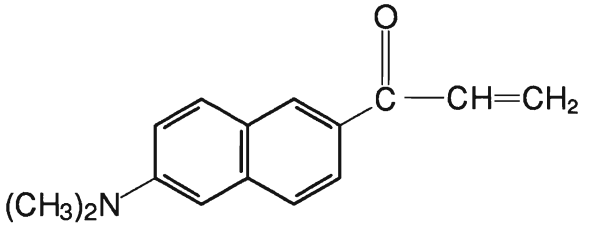

Figure 5.1: Structure of Acrylodan

One of the issues that is of interest for both free and immobilized proteins is the retention of protein function and how this relates to changes in the protein structure. This becomes especially important when one desires information on the effects of different encapsulation or immobilization protocols on protein structure and/or function. Several studies have appeared which have examined the structure, stability and unfolding pathway of unlabelled HSA in solution. [15-23] A variety of techniques have been applied, including nuclear magnetic resonance,[24] circular dichroism,[18] differential scanning calorimetry [15-17] and measurement of intrinsic fluorescence.[15,22] In addition, there is a recent report where the steady-state and time-resolved fluorescence of the acrylodan label has been monitored during chemical denaturation of HSA-Ac in solution.[8] Unfortunately, most of these techniques, with

the exception of fluorescence spectroscopy, are not amenable to studies of entrapped or immobilized proteins. Furthermore, the information which is normally obtained from fluorescence studies is often not sufficient to characterize subtle changes in the structure of large proteins. It is important to recognize that no studies have appeared which comprehensively describe the fluorescence behaviour of both labelled and unlabelled HSA and how the fluorescence is affected by changes in structure and dynamics which are caused by thermally and chemically denaturing the protein.

In the chapter, the emission of the acrylodan moiety attached at Cys-34 is used to provide information on the local structure and dynamics of domain I, while the fluorescence of the single Trp residue is used to provide information on the local structure and dynamics of domain II during thermal and chemical denaturation. We report a detailed investigation of the steady-state fluorescence, steady-state anisotropy, and time-resolved fluorescence behaviour of both Trp and acrylodan. Such studies provide a large amount of information including local polarity, dynamics, and probe accessibility from two locations within the protein. In addition, we show here for the first time that the monitoring of Trp fluorescence from HSA-Ac provides the ability to investigate the spatial relationship between the Trp and acrylodan probes using resonance energy transfer techniques, owing to the overlap of the acrylodan excitation spectrum and the Trp emission spectrum. HSA has been labelled at the Cys residue previously for the purpose of examining interdomain spacings via energy transfer.[3,4] However, in this previous work only the effects of pH induced structural alterations on the energy transfer efficiency were examined. Unfolding studies were not done with the labelled protein. In the present work, energy transfer measurements are used to provide a

convenient method for examining changes in interdomain distances during denaturation and refolding, providing information on the spatial relationships between domains I and II.

The reversibility of unfolding at different stages and its correlation to protein function is also examined via binding of the fluorescent ligand salicylate. [25-27] Salicylate binding studies provide information on the relationship between protein structure and function. By combining all of the fluorescence and binding data we have been able to elucidate subtle features of the protein unfolding pathway which are not easily observed by other methods. These observations provide the key groundwork for future studies involving entrapped HSA and HSA-Ac.

5.2 Materials and methods

5.2.1 Materials

Human serum albumin (HSA, essentially fatty acid free), sodium salicylate, *N*-acetyltryptophan-amide (NATA) and 3500 MW cutoff dialysis tubing were obtained from Sigma (St. Louis, MO). 6-acryloyl-2-(dimethylamino)naphthalene (acrylodan) was obtained from Molecular Probes (Eugene, OR). 1,4-bis(4-methyl-5-phenyl-2-oxazolyl)benzene (Me_2-POPOP), acrylamide (99+%) and sodium azide (99%) were supplied by Aldrich (Milwaukee, WS). The guanidine hydrochloride (GdHCl, Sequanol grade) was from Pierce (Rockford, IL). The Sephadex G-25 fine powder was supplied by Pharmacia Biotech (Uppsala, Sweden). All water was twice distilled and deionized to a specific resistivity of at least 18 MΩ·cm using an Elga "Prima" 5-stage stage water purification system. All other chemicals were of analytical grade and were used without further purification.

5.2.2 Experiments

5.2.2.1 Protein Labelling and Purification

A small amount of protein (1 mg) was dissolved into 1 mL of 10 mM phosphate buffer containing 100 mM KCl at pH 7.2. This was then passed through a Sephadex G-25 column (height 10-20 cm, diameter 1 cm) using 10 mM phosphate buffer to elute the protein. The purified protein was labelled as described elsewhere. [7] Briefly, acrylodan and HSA were mixed in a 2:1 molar ratio and allowed to stir in the dark for 24 hours at room temperature. Unlabelled acrylodan was dialyzed against 10 mM phosphate buffer over a 4 day period with an exchange of buffer every 12 hours. The labelled protein was then passed through a G-25 sephadex column to dislodge any unreacted label. The concentration of labeled protein was found using $\varepsilon_{278} = 8700\ M^{-1}cm^{-1}$ and $\varepsilon_{365} = 12\ 800\ M^{-1}cm^{-1}$ for acrylodan [28] and $\varepsilon_{277} = 36\ 000\ M^{-1}cm^{-1}$ for HSA. [17] The labelling efficiency was determined to be >80%.

5.2.2.2 Steady-State Fluorescence Measurements

Fluorescence excitation and emission spectra were collected from labelled and unlabelled HSA using instrumentation which has been described previously. [29] Samples containing unlabelled HSA were excited at 295 nm and emission was collected from 305 nm to 450 nm in 1 nm increments with an integration time of 0.50 s using 4 nm bandpasses in both the excitation and emission paths. Acrylodan-labelled HSA was excited at 360 nm, with emission collected from 400 nm to 600 nm to examine the acrylodan residue alone. For energy transfer experiments, the labelled protein was excited at 295 nm and emission was collected from 305 nm to 600 nm. Excitation spectra of acrylodan were collected from 315 nm to 470 nm with emission at 500 nm.

Steady-state fluorescence anisotropy measurements were done as described elsewhere[30] with excitation at 295 nm and emission at 340 nm for studies of Trp, 360 nm excitation and 500 nm emission to measure the anisotropy of acrylodan, or 295 nm excitation and 500 nm emission to measure the effects of energy transfer on anisotropy. All experiments were done with 30 μM of protein to provide sufficient signal with the polarizers in place.

5.2.2.3 Time-Resolved Fluorescence Measurements

Time-resolved fluorescence measurements of Trp were performed using the time-correlated single photon counting method,[31] available at the University of Windsor. The excitation source was a cavity dumped dye laser synchronously pumped by an actively mode-locked argon ion laser (Spectra Physics) operating at 825 kHz with a pulse width of 15 ps. Emission, following vertically polarized excitation at 295 nm, was detected (right angle geometry) after passing through a polarizer set at 55° to the vertical and a JY H10 monochromator with a 4 nm bandpass, using a Hamamatsu 1564U-01 microchannel plate photomultiplier tube. The channel width was 10 ps/channel, and data were collected in 1024 channels. The instrument response function was determined from the Raman scattering of water and typically had a fwhm of *ca.* 70 ps. Counts from a blank were measured for each sample for the same accumulation time, and the blank counts were subtracted from the sample decay curve.

Time-resolved intensity and anisotropy decay data for the acrylodan label were collected by Frank V. Bright's research group. All data was acquired in the frequency-domain using a SLM 48000 MHF multi-frequency phase-modulation fluorometer, present at the State University of New York at Buffalo. An argon ion laser (Coherent, Model Innova

90-6) operating at 351.1 nm was used as the excitation source. A bandpass filter was placed in the excitation path to minimize extraneous plasma discharge from reaching the detection system. Magic angle polarization was used for all excited-state intensity decay experiments. Me_2POPOP in ethanol served as the reference lifetime standard; its lifetime was assigned a value of 1.45 ns. For all experiments, the Pockel's cell was operated at a repetition rate of 5 MHz. Typically, data were collected for 60-90 s over a frequency range of 5-250 MHz. All multifrequency phase and modulation data were analyzed according to the global analysis method described elsewhere.[30]

5.2.2.4 Acrylamide Quenching Studies

A volume of 2.0 mL of a 0.5 μM HSA solution was titrated by adding a total of twenty-two 10 μL aliquots of 8.0 M acrylamide in buffer. A fluorescence spectrum was collected from the sample and an appropriate blank after each addition. Spectra were corrected for sample dilution and were integrated from 310 nm to 450 nm. The quenching data was fit using a modified version of the Stern Volmer equation which accounted for both dynamic and static contributions to the quenching process, as shown in equation 18.

5.2.2.5 O_2 Quenching of HSA-Ac

The oxygen quenching of the Ac residue of HSA-Ac was done in the laboritories of Prof. Frank V. Bright, at State University of New York at Buffalo, using a stainless steel high-pressure O_2 cell similar to the one described by Lakowicz et al.[32] (Note: These experiments require the use of moderately high pressures. One must exercise extreme caution when working with high pressure gases, especially O_2). A temperature-regulated

fluid was pumped directly through a coil within the cell to ensure temperature control (20 ± 1 °C). O_2 from a standard gas cylinder was introduced directly into the cell through stainless steel tubing and a valve. The internal cell pressure was monitored (± 1 psia) with a standard digital pressure transducer. The solution was constantly stirred throughout the experiment and all samples were allowed to equilibrate until the fluorescence was constant [5]. The concentration of HSA-Ac within the cell was 2 μM. Data were analyzed following the protocol outlined in reference [5].

5.2.2.6 Thermal Denaturation Studies

A volume of 1.5 mL of 0.5 μM HSA was placed into a quartz fluorimeter cuvette. The temperature was raised in *ca.* 5°C increments starting at 20°C and going to 70°C or 80°C. A fluorescence spectrum or anisotropy value was collected from the sample and from an appropriate blank at each temperature, as described in Chapter 3. All thermodynamic analysis was done as described in Chapter 3.

5.2.2.7 Chemical Denaturation Studies

Chemical denatuation studies were done using a volume of 1.50 mL of a 0.5 μM HSA solution. A total of twenty aliquots of 8.0 M GdHCl in buffer were added with constant stirring and a minimum of 10 minutes was allowed for equilibration (with a shutter blocking the excitation light). A fluorescence spectrum or a steady-state anisotropy value was collected at each point for both the sample and a blank containing an identical concentration of GdHCl. The spectra were corrected for contributions from the blank and instrument

factors as well as dilution factors. The titration curves for these experiments were obtained by integrating and normalizing the spectra.

5.2.2.8 Salicylate Titrations of HSA

A solution of 5 μM HSA in 10 mM phosphate buffer was titrated with salicylate in 10 mM phosphate buffer at pH 7.2. Twenty 10 μl aliquots of 50 μM salicylate were added to a starting volume of 1300 μL of protein solution. Spectra were collected for both the sample and the appropriate blank. All spectra had appropriate blanks subtracted and were dilution corrected. A 40 nm window centered about the wavelength maximum at 408 nm was integrated to provide intensity values for the ligand at each salicylate concentration. A linear regression was performed on the integrated intensity to quantitate the relative binding affinity of the HSA. [25] This experiment was performed on native, thermally denatured and chemically denatured protein samples.

5.3 Results and Discussion

5.3.1 Chemical Denaturation

The unfolding behaviour of HSA and HSA-Ac was first examined by chemical denaturation with GdHCl. The changes in the steady-state and time-resolved fluorescence intensity and anisotropy were monitored for both the Trp in HSA and HSA-Ac and for the acrylodan moiety of HSA-Ac. The Trp residue within the native, unlabelled protein had an emission maximum of 335 nm, a quantum yield of 0.14 ± 0.01 and a steady-state anisotropy value of 0.180 ± 0.002. From equation 13, this indicates that the average rotational correlation time for native HSA is 4.15 ± 0.04 ns. These values are consistent with the Trp

residue being located in an environment of intermediate polarity with an intermediate degree of motion (i.e., some local motion which reduces *r*).

Denaturation of HSA using GdHCl was monitored by changes in integrated fluorescence intensity and steady-state anisotropy, as shown in Figures 5.2a and 5.3. Initially, there was a pre-unfolding baseline with no major changes in intensity or anisotropy. However, there was a slight blue shift in the emission wavelength of the Trp residue before the first stage of unfolding, as shown in Figure 5.2a. The intensity data, shown in Figure 5.2a, indicated that the protein denatured by a two-stage process. The first unfolding transition occurred between 1.0 M and 2.2 M with a large change in intensity (50%). This transition was accompanied by a red-shift in the wavelength from 330 nm to 345 nm. The intensity data also indicated that there was a second unfolding transition between 2.2 M and 3.0 M, with a much smaller change in intensity (~20%), and no further wavelength shift. Anisotropy changes, shown in Figure 5.3 (lower curve), showed one distinct unfolding step at a denaturant level similar to that observed using intensity measurements, and a drawn out baseline, which is presumably due to the second unfolding step. The final anisotropy value was 0.070 ± 0.002 at 4.0 M GdHCl, corresponding to an average rotational correlation time of 0.58 ± 0.02 ns. The decrease in anisotropy is indicative of a substantial increase in the mobility of the Trp residue, and is consistent with unfolding of the protein. The transition reported by steady-state fluorescence anisotropy measurements was broader than that reported by intensity measurements, consistent with the differential quantum yield weighting of the folded and unfolded forms of the protein.[33]

Acrylamide quenching of the Trp residue at different levels of GdHCl indicated that the value of k_q increased from 0.6 x 10^9 to 1.1 x 10^9 $M^{-1} \cdot s^{-1}$ on going from 0.0 M to 2.0 M

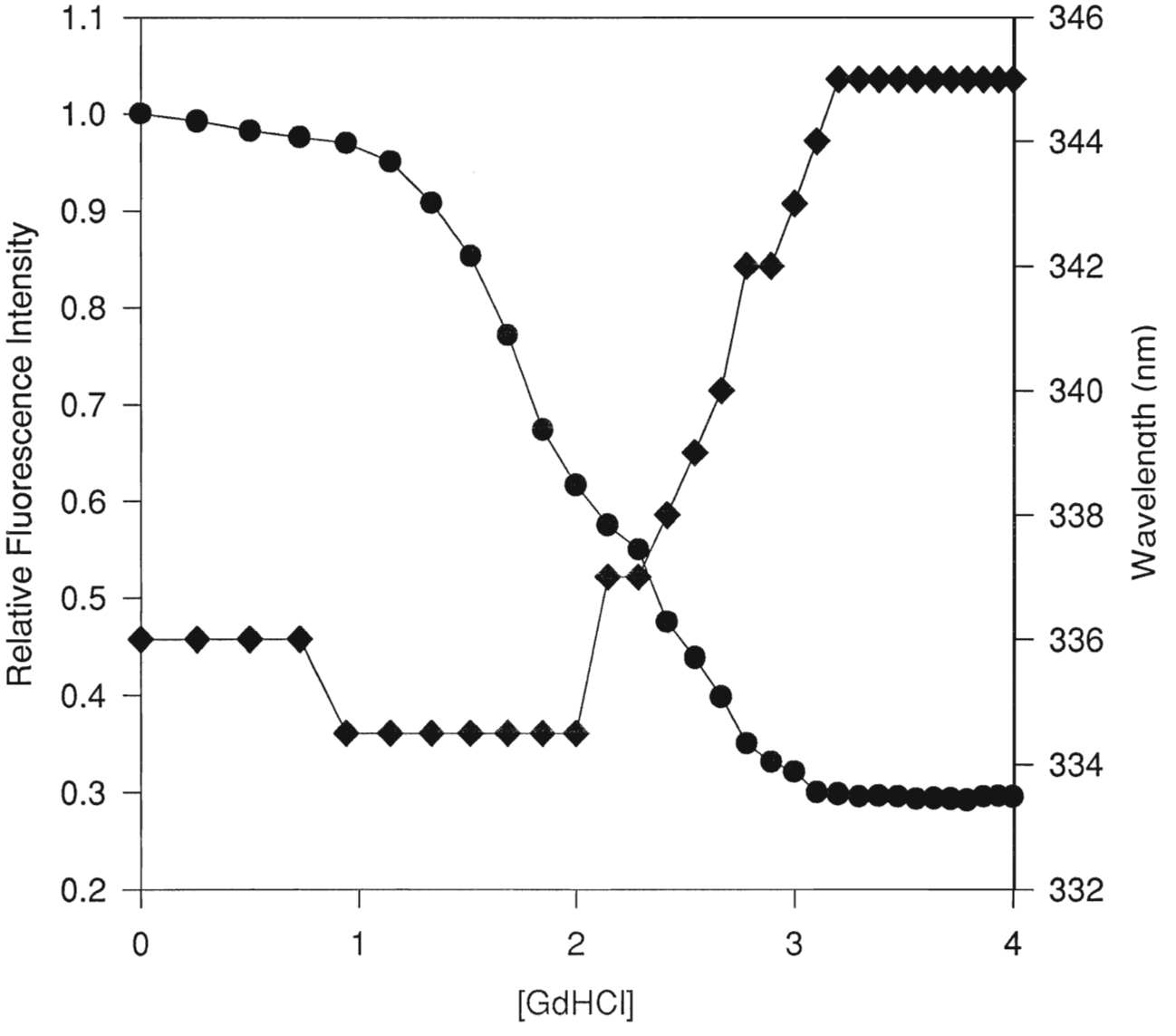

Figure 5.2a. Changes in integrated intensity of Trp emission (●) and wavelength (◆) from HSA excited at 295 nm during chemical denaturation of HSA using GdHCl..

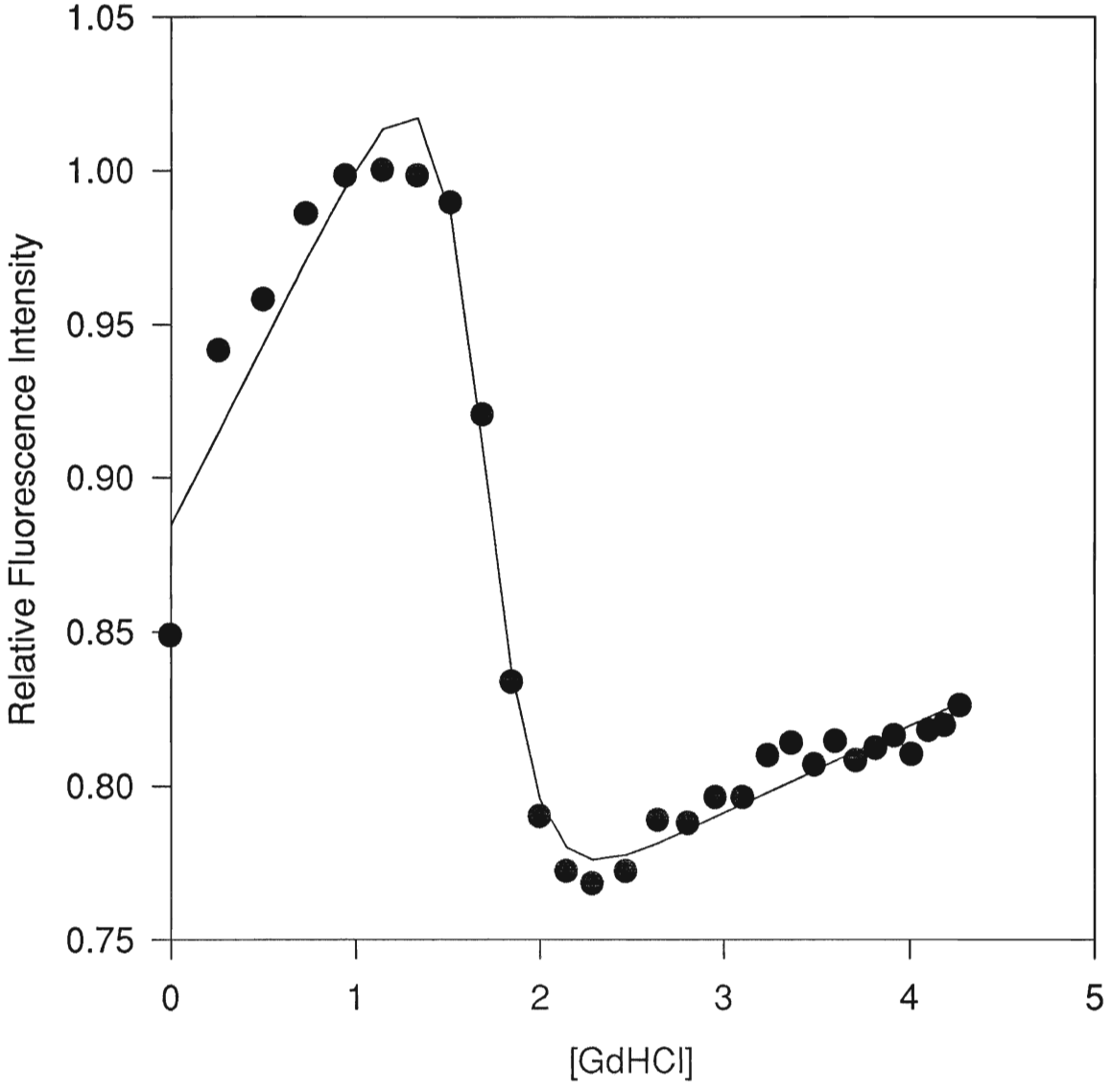

Figure 5.2b. Changes in integrated intensity of Trp emission from HSA-Ac excited at 295 nm during chemical denaturation of HSA-Ac using GdHCl.

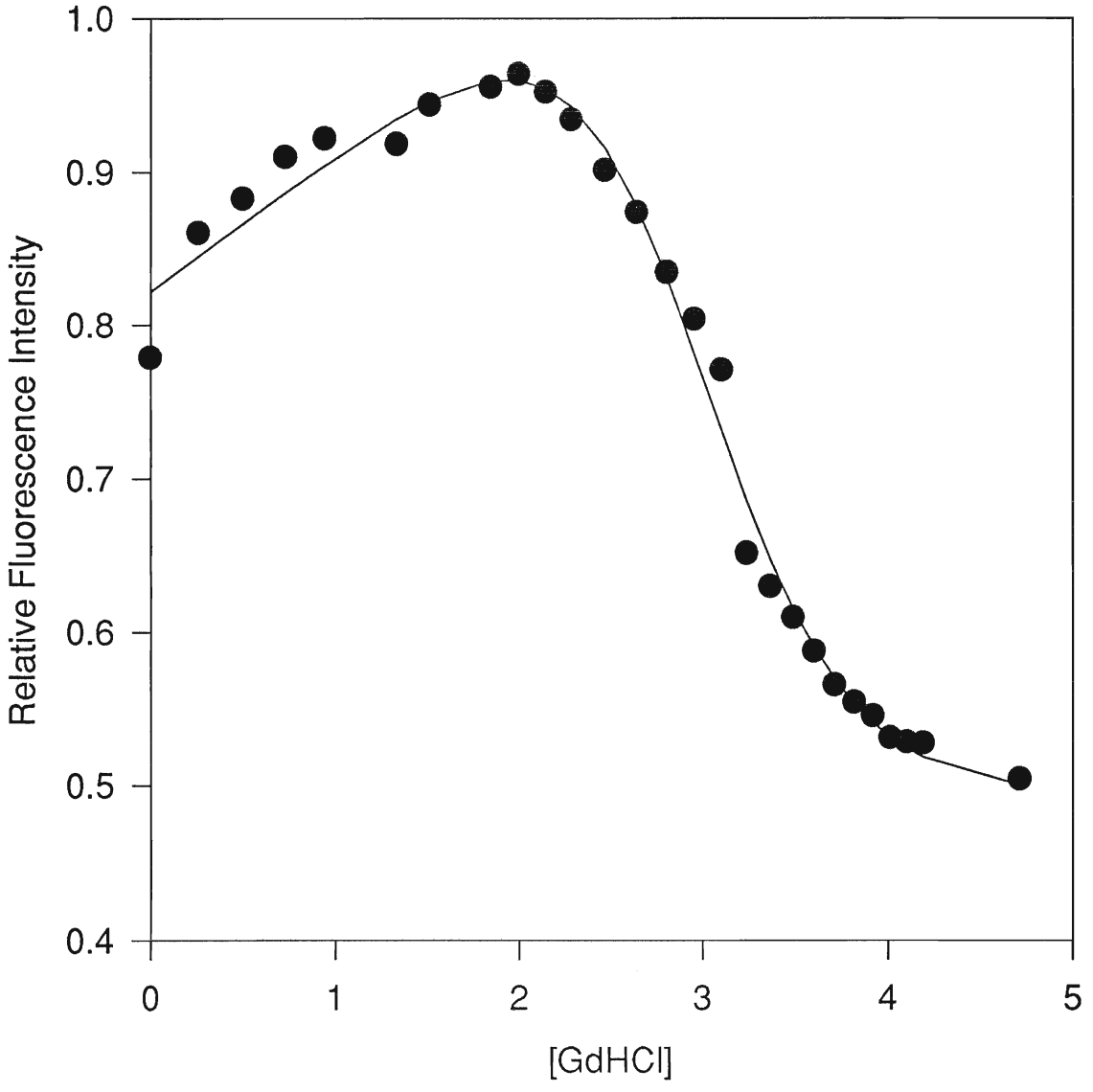

Figure 5.2c. Changes in integrated intensity of acrylodan emission from HSA-Ac excited at 360 nm during chemical denaturation of HSA-Ac using GdHCl.

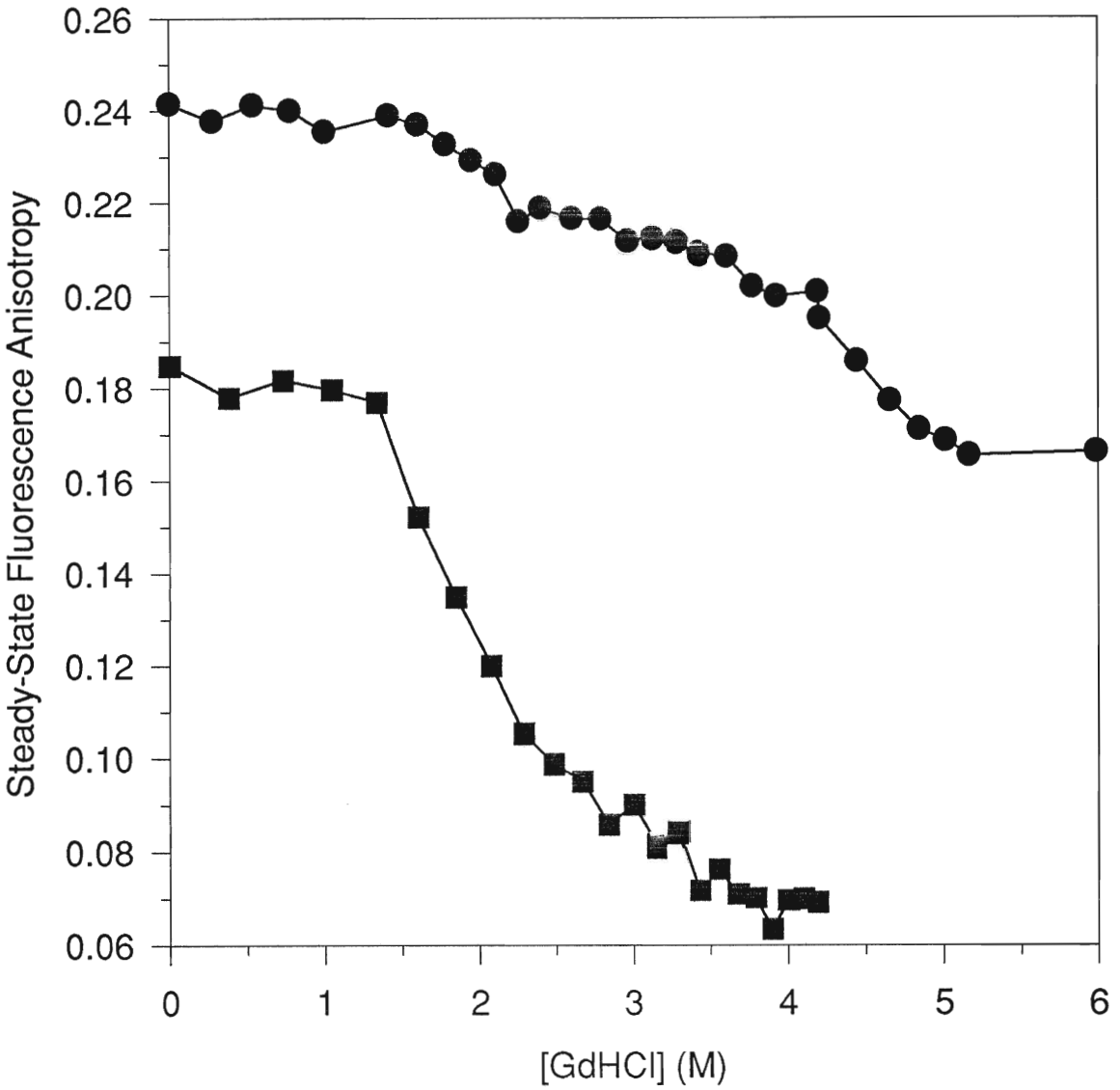

Figure 5.3. Steady-state anisotropy of HSA and HSA-Ac during chemical denaturation. (■) anisotropy of Trp from HSA with excitation at 295 nm, (●) anisotropy of acrylodan within HSA-Ac with excitation at 360 nm.

GdHCl. The results are consistent with the unfolding of domain II causing increased exposure of the Trp residue, and correspond to the range for the major emission wavelength shift. Beyond 2.0 M the k_q value remained constant at 1.0 x 10^9 $M^{-1}\cdot s^{-1}$, indicating that the second unfolding step did not cause changes in the exposure of the Trp residue. From this data, it appears that the unfolding of domain II occurs over the denaturant range between 1.0 and 2.0 M, while a second unfolding step not directly involving domain II occurs at denaturant levels above 2.0 M.

Analysis of the unfolding curve (Fig. 5.2a) using equation 24 provided $\Delta G_{(F\rightarrow U)}$ values of 30.0 ± 1.3 $kJ\cdot mol^{-1}$ for the first stage of unfolding, and 35.0 ± 1.5 $kJ\cdot mol^{-1}$ for the second stage of unfolding, as shown in Table 5.1. Thus, the total change in free energy for unfolding of HSA was 65.0 ± 4.8 $kJ\cdot mol^{-1}$. Farruggia et al. [22] obtained a value of 23 $kJ\cdot mol^{-1}$ with a $D_{1/2}$ of 2.75 M for unfolding of HSA but did not witness a two-stage unfolding process. Our initial experimental results indicated a one-step unfolding with a $\Delta G_{(F\rightarrow U)}$ value of 25.9 ± 2.2 $kJ\cdot mol^{-1}$, but these results were obtained under conditions where samples were not given sufficient time to reach equilibrium after addition of GdHCl. Only when sufficiently long equilibration times were used (10 mins per aliquot of denaturant) was the unfolding of HSA observed to be a multistep process.

Removal of GdHCl by dialysis resulted in a recovery of the shape of the spectral contour for Trp along with recovery in terms of emission wavelength, anisotropy and quencher accessibility. However, the intensity did not recover to the initial value before unfolding, suggesting that the native structure may not have been fully recovered. To further examine the changes in protein structure and function on denaturation and recovery, the binding of salicylate to HSA was measured at different denaturant levels and for protein

which had the GdHCl removed by dialysis. HSA containing even low levels of GdHCl (less than 1.0 M) was unable to bind salicylate. However, at such levels the removal of the denaturant by dialysis restored the binding capability of the protein, indicating that the initial conformational changes reported by the blue shift in the Trp emission wavelength were reversible. Denaturation and recovery of HSA using GdHCl at levels of 2.0 M or higher, where domain II was fully unfolded, resulted in a large decrease in the ability of the protein to bind salicylate, showing that domain II unfolding was not fully reversible. Thus, even though the spectral and quenching data suggest a similar environment for the Trp residue for native and refolded HSA, the binding studies clearly show that unfolding of domain II causes irreversible changes in the structure and function of the protein.

Table 5.1. Thermodynamic parameters for GdHCl induced unfolding of HSA.

Sample	$\Delta G_{(F\rightarrow U)}$ (kJ.mol^{-1})[a]	-m_G (kJ.L.mol^{-2})[a]	$D_{1/2}$ (M)[b]	$\chi^{2(c)}$
Trp in HSA (Stage 1)[d]	30.0 ± 1.8	20.1 ± 1.1	1.5 ± 0.2	0.97
Stage (2)[e]	35.0 ± 1.5	13.0 ± 0.9	2.7 ± 0.2	0.97
Trp in HSA-Ac[f]	29.7 ± 5.0	15.0 ± 2.4	2.0 ± 0.2	0.98
Acrylodan in HSA-Ac[g]	14.7 ±1.1	5.7 ± 0.5	2.6 ± 0.3	0.99

a) These values were obtained by fitting of unfolding curves to equation 24; b) this value was obtained by dividing ΔG_{un} by $-m_G$; c) determined from non-linear curve fitting using SigmaPlot 1.02 for Windows; d) fitting parameters: $F_N = 0.999$, $F_U = 1.104$, $m_N = -0.033$, $m_U = -0.245$; e) fitting parameters: $F_N = 1.044$, $F_U = 0.332$, $m_N = -0.245$, $m_U = -0.011$; f) fitting parameters: $F_N = 0.942$, $F_U = 0.632$, $m_N = 0.050$, $m_U = 0.016$; g) fitting parameters: $F_N = 0.862$, $F_U = 0.832$, $m_N = 0.093$, $m_U =$ -0.046.

To examine the unfolding behaviour of domain I, denaturation of HSA-Ac was done. Incorporation of the acrylodan label resulted in dramatic changes in the intensity of the Trp

signal for both the native and the unfolded protein, although the spectral contours corresponding to these forms (i.e., emission maximum and full-width at half maximum) were identical to those obtained for the unlabelled protein. The measured quantum yield of the native protein dropped from 0.14 ± 0.01 to 0.03 ± 0.01, indicating that the acrylodan was able to quench the Trp fluorescence. These results strongly suggest that the acrylodan label influenced the Trp signal owing to a resonance energy transfer effect with the Trp residue acting as the donor and the acrylodan label acting as the acceptor. This effect is described in more detail below.

Chemical denaturation of HSA-Ac resulted in a significantly different unfolding curve when the Trp emission was monitored, as shown in Figure 5.2b. The unfolding curve for the protein was altered such that the intensity of the Trp signal increased significantly (15%) between 0.0 M and 1.0 M of denaturant. This range is similar to that for the blue shift in the Trp emission wavelength maximum, and is consistent with a separation of domain I and domain II such that the quenching of the Trp residue is partially relieved. The main unfolding transition occurred between 1.0 M and 2.0 M of GdHCl, and had a $D_{1/2}$ value of 1.7 M which was similar to that obtained for the unfolding of unlabelled HSA. Beyond 2.0 M the intensity of the Trp emission increased in a fairly linear fashion, suggesting that the unfolding of domain I containing the acrylodan label was affecting the Trp signal from domain II, in agreement with the behaviour observed for unlabelled HSA (Fig 5.2a). It is interesting to note that the second unfolding step is not observable, unlike the case of unlabelled HSA. This is likely due to a broad distribution of Trp-acrylodan donor-acceptor distances within the partially denatured HSA-Ac, causing a broadening of the unfolding transition.

Unfolding curves were also obtained for HSA-Ac when the acrylodan label was excited directly at 360 nm and the acrylodan emission was observed during denaturation. Figure 5.2c shows the changes in integrated intensity during denaturation, while Figure 5.3 (upper curve) shows the changes in steady-state anisotropy. O_2 quenching of the acrylodan label was also done at various denaturant levels. In this case, the intensity of the acrylodan label increased by approximately 15% during the addition of the first 2.0 M of denaturant, reaching a maximum between 1.5 and 2.0 M GdHCl, although the anisotropy and k_q value remained relatively constant over this range. This range correlates to that for the initial domain separation and unfolding of domain II, as shown by the Trp fluorescence of HSA and HSA-Ac, and indicates that these processes result in a change in the local conformation of domain I in the region surrounding Cys-34. The main unfolding transition reported by the acrylodan intensity changes occurred over a fairly broad range between 2.0 M and 4.0 M GdHCl, with a $D_{1/2}$ value of 2.7 M. The k_q value also increased by nearly 2-fold over this range, indicating that the acrylodan moiety became more solvent exposed. Beyond 4.0 M GdHCl the intensity and k_q value remained relatively constant, indicating that full unfolding of the structure occurred upon addition of ~ 4.0 M GdHCl. The corresponding anisotropy decrease for the acrylodan label occurs in two stages, with a small anisotropy change between 1.0 M and 2.2 M of denaturant, and a larger change between 4.0 and 5.0 M GdHCl. The initial change is consistent with an overall increase in the global motion of the protein upon unfolding of domain II. The second step is consistent with the unfolding of domain I. The steady-state anisotropy changes again lag behind the integrated intensity changes, as observed for Trp, owing to the differential quantum yield weighting of the native and unfolded states (Eftink, 1994). Overall, the results from the acrylodan emission clearly shows that the

unfolding of domain I occurs only after domain II has fully unfolded, and supports the presence of a multi-step unfolding process as suggested by changes in the Trp fluorescence of HSA.

The multi-step unfolding profile reported by the intensity and anisotropy data provides evidence that the protein unfolding pathway involves at least one intermediate. This is contrary to the findings of Tayyab et al.,[19] who examined urea-induced denaturation of HSA using fluorescence measurements and found that unfolding apparently occurred in a single, concerted step. However, studies by Wallevik [21] suggested that the unfolding of HSA with GdHCl is a multistep process at physiological pH values, in agreement with our findings. Chmelik et al. [23] have also reported a two-step unfolding of HSA by urea using polarography.

Time-resolved intensity data for Ac was collected by Frank Bright and co-workers. Data was collected for the Trp residue within HSA and for the Trp and acrylodan within HSA-Ac was obtained for proteins in the presence of 0 M, 1.0 M, 2.0 M and 4.0 M GdHCl, as shown in Table 5.2. The mean lifetime value for Trp in native HSA was 5.28 ± 0.03 ns, is in reasonable agreement with the value of 5.60 ns reported elsewhere [34]. Comparison of Trp lifetime values for HSA and HSA-Ac allowed for an examination of interdomain distance relationships at different denaturant levels using equation 19. The value of R_0 for the native protein was first calculated, and was determined to be 2.70 ± 0.03 nm, using a donor quantum yield of 0.14, a J value of (8.91 ± 0.09) x 10^{-15} cm^3M^{-1}, and with κ^2 set to 2/3, and n set to 1.50. Based on the differences in the intensity-weighted mean lifetime of native HSA and HSA-Ac, the energy transfer efficiency of the folded protein was determined to be 28.3 ± 0.2%, corresponding to an interdomain distance of 3.15 ± 0.03 nm. This value is in excellent

Table 5.2. Fluorescence intensity decay parameters for the Trp residue within HSA and HSA-Ac as a function of denaturant concentration.

Sample	α_1	α_2	α_3	f_1[a]	f_2	f_3	τ_1 (ns)	τ_2 (ns)	τ_3 (ns)	$\langle\tau\rangle$ (ns)[b]	χ^2
Tryptophan in HSA											
0 M GdHCl	0.57	0.29	0.14	0.79	0.20	0.01	5.913	3.046	0.231	5.28	1.054
1 M GdHCl	0.59	0.24	0.17	0.85	0.14	0.01	5.453	2.135	0.080	4.98	1.103
2 M GdHCl	0.38	0.37	0.25	0.73	0.25	0.02	5.114	1.857	0.214	4.19	1.062
4 M GdHCl	0.48	0.41	0.11	0.70	0.28	0.02	3.230	1.516	0.310	2.73	1.004
0 M GdHCl (recovered)	0.40	0.35	0.25	0.73	0.25	0.02	5.951	2.251	0.257	4.92	1.089
Tryptophan in HSA-Ac											
0 M GdHCl	0.36	0.27	0.37	0.79	0.19	0.02	4.473	1.420	0.143	3.79	1.070
1 M GdHCl	0.31	0.29	0.40	0.77	0.21	0.02	4.439	1.325	0.074	3.70	1.010
2 M GdHCl	0.30	0.35	0.25	0.73	0.24	0.03	3.314	0.930	0.152	2.65	1.011
4 M GdHCl	0.22	0.35	0.42	0.61	0.34	0.05	3.229	1.118	0.147	2.36	1.020
Acrylodan in HSA-Ac											
0 M GdHCl	0.60	0.40	-	0.77	0.23	-	4.330	1.886	-	3.775	1.005
0.5 M GdHCl	0.61	0.39	-	0.80	0.20	-	4.212	1.656	-	3.698	1.017
1M GdHCl	0.65	0.35	-	0.85	0.15	-	4.002	1.325	-	3.606	1.021
2M GdHCl	0.65	0.35	-	0.84	0.16	-	3.972	1.377	-	3.562	1.009
4 M GdHCl	0.62	0.38	-	0.83	0.17	-	3.779	1.282	-	3.365	1.029
5 M GdHCl	0.61	0.39	-	0.81	0.19	-	3.610	1.312	-	3.166	1.045
6M GdHCl	0.48	0.52	-	0.71	0.29	-	3.470	1.320	-	2.853	1.121

a) calculated from equation 8, b) calculated from equation 9.

slight decrease in energy transfer efficiency to 25.0 ± 0.2 %. This indicated that the interdomain distance had increased to 3.26 ± 0.03 nm, suggesting that interdomain separation likely occurred before domain unfolding took place. This interpretation is in agreement with the increase in Trp emission intensity observed during the initial stages of denaturation for HSA-Ac (Fig. 5.2b).

At 2.0 M GdHCl, the mean lifetime value of Trp in both proteins dropped significantly, indicating a large change in the environment of the Trp residue. Comparison of the lifetime values for the two proteins indicated energy transfer efficiency increased to 36.7 ± 0.4%, corresponding to a decrease in the Trp-acrylodan distance to 2.96 ± 0.03 nm. This decrease in the donor-acceptor distance occurs at a point where domain II is unfolded but domain I is intact. Thus, under these conditions the Trp residue is apparently free to move closer to the acrylodan moiety, producing a slight decrease in the average Trp-acrylodan distance. The overall structural change in the protein may explain the observed increase in the directly-excited acrylodan emission intensity between 0.0 and 2.0 M GdHCl, shown in Figure 5.2c.

At 4.0 M GdHCl, the mean lifetime values of the Trp within HSA and HSA-Ac show a further decrease, and the fractional contribution of each decay component shifts to emphasize the two longer decay components. The energy transfer efficiency drops to 13.2 ± 0.1%, corresponding to an average Trp-acrylodan distance of 3.69 ± 0.05 nm. Thus, after domain I unfolds the protein adopts an extended conformation with the distance between the Trp and acrylodan moieties increasing substantially. The relative closeness of the two probes for the unfolded protein may be explained by the fact that the disulfides were not reduced, thus complete unfolding does not occur.

for the unfolded protein may be explained by the fact that the disulfides were not reduced, thus complete unfolding does not occur.

Refolding the protein by dialysis of the GdHCl resulted in the lifetime recovering to a value of 4.92 ± 0.04 ns. However, the fractional contribution of each decay component was different than those observed for the native protein. The results clearly indicated that the native structure was not recovered upon protein refolding, at least in the region of the Trp residue. The decay of Trp fluorescence intensity for refolded HSA-Ac could not be reliably fit and therefore it was not possible to obtain Trp-acrylodan distance information in this case.

Time-resolved intensity measurements of acrylodan within HSA-Ac were also done as a function of GdHCl concentration. The results are shown in Table 5.2. Both the long and short lifetime components decrease as the GdHCl concentration increases, as expected based on the unfolding model proposed above for HSA. The initial changes seen at between 0.5 and 1.0 M GdHCl are consistent with changes in the local environment of the probe, while changes of the global protein structure are observed between 1.0 and 6.0 M GdHCl. These results support the suggestion that the major changes in the environment of the acrylodan label occur at higher levels of denaturant, which is consistent with the suggestion that the unfolding of domain I containing the acrylodan label occurs at high denaturant levels.

Time-resolved fluorescence anisotropy decays of the acrylodan moiety in HSA-Ac were also measured. This data was collected by Frank Bright and co-workers. These results are summarized in Figure 5.4. The results show that the initial global reorientation time is quite large (~ 80 ns), suggesting that multimers of the protein may have been present. A small decrease in the global rotational reorientation time occurs between 1.0 M and 3.0 M, suggesting that the global motion of the entire protein increases over this range of denaturant.

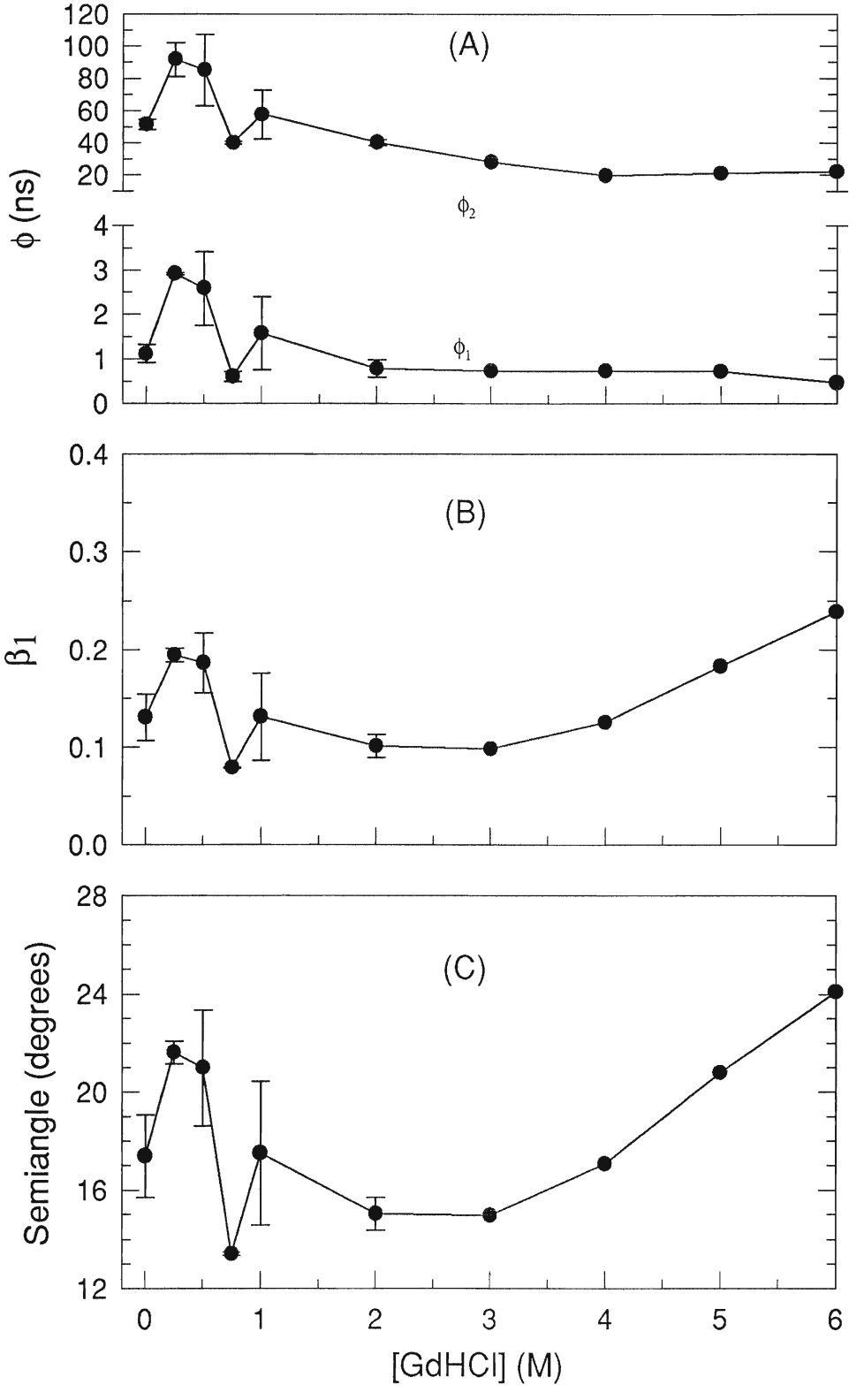

Figure 5.4. Time-resolved decay of the acrylodan anisotropy during chemical denaturation of HSA-Ac. (A) fluorescence rotational correlation times for global (ϕ_2) and local (ϕ_1) rotational components, (B) fractional contribution of ϕ_1 as a function of denaturant concentration, (C) semi-angle of probe rotation obtained during chemical denaturation of the protein. The error bars on each panel denote ± 1 standard deviation from at least three discrete measurements.

There is also a small increase in the fractional contribution of the shorter rotational correlation time, suggesting greater acrylodan residue freedom. Between 3.0 M and 6.0 M GdHCl, the two rotational correlation times remain essentially constant, however the contribution from the shorter component and the semi-angle of rotation for the acrylodan label increase significantly. This is consistent with an opening of the pocket hosting the acrylodan reporter group such that a higher proportion of acrylodan labels are able to freely rotate.

5.3.2 Thermal Denaturation

Thermal denaturation experiments were also performed, and were used to validate the model outlined above. The changes in the emission spectrum of HSA and HSA-Ac during thermal denaturation and recovery are shown in Figure 5.5a and 5.5b. Figures 5.6 and 5.7 present the changes in integrated intensity and steady-state anisotropy as a function of temperature for HSA, HSA-Ac excited at 295 nm (Trp emission, not shown on Fig. 5.7), and HSA-Ac excited at 360 nm (acrylodan emission). Unfolding of HSA (circles in Fig. 5.6) appeared to occur as a single step, contrary to the results obtained for chemical denaturation of HSA as monitored by Trp intensity. The Trp intensity decreased by 60%, with the emission wavelength maximum blue shifting, as shown in Figure 5.5a, and the anisotropy decreasing from 0.180 ± 0.003 to 0.118 ± 0.002 during the unfolding transition. The latter anisotropy value corresponds to an average rotational correlation time of 1.25 ± 0.02 ns, which is double that obtained during chemical denaturation. Furthermore, above 60°C, the anisotropy of the Trp residue increased. Taken together, these results provide evidence that protein aggregates on thermal unfolding, and thus does not end up in the same final state as is

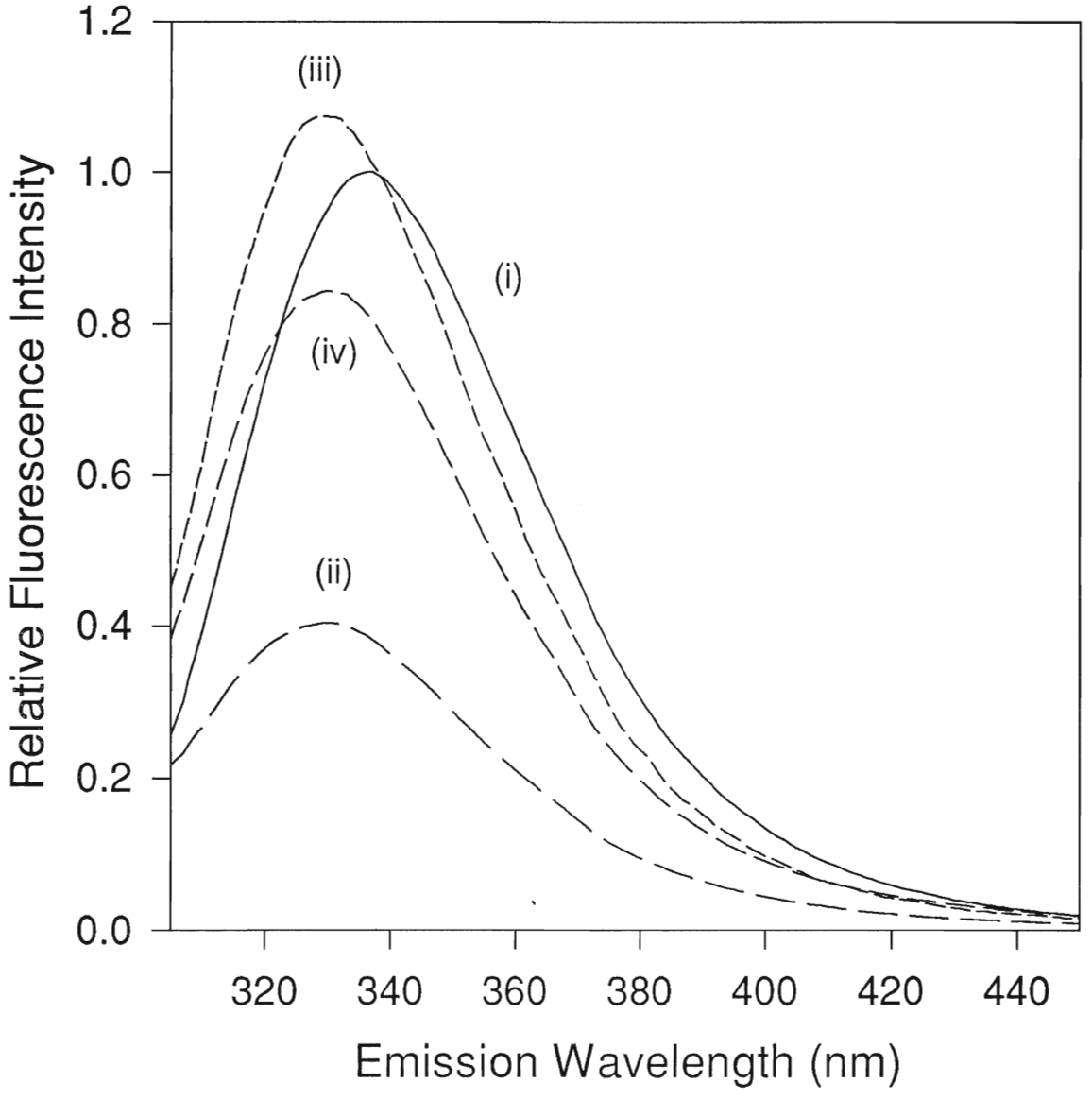

Figure 5.5a. Changes in the emission spectrum of Trp from HSA during thermal denaturation. (i) 20°C, ii) 80°C, iii) recovered from 70°C, iv) recovered from 80°C.

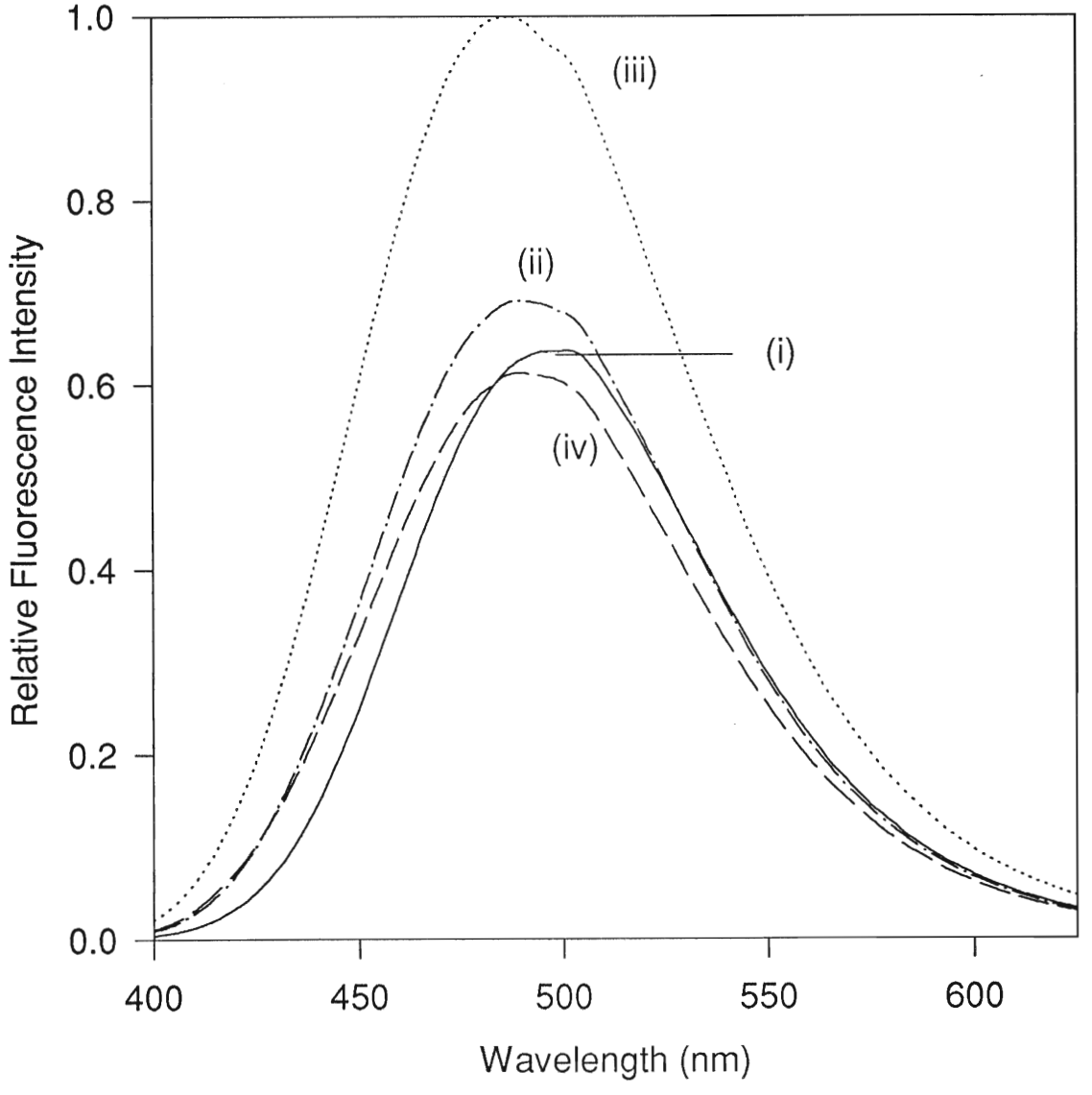

Figure 5.5b. Changes in the emission spectrum of acrylodan from HSA-Ac during thermal denaturation. (i) 20°C, ii) 80°C, iii) recovered from 70°C, iv) recovered from 80°C.

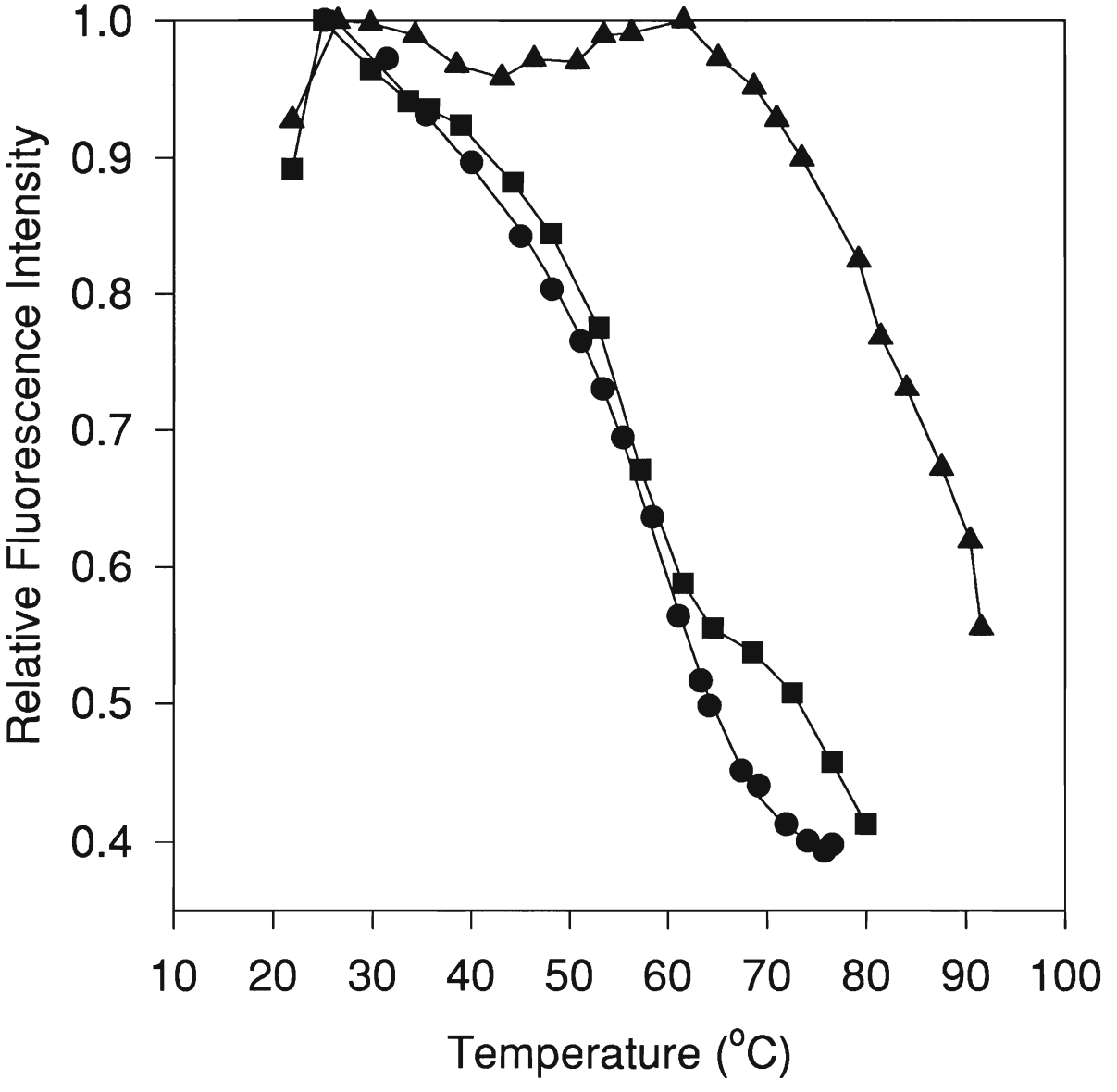

Figure 5.6. Changes in integrated intensity of HSA and HSA-Ac monitored as a function of temperature. (●) Trp emission of HSA, (■) Trp emission from HSA-Ac, (▲) acrylodan emission from HSA-Ac.

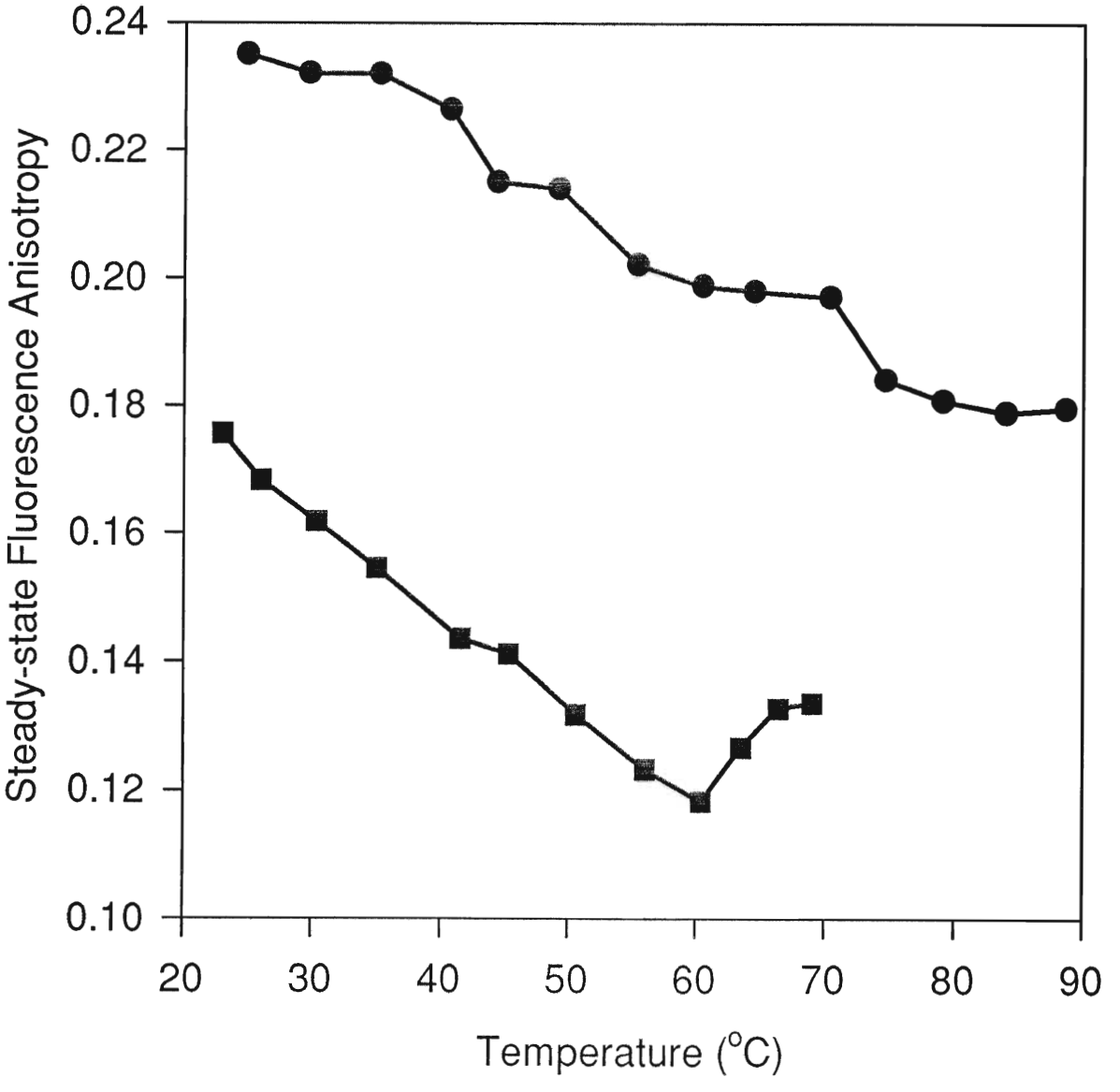

Figure 5.7. Steady-state fluorescence anisotropy of HSA and HSA-Ac during thermal denaturation. (■) anisotropy of Trp from HSA with excitation at 295 nm, (●) anisotropy of acrylodan within HSA-Ac with excitation at 360 nm.

Taable 5.3. Fluorescence intensity decay parameters for the Trp residue within HSA and the acrylodan moiety of HSA-Ac as a function of temperature.

Sample	α_1	α_2	α_3	f_1[a]	f_2	f_3	τ_1 (ns)	τ_2 (ns)	τ_3 (ns)	$\langle\tau\rangle$ (ns)[b]	χ^2
Tryptophan in HSA											
20°C	0.57	0.29	0.14	0.79	0.20	0.01	5.913	3.046	0.231	5.28	1.054
75°C	0.38	0.62	-	0.67	0.33	-	3.251	0.984	-	2.50	1.030
20°C (recovered)	0.42	0.33	0.25	0.77	0.21	0.02	5.628	1.920	0.195	4.72	1.033
Acrylodan in HSA-Ac											
20°C	0.56	0.44	-	0.87	0.13	-	4.137	1.363	-	3.77	1.083
80°C	0.54	0.46	-	0.79	0.21	-	3.327	1.195		2.88	1.005
20°C (recovered)	0.64	0.36	-	0.85	0.15	-	4.046	1.269	- -	3.62	1.022

a) calculated from equation 8, b) calculated from equation 9.

the protein to 20°C, the anisotropy of the Trp residue returned to the initial value of 0.180 ± 0.002. However, the mean fluorescence lifetime (from Table 5.3) did not return to the value obtained for the native protein, resulting in a mean rotational correlation time of 3.71 ± 0.07 ns. Hence the mobility of the Trp residue was greater in the refolded state as compared to the native state. This clearly indicated that the protein did not refold to its original form after a single heating and cooling cycle.

Monitoring of Trp emission from HSA-Ac (squares in Fig. 5.6) provided evidence of two unfolding steps, in qualitative agreement with the multi-step unfolding observed during chemical denaturation. In addition, the intensity of the Trp signal of HSA-Ac initially increased upon unfolding, consistent with an initial increase in the donor-acceptor distance with increasing temperature. With the exception of the two-step unfolding profile, the changes in Trp emission characteristics (intensity, wavelength, anisotropy) during unfolding were similar to those for unlabelled HSA.

Monitoring of acrylodan fluorescence (triangles in Fig. 5.6) also showed an initial increase in acrylodan intensity between 20°C and 30°C. Given that energy transfer is not possible under these experimental conditions, the spectroscopic changes provide evidence of a global change in protein structure which affected the environment in the region of both the Trp and the acrylodan label. Hence, the initial structural changes involving domain separation must also have a direct effect on the environment surrounding Trp-214 and Cys-34. Salicylate binding studies done at 40°C showed retention of partial binding function, hence complete domain separation was not evident at this point. Recovery of the temperature to 20°C resulted in almost full recovery of salicylate binding, suggesting that the

temperature to 20°C resulted in almost full recovery of salicylate binding, suggesting that the initial changes in structure were reversible, in agreement with the chemical denaturation studies.

Between 30°C and 60°C, the acrylodan intensity varies somewhat, while the emission maximum blue shifts from 495 nm to 490 nm. The steady-state fluorescence anisotropy of the acrylodan label (Figure 5.7, circles) also showed a significant decrease, corresponding reasonably well to the pretransition region (30-50°C). This clearly shows that the unfolding of domain II has a major effect on the environment of the acrylodan probe in domain I. Between 60°C and 90°C, the intensity and anisotropy of the acrylodan label decreased substantially, indicating the main unfolding transition of domain I. Over this range, the emission maximum of the acrylodan label blue-shifted to 480 nm, indicating a decrease in the polarity in the local region of Cys-34. It is interesting to note that the emission maximum of the acrylodan label red-shifted during chemically-induced unfolding, opposite to the trend observed during thermal denaturation. This suggests that domain I was able to fully unfold upon exposure to GdHCl, but could not unfold at high temperature. This is further supported by the final anisotropy value of 0.180 at 90°C, which is substantially higher that that for acrylodan in solution ($r_{acrylodan}$ = 0.005), indicating that the protein was not unfolded fully at this temperature. The data are consistent with aggregation of the protein at higher temperatures. Salicylate binding studies of protein which was recovered from heating at 80°C indicated a large loss of binding function, confirming that the recovered protein was only partially functional.

The thermal melting curves derived from measurements of Trp intensity in HSA and HSA-Ac were examined using equation 22. The thermodynamic parameters for HSA

indicated an enthalpy of unfolding of 350 ± 23 kJ·mol^{-1}, an entropy of unfolding of 1050 ± 71 J·K^{-1}·mol^{-1}, and a T_{un} value of 60 ± 4°C (note: other fitting parameters were as follows; F_{0N} = 1.251, F_{0U} = 0.850, s_N = -0.009, s_U = -0.006). These values are in excellent agreement with literature values.[15-17] The ΔG_{un} value was determined to be 42 kJ·mol^{-1} if the $\Delta C_{p,un}$ value was set to zero. Use of the $\Delta C_{p,un}$ values provided by Pico [17] resulted in negative free energy values at a reference temperature of 20°C, suggesting that these values may be erroneous. Thus, all ΔG_{un} values reported herein use a $\Delta C_{p,un}$ value of zero. Thermodynamic analysis of the first unfolding step for HSA-Ac yielded thermophysical values that were similar to those obtained for unlabelled, native HSA (ΔH_{un} = 380 ± 25 kJ·mol^{-1}, ΔS_{un} = 1160 ± 60 J.K^{-1}·mol^{-1}, ΔG_{un} = 39.6 ± 6.7 kJ·mol^{-1}, F_{0N} = 1.142, F_{0U} = 1.012, s_N = -0.006, s_U = -0.007). From these values, the unfolding temperature was calculated to be 55 ± 3°C, which is in reasonable agreement with the value obtained for unlabelled, native HSA. The small differences in the T_{un} values likely reflect the influence of the acrylodan label on the emission properties of Trp within HSA-Ac, due to energy transfer. Circular dichroism spectra of HSA-Ac obtained in 10 mM phosphate buffer containing 100 mM KCl, pH 7.2, suggested that the labelled protein was 64% α-helix, 21% β-sheet and 15% random coil (data not shown). These values are in excellent agreement with those obtained by Wetzel et al [18] for native HSA under similar conditions (61% α-helix, 22% β-sheet, 17% random coil). These results indicate that labelling of Cys-34 had no significant effect on the conformation of the native protein, ruling out such changes as the basis of the lower T_{un} for HSA-Ac.

The unfolding curve derived from measurements of acrylodan fluorescence intensity could not be fit to equation 22 since there was no postunfolding region, owing to the inability of our instrument to heat samples beyond 92°C. However, qualitative analysis of the

unfolding curve suggests that the T_{un} is at least 75°C. It must be noted that the determination of thermodynamic parameters relies on the protein unfolding being reversible. The spectroscopic parameters strongly suggest that this is not a valid assumption for HSA, thus the thermodynamic data presented above should be treated with caution.

The time-resolved decay of fluorescence intensity for Ac was examined by Frank Bright and co-workers. Data was collected for the Trp residue of HSA and the acrylodan probe of HSA-Ac at different temperatures and upon recovery from 75°C (for HSA) or 80°C (for HSA-Ac). The results are given in Table 5.3. Unfolding of the protein by raising the temperature to 75°C resulted in the decay being best fit by two decay components and also caused a decrease in the intensity-weighted mean fluorescence lifetime from 5.28 ± 0.03 ns to a value of 2.50 ± 0.05 ns. Refolding the protein by decreasing the temperature to 20°C resulted in the reappearance of the third decay component, however the lifetime recovered to only 4.72 ± 0.09 ns. In addition, the fractional contributions of each decay component were different that those observed for the native protein, with the fraction of the shortest component increasing at the expense of the longest component. This clearly indicated that the native protein structure was not fully recovered upon protein refolding, at least in the region of the Trp residue, in agreement the chemical denaturation studies described above. Previous studies of the unfolding and refolding behaviour of HSA using circular dichroism measurements indicated that the α-helical content of the protein decreased upon thermal denaturation to 75°C and did not fully recover upon subsequent cooling (Wetzel et al, 1980). Thus, the α-helix containing the Trp residue may have been altered to a looser structure similar to a random coil upon unfolding, and the new conformation was likely unable to refold into the original form. The fluorescence lifetime characteristics of the refolded state

obtained after chemical denaturation were effectively identical to those measured for the protein after recovery from thermal denaturation. This was not expected since the spectra of the two recovered proteins are quite different in terms of wavelength and intensity.

Table 3.3 also shows the pre-exponential terms and fluorescence lifetime components for the acrylodan probe within HSA-Ac obtained at 20°C, after heating to 80°C and after subsequent recovery to 20°C. These data clearly show that both lifetime components decrease upon heating; however, the shorter of the two components decreases 63%, while the longer component only drops by 18%. Cooling to 20°C caused the mean lifetime to recover to within a few percent of the original value; however, there was once again a significant difference in the value and the contribution of the short lifetime component, indicating that the environment within the cybotactic region surrounding the acrylodan probe did not recover to the initial conditions before heating. These results are consistent with those for the Trp residue in HSA, and overall suggest that the protein does not refold to its native structure after heating beyond the protein T_{un}.

Time-resolved anisotropy was collected by Frank Bright and co-workers. This data provided evidence of increased rotational motion of the acrylodan probe upon heating of the protein, as shown in Figure 5.8. The global reorientation time was again higher than expected (~ 55 ns), as was found during chemical denaturation studies, further supporting the presence of protein dimers or multimers. Interestingly, both the global and local rotational correlation times decreased substantially over the first 10°C increase (20°C to 30°C). This corresponds to the temperature range for the initial increases observed in the intensity of the acrylodan label and the increase in the Trp signal when HSA-Ac was denatured. This suggests that there may be a pre-transition, or perhaps a local change in the environment of

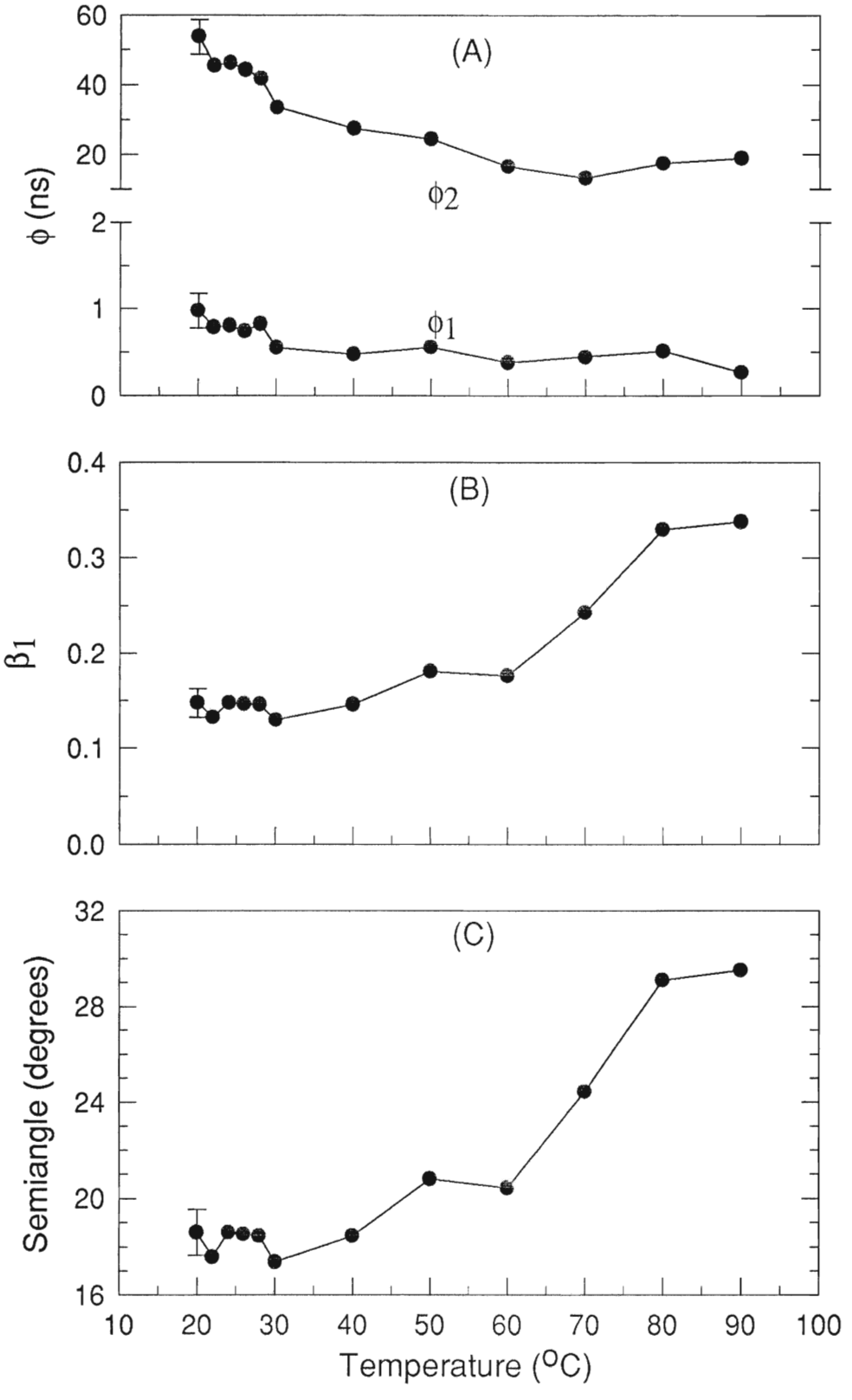

Figure 5.8. Time-resolved anisotropy of acrylodan within HSA-Ac during thermal denaturation. (A) fluorescence rotational correlation times for global (ϕ_2) and local (ϕ_1) rotational components, (B) fractional contribution of ϕ_1 as a function of temperature, (C) semi-angle of probe rotation obtained during heating of the protein. The error bars on each panel denote ± 1 standard deviation from at least three discrete measurements.

the acrylodan label (domain separation). However, there appears to be no corresponding changes in steady-state anisotropy. Further increases in temperature up to 90°C caused the global correlation time to decrease until a temperature of 70°C was reached, at which point a slight increase in ϕ_2 was observed. The most striking change in the time-resolved fluorescence anisotropy was the significant increase in the contribution from the local rotational motion, as evidenced by the large increase in β_1 between 60°C and 80°C, which corresponds well to the region where the acrylodan intensity reported the unfolding of domain I.

5.3.3 A Model for Unfolding of HSA

Based on the results presented above, the following model for unfolding of HSA can be developed. Based on salicylate binding studies, it is clear that raising the temperature to < 50°C or adding up to 1.0 M of GdHCl causes a complete loss of protein function, but that this process is almost fully reversible. Energy transfer results suggest that a domain I and II move apart during this stage, causing slight alterations in the local environment of both the Trp and acrylodan residue. This conclusion is based on the observed changes in emission maximum values for both probes, the increase in Trp intensity over this range for HSA-Ac (Figure 5.2B), and on the slight changes in the time-resolved decay of intensity and anisotropy for the acrylodan moiety. Increasing the temperature to above 60°C or increasing the level of denaturant to 2.0 M resulted in substantial changes in the spectroscopic parameters for the Trp residue. Both the integrated intensity and the steady-state anisotropy of the Trp residue drop significantly over this range. In the case of chemical denaturation, this change was accompanied by a 15 nm red-shift in the emission maximum, a doubling of

the k_q value, and a decrease of 16% in the mean fluorescence lifetime. For thermal unfolding, the emission maximum did not shift significantly. However, the fluorescence lifetime dropped by 53%. Together, these changes indicate a major structural change for the protein which is consistent with the unfolding of domain II. The spectroscopic parameters for the acrylodan probe over this temperature or denaturant range changed only slightly, with most parameters changing value by only a few percent. The most notable changes for acrylodan were the slight decrease in semi-angle which was accompanied by a 5 nm blue-shift in the emission maximum for the probe. These changes are consistent with a slight closing of the pocket surrounding the acrylodan moiety, and may be indicative of an indirect effect of domain II unfolding on the environment of domain I. Salicylate binding studies indicated that this stage of unfolding was only partially reversible, in agreement with the altered spectroscopic parameters for the Trp residue for the recovered protein.

Increasing the temperature above 70°C or higher, or the level of GdHCl to 4.0 M or above, resulted in small changes in the spectroscopic behaviour of the Trp residue beyond those obtained at 60°C, but had a significant effect on the emission properties of the acrylodan moiety. For example, the integrated intensity and anisotropy of Ac both decreased substantially between 2.2 M and 5.0 M GdHCl, with corresponding decreases in the mean fluorescence lifetime. For chemical denaturation, a 10 nm red-shift in the emission maximum and a 70% increase in the k_q value of the acrylodan moiety were also observed, with the semi-angle for acrylodan rotation increasing by 9°. Overall, these changes indicate that the acrylodan moiety becomes much more solvent exposed and more mobile, consistent with the unfolding of domain I. In addition, the energy transfer experiment indicated a significant increase in the average Trp-to-acrylodan distance, providing further evidence of an overall

expansion in the size of the protein. Salicylate binding experiments indicated that these structural alterations were only partially reversible. Thus, the unfolding of either domain I or domain II causes a significant loss in protein function.

The denaturation experiments indicate that the unfolding of HSA proceeds by the following scheme:

$$N \xleftrightarrow{Step1} E \xrightarrow{Step2} I \xrightarrow{Step3} U$$

where N is the native form of the protein, E is the expanded form, I is an intermediate where domain II is unfolded but domain I is intact, and U is the unfolded protein. The scheme proposed above is consistent with previous reports which show that heating HSA to temperatures less than 60°C results in refolding being fully reversible, while heating to higher temperatures results in a substantial loss of reversibility for the unfolding transition [17]. This model is also consistent with previous reports which suggest a multi-step unfolding pathway for HSA [17,21,23]. However, the new model is the first to provide detailed insights into the nature of the various unfolding intermediates, and is also the first to show that unfolding of domain I occurs only after the unfolding of domain II is complete. Spectroscopic data from both the Trp and acrylodan probes suggests that the U state shown in Scheme I is not a fully unfolded random coil, but rather a partially unfolded, or molten globule, state. This is likely the result of intact disulfide bonds within the various domains which act to maintain a degree of structure [20]. The addition of a disulfide reducing agent was not attempted since this would have removed the acrylodan label from Cys-34.

5.4. Conclusions

Combining the results from thermal and chemical denaturation of HSA and HSA-Ac, the following partial model can be proposed for the unfolding. In both cases, there is an

initial, reversible movement of domain I from domain II, resulting in a slight expansion of the protein structure. As the temperature or level of denaturant increases, domain II of the protein unfolds, causing major changes in the emission of Trp-214. At this point, the protein can be refolded to a non-functional state with a higher emission yield and a blue-shifted emission wavelength. Further increases in temperature or denaturant concentration cause the irreversible unfolding of domain I to occur, with a resultant alteration in the fluorescence properties of the Ac label. Unfolding of domain I results in an inability to properly refold the protein, and also results in aggregation with thermal denaturation. As domain I unfolds it appears that the average distance between the Ac and Trp probes decreases based on the slight increases in Trp emission beyond 2 M GdHCl. There is also a reduction in the accessibility of the Trp residue. This indicates that the protein likely adopts a new conformation which is not a random coil, but perhaps a rearrangement such that hydrophobic regions of the protein are protected from solvent. The protein does not fully unfold under any conditions, as evidenced by the high anisotropy of the Ac label under denaturing conditions. This is likely the result of intact disulfide bonds within the various domains which act to maintain some degree of structure. Evidence from other groups has shown that cleavage of disulfide bonds does result in substantial changes in the emission of the Trp residue. However, it is expected that such conditions would also remove the Ac label from Cys-34, and thus could not be employed in the present work. Overall, the results of this study show the potential of site-specific labelling of single Trp proteins as a method for gaining detailed information regarding the unfolding pathway and thermodynamic stability of such proteins.

5.5 References for Chapter 5

1)Carter, D. C.; Ho, J. X. *Adv. Prot. Chem.* **1994**, *45*, 153.

2)Brown, J. R. *Albumin Structure, Function and Uses*; Pergamon: Oxford, 1977.

3)Suzukida, M.; Le, H. P.; Shahid, F.; McPherson, R. A.; Birnbaum, E. R.; Darnall, D. W. *Biochem.* **1983**, *22*, 2415.

4)Hagag, N.; Birnbaum, E. R.; Darnall, D. W. *Biochem* **1983**, *22*, 2420.

5)Ingersoll, C. M.; Jordon, J. D.; Bright, F. V. *Anal. Chem.* **1996**, *68*, 3194.

6)Jordon, J. D.; Dunbar, R. A.; Bright, F. V. *Anal. Chem.* **1995**, *67*, 2436.

7)Wang, R.; Sun, S.; Bekos, E. J.; Bright, F. V. *Anal. Chem.* **1996**, *67*, 149.

8)Narazaki, R.; Maruyama, T.; Otagiri, M. *Biochim. Biophys. Acta.* **1997**, *1338*, 275.

9)Lundgren, J. S.; Heitz, M. P.; Bright, F. V. *Anal. Chem.* **1995**, *67*, 3775.

10)Sudlow, G.; Birkett, D. J.; Wade, D. N. *Molec. Pharmacol.* **1976**, 1052-1061.

11)Prendergast, F. G.; Meyer, M.; Carlson, G. L.; Iida, S.; Potter, J. D. *J. Biol. Chem.* **1983**, *258*, 7541.

12)Ilich, P.; Prendergast, F. G. *J. Phys. Chem.* **1989**, *93*, 4441.

13)Clark, I. D.; Burtnick, L. D. *Arch. Biochem. Biophys.* **1988**, *260*, 595.

14)Yem, A. W.; Epps, D. E.; Matthews, W. R.; Guido, D. M.; Richard, K. A.; Staite, N. D.; M.R. Deibel, J. *J. Biol. Chem.* **1992**, *267*, 3122.

15)Pico, G. A. *Biochem. Molec. Biol. Int.* **1995**, *36*, 1017.

16)Pico, G. A. . *Biochem. Molec. Biol. Int.* **1996**, *38*, 1.

17)Pico, G. A. *Int. J. Biol. Macromolec.* **1997**, *20*, 63.

18)Wetzel, R.; Becker, M.; Behlke, J.; Wite, H.; Bohn, S.; Ebert, B.; Hamaann, H.; Krumbiegel, J.; Lasiman, G. *Eur. J. Biochem.* **1980**, *104*, 469.

19)Tayyab, S.; Siddiqui, M. U.; Ahmad, N. *Biochem.* **1995**, *23*, 162.

20)Lee, J. Y.; Hirose, M. *J. Biol. Chem.* **1992**, *267*, 14753.

21)Wallevik, K. *J. Biol. Chem.* **1973**, *248*, 2650.

22)Farruggia, B.; Gabriela, G.; D'Angelo, C.; Pico., G. *Int. J. Macromolec.* **1997**, *20*, 43.

23)Chmelik, J.; Kalous, V. *Bioelectrochem. Bioenerg.* **1982**, *9*, 7.

24)Price, W. S.; Ge, N. H.; Hong, L. Z.; Hwang, L. P. *J. Am. Chem. Soc.* **1993**, *115*, 1095.

25)Brown, K. F.; Crooks, M. J. *Biochem. Pharmacol.* **1976**, 1175.

26)Kerestes-Nagy, S.; Mais, R. F.; Dester, Y. T.; Zaroslinski, J. F. *Anal. Biochem.* **1972**, *48*, 80.

27)Hultmark, D.; Borg, K.; Elofsson, R.; Palme, L. *Acta. Pharm. Suec.* **1975**, *12*, 259.

28)Edminston, P. L.; Wambolt, C. L.; Smith, M. K.; Saavedra, S. S. *J. Coll. Int. Sci.* **1994**, *163*, 395.

29)Zheng, L.; Reid, W. R.; Brennan, J. D. *Anal. Chem.* **1997**, *69*, 3940.

30)Wang, R.; Bright, F. V. *J. Phys. Chem.* **1993**, 4231-4238.

31)O'Connor; Phillips, D. V. *Time-Correlated Single Photon Counting*; Academic Press: London, 1984.

32)Lakowicz, J. R.; Weber, G. *Biochem.* **1973**, *12*, 4161.

33)Eftink, M. R. *Biophys. J.* **1994**, *66*, 482.

34)Helms, M. K.; Petersen, C. E.; Bhagavan, N. V.; Jameson, D. M. *FEBS Lett.* **1997**, *408*, 67.

Chapter 6: Investigation of HSA and HSA-Ac in TEOS derived Matrices

6.1 Introduction

The unfolding behaviour of HSA occurs by a multi-step process which can be elucidated using a combination of fluorescence techniques in solution. It is of interest to examine the unfolding behaviour and structure-function relationships of HSA encapsulated into TEOS derived matrices to investigate whether the entrapped protein undergoes similar changes in structure, conformation, stability and functionality upon denaturation. Studies have previously been conducted on HSA/BSA and HSA-Ac/BSA-Ac while immobilized to inorganic surfaces, or entrapped in sol-gel derived media. [1-5] However, the questions of whether or not HSA and HSA-Ac are able to retain its structure and/or function and whether protein stability is allowed by entrapment still need to be addressed.

Given the size and structural complexity of HSA several interesting questions can be addressed, including: Is the sol-gel-derived matrix able to entrap large proteins with retention of structure and function? Are the pores of the sol-gel-derived matrix large enough to allow the biomolecule to undergo large scale conformational changes? Will the protein unfold in the same manner as it does in solution while encapsulated? These questions are addressed using the fluorescence techniques outlined in Chapter 5.

6.2 Experimental

All chemicals used and procedures followed are as described in Chapters 3 and 5.

6.2.1 Entrapment of HSA and HSA-Ac into TEOS-derived matrices

Monoliths were prepared and mounted for fluorescence studies as described in Chapter 3. After gelation, the sol-gel-derived matrices were rinsed twice with buffer for 30 minutes each cycle. The samples were aged for 12 days, prior to testing.

6.2.2 Salicylate Binding

Salicylate binding titrations were performed on the mounted monolith as described in Chapter 5. 12 minutes were allowed to reach equilibrium between additions, before spectra were collected. Spectra collection and data analysis were done as described in Chapter 5.

6.3 Results and Discussion

6.3.1. Structure of Encapsulated HSA and HSA-Ac

As shown in Figure 6.1, the fluorescence spectra of encapsulated HSA and HSA-Ac are similar to the spectra of the proteins in solution. This indicates that the protein was able to survive the high ethanol concentrations of encapsulation. An ethanol titration was performed on the native protein in solution to investigate the effects of alcohol on the emission spectra of HSA. It was found that a blue shift of the Trp emission occurs as a function of increasing concenctration of ethanol. In solution, at 36% ethanol the emission maximum is at 325 nm in comparison to 337 nm with no ethanol present. Figure 6.2 shows the effects of ethanol on the emission spectrum of HSA. Thus, the slight blue shift of the encapsulated protein in Figure 6.1 is most likely due to the presence of residual ethanol, which remained after washing steps were complete.

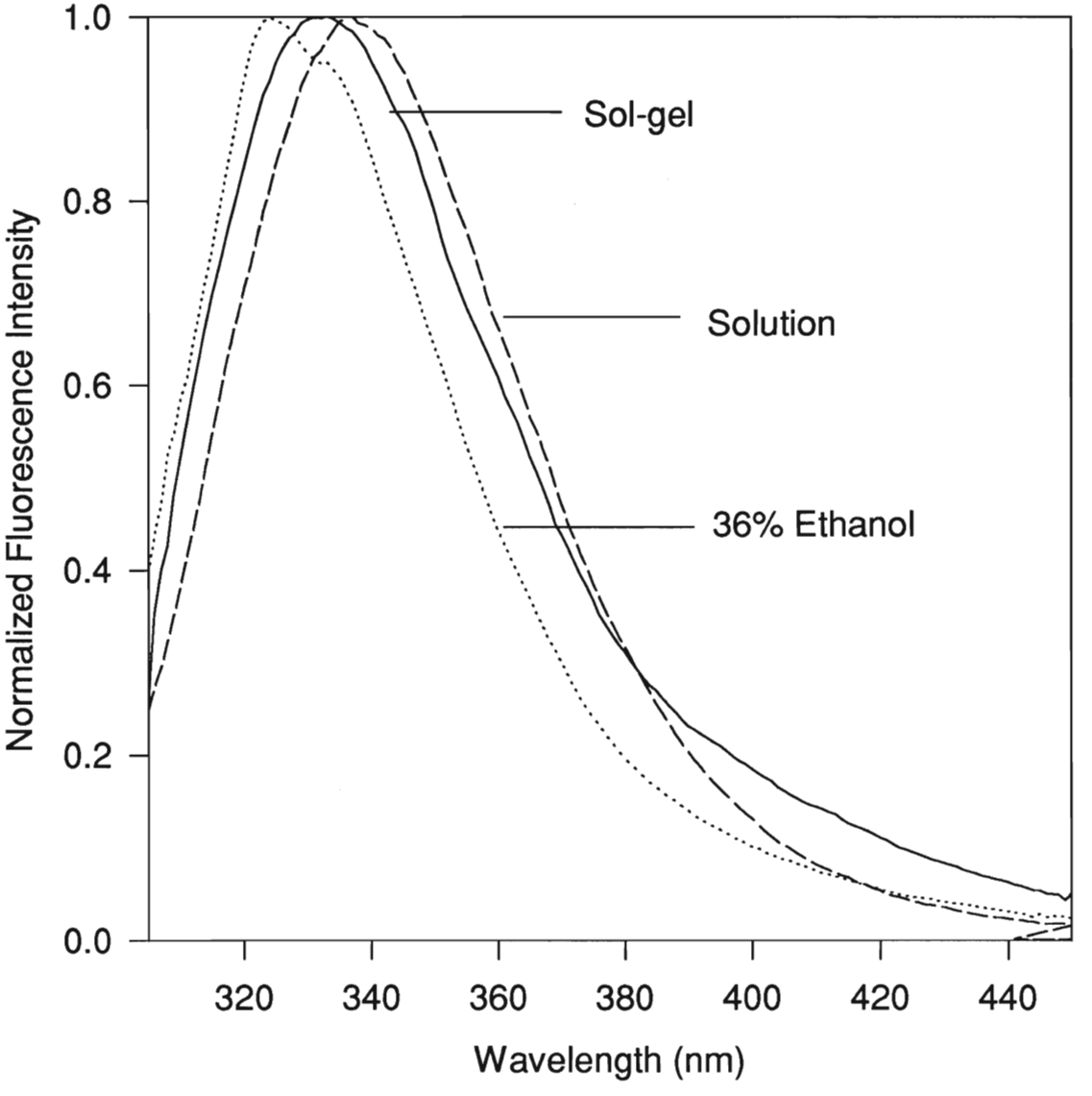

Figure 6.1. Fluorescence emission entrapped HSA and free HSA both native and in the presence of 36% ethanol.

6.3.2 Salicylate Binding of Entapped Protein

The ability of entrapped HSA to bind salicylate was examined to characterize the function of the entrapped HSA. Binding studies showed that encapsulated HSA remained in a funtional state while entrapped in the sol-gel-derived matrix. These results could not be correlated directly with the results obtained in solution, owing to difficulties encountered with direct interactions between salicylic acid and the silicate matrix, which made it appear that the binding affinity is actually elevated in the sol-gel matrix. The free form of salicylic acid fluoresces at 408 nm, and upon binding to HSA the fluorescence intensity increases with a corresponding decrease in Trp emission intensity. The changes in fluorescence emission are due to an energy transfer phenomena where the Trp residue transfers energy to salicylic acid, due to an ovelap of the acid excitation spectra and the Trp emission spectra. The apparent increase in binding ability may be due to enhancement in the process, resulting from improved overlap of the excitation spectrum of salicylic acid and the emission spectrum of Trp. As a control experiment, binding studies were also done for the entrapped protein after heating to 80°C. It was found that the extent of salicylic acid binding was 3.5 fold greater for the native protein at room temperature relative to the heated protein. The extent of binding at 80°C which is 4.4-fold greater than for free HSA heated to 40°C, suggesting that the protein has not lost its function. In solution, the protein loses most of its function at 40°C (1.5-fold less than native), where domain II has unfolded. Further studies are required to confirm this result.

6.3.3 Thermal Denaturation of Encapsulated HSA and HSA-Ac

Thermal denaturation experiments for both entrapped HSA and HSA-Ac were performed with matrices hosting the entrapped proteins aged for 12 days. Figure 6.2 shows the thermal unfolding curve of entrapped HSA and the respective unfolding curve generated in solution.

As seen in Figure 6.2, free HSA (closed circles) unfolds at a much lower temperature than entrapped HSA (open circles). Although a post unfolding baseline is not evident for the entrapped protein, it appears to have fully unfolded based on changes in intensity, maximum emission wavelength and the spectral half-width at half-maximum (HWHM), as illustrated in Table 6.1. For example, in solution the intensity decreased 60% by 78°C while in the silicate matrix the intensity only decreased 32% at 78°C, and decreased a total of 65% by 95°C. This is again suggesting that the protein was able to unfold completely in the sol-gel matrix, but not shown due to instrument limitations. Based on the unfolding curves, it appears that HSA is actually stabilized upon entrapment by approximately 20°C. An increase in thermal stablilty of 14°C ± 1°C has been previously shown with sol-gel entrapped monellin. [6] Furthermore, by investigating Figure 6.2, it can be seen that the unfolding transition is much broader than that obtained for the free protein. This is again indicative of a distribution of environments, as was observed for cod III parvalbumin in chapter 3 of this thesis. Thermodynamic parameters could not be calculated for the entrapped protein since there was not a level post transition region present.

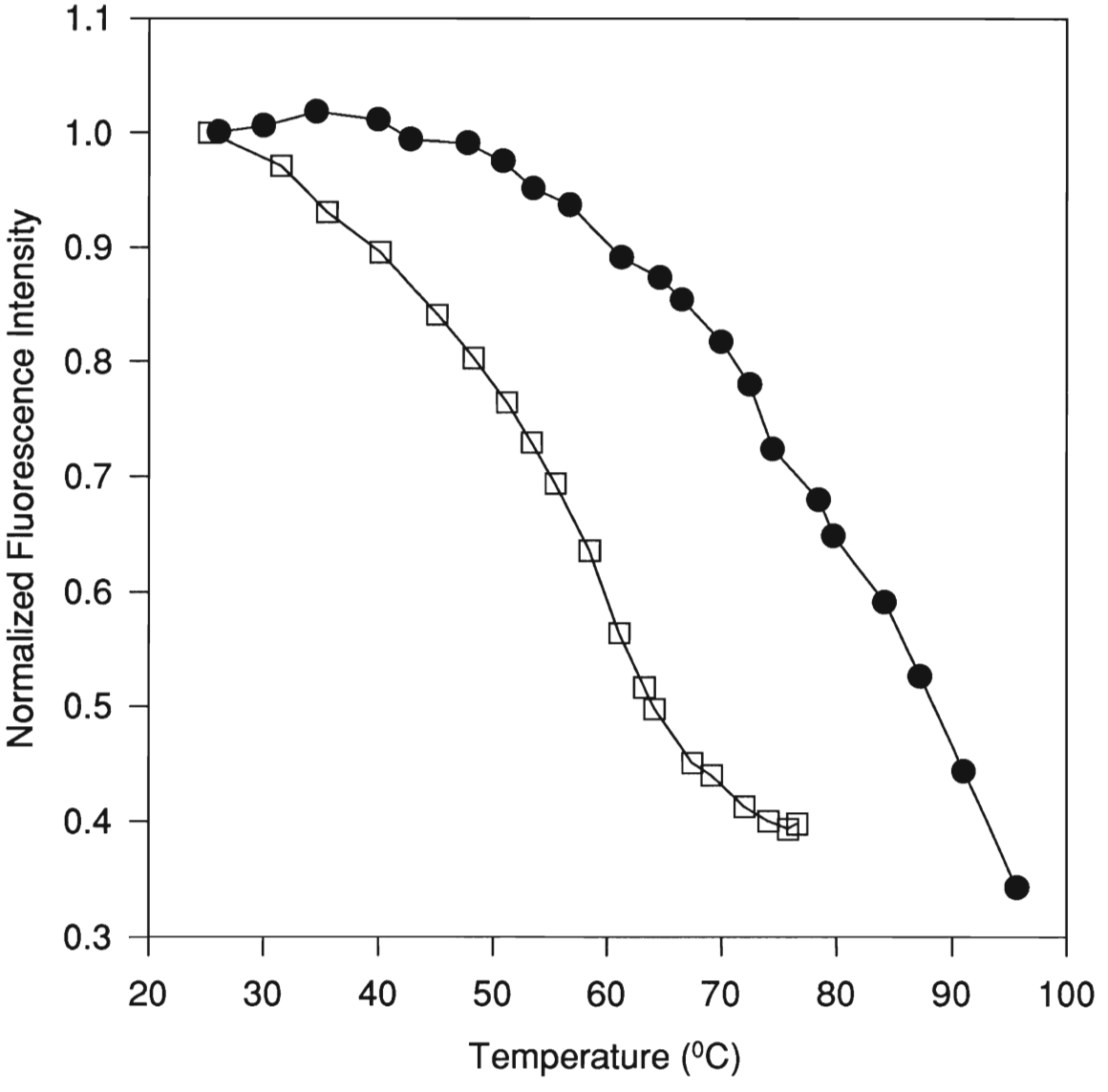

Figure 6.2. Unfolding curves from thermal denaturation of free (●) and entrapped HSA (○).

Spectra collected before, during and after thermal denaturation of HSA are shown in Figure 6.3. As in solution, the entrapped protein blue shifted with increasing temperature indicating, that some unfolding is able to take place. Table 6.1 gives quantitative information of the spectra obtained for heating and recovering free and entrapped HSA. What is interesting to note is that the intensity changes of the denatured and recovered states are identical for the free and entrapped protein. This again indicates that unfolding has taken place and that the same recovered state is obtained for the free and entrapped protein indicating, that similar unfolding patterns have taken place.

Table 6.1. Spectral Information for Entrapped and Free HSA before, during and after thermal denaturation.

	HWHM (nm)	Emission Max. (nm)	Intensity Changes
Free			
Native	32	336	100%
Denatured	31	330	65 %
Recovered	31	330	82%
Entrapped			
Native	33	334	100%
Denatured	35	330	65%
Recovered	31	329	82%

Figure 6.4 shows the changes in anisotropy for entrapped HSA during thermal denaturation. The anisotropy drops from 0.20 to only 0.18 for the entrapped protein in comparison to a drop fom 0.18 to 0.12 for the free protein on going from room temperature to 60°C. The anisotropy of the entrapped protein then increases to 0.20 at 80°C. This indicates that the entrapped protein has not undergone a substantial change in average mobility upon heating. This may be due to a higher viscosity in the entrapped local

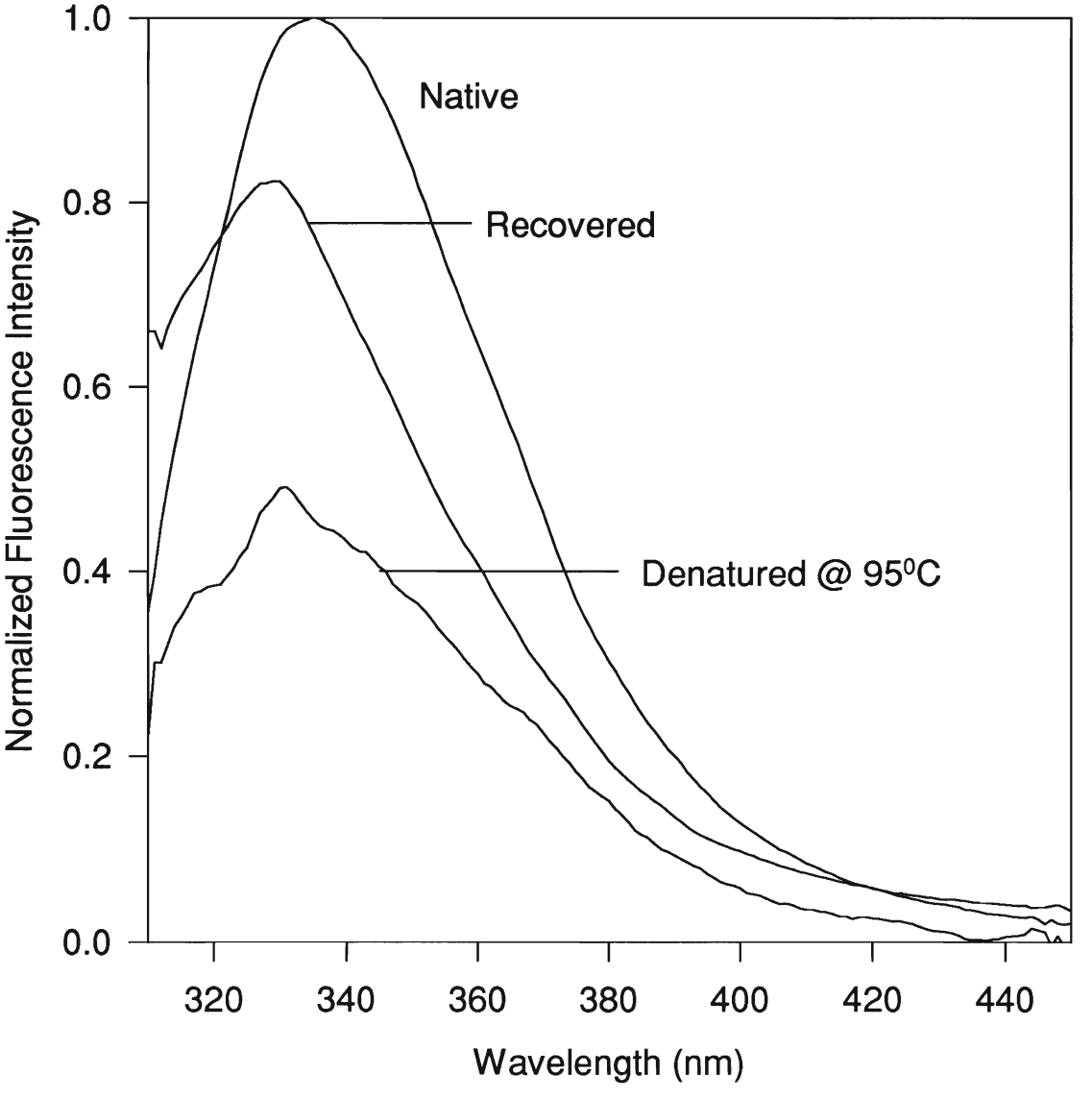

Figure 6.3. Changes in emission spectra of entrapped HSA as a function of heating

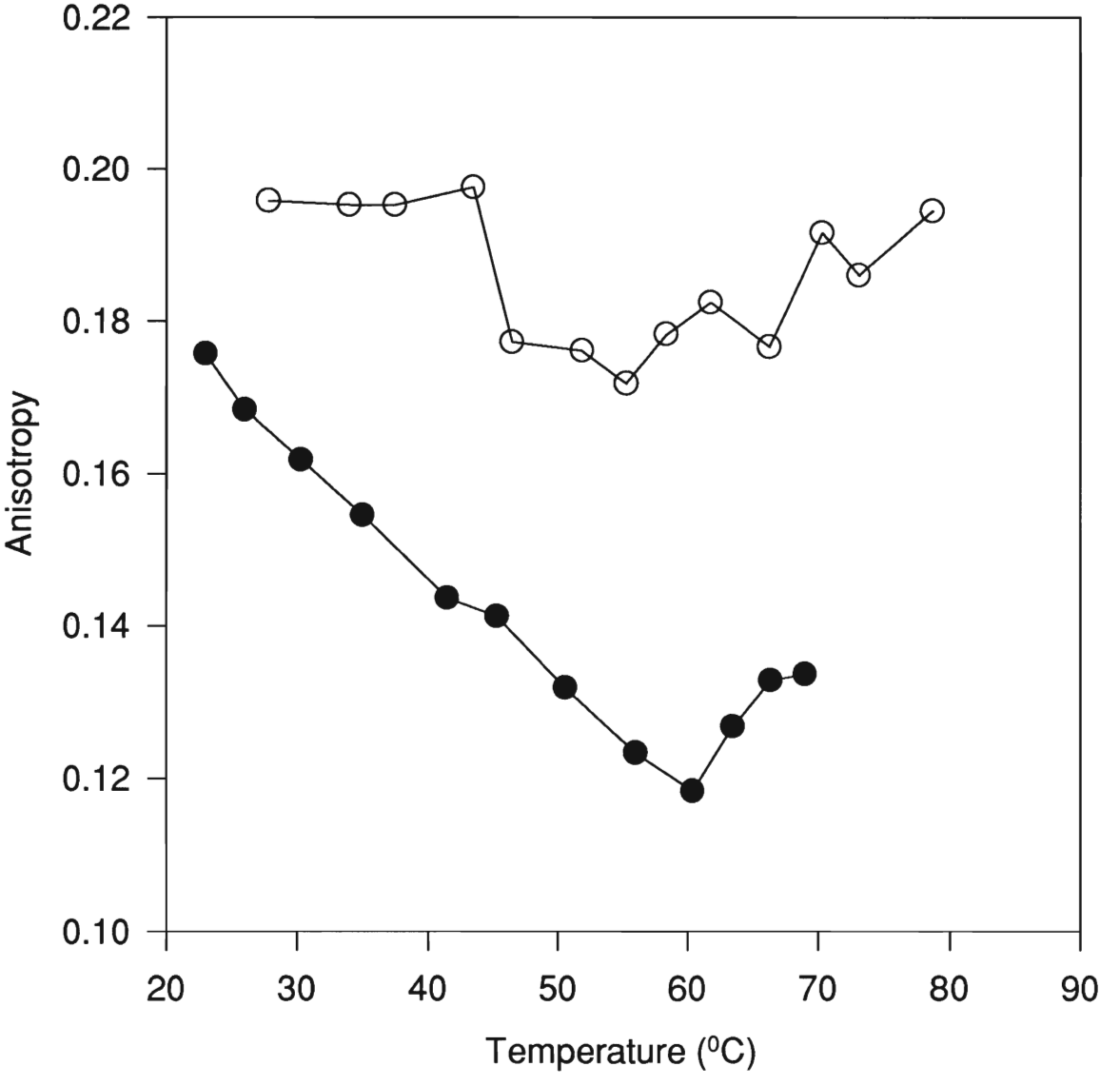

Figure 6.4. Monitoring of anisotropy of free (●) and entrapped HSA (○) during thermal denaturation.

environment of the protein or perhaps some adsorption of the protein to the pore walls of the matrix, or perhaps incomplete unfolding due to the presence of a distribution of environments. Time resolved measurements are required to further explore this issue.

Figure 6.5 shows the unfolding of HSA-Ac obtained by monitoring the Trp residue via excitation at 295 nm. In this case, the unfolding of the free protein (closed circles) and the entrapped protein (open circles) follow each other relatively closely throughout most of the unfolding curve, until the end where again the entrapped protein displays a broader unfolding transition and an increase in T_{un} of about 10°C. The appearance of a two-step unfolding process for the entrapped protein is in agreement with the results for the protein in solution. Based on solution studies, it is likely that the first stage is representative of the unfolding of domain II, while the second stage represents the unfolding of domain I. Although the two curves shown in this figure don't overlap completely, they do decrease in intensity the same amount, 60%. The differences in thermal stability of HSA as compared to HSA-Ac is not known at this time. This needs to be examined further.

Figure 6.6 shows the unfolding curve obtained by directly exciting the Ac residue in the labelled protein. The unfolding curve of the free protein (closed cicles) appears to have its unfolding transition *later* than the entrapped protein (open circles), although again the unfolding transition is actually broader in the gel. However, the intensity drops 60% for the entrapped protein (at 90°C) compared to 45% for the free protein. This indicates that unfolding must be occuring. The reason for the larger drop in intensity for the entrapped protein is likely due to photobleaching of the Ac probe owing to diffusional limitations or the presence of O_2. Visual inspection of the two unfolding curves suggests a similar value for T_{un}, ~80°C. Note, however, that the T_{un} value for free HSA-Ac is diffucult to accurately

determine due to lack of the post unfolding region. Monitoring of the Ac probe actually represents the unfolding of domain I in HSA. For both free and entrapped HSA-Ac, the instrument is not able to heat the protein high enough to see the complete unfolding of domain I. However, the Ac emission spectra blue shifted, indicating that a change is taking place in the environment surrounding the probe.

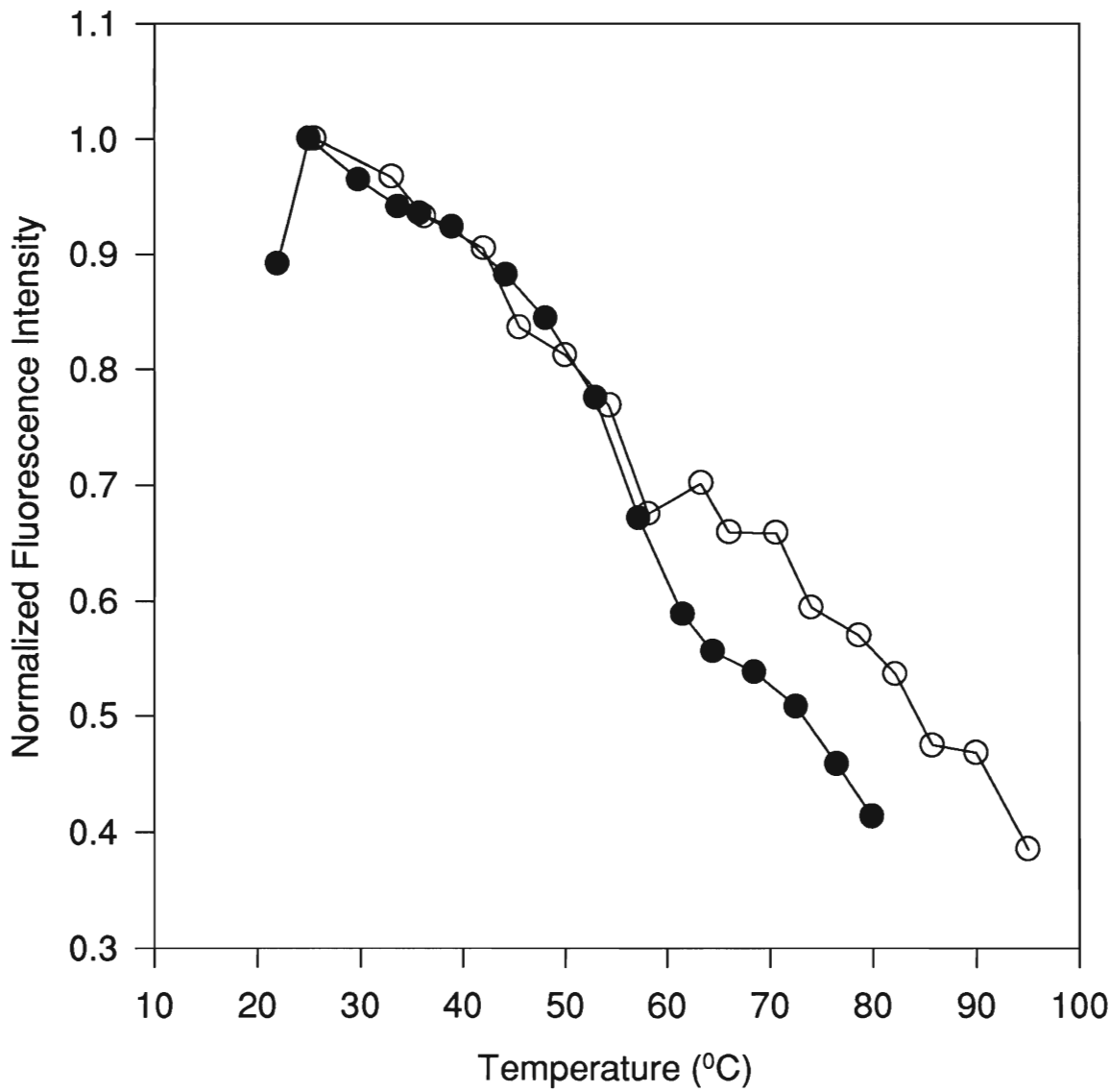

Figure 6.5. Monitoring the changes in Trp fluorescence intensity of free (●) and entrapped (○) HSA-Ac through direct excitation of the Trp residue at 285 nm.

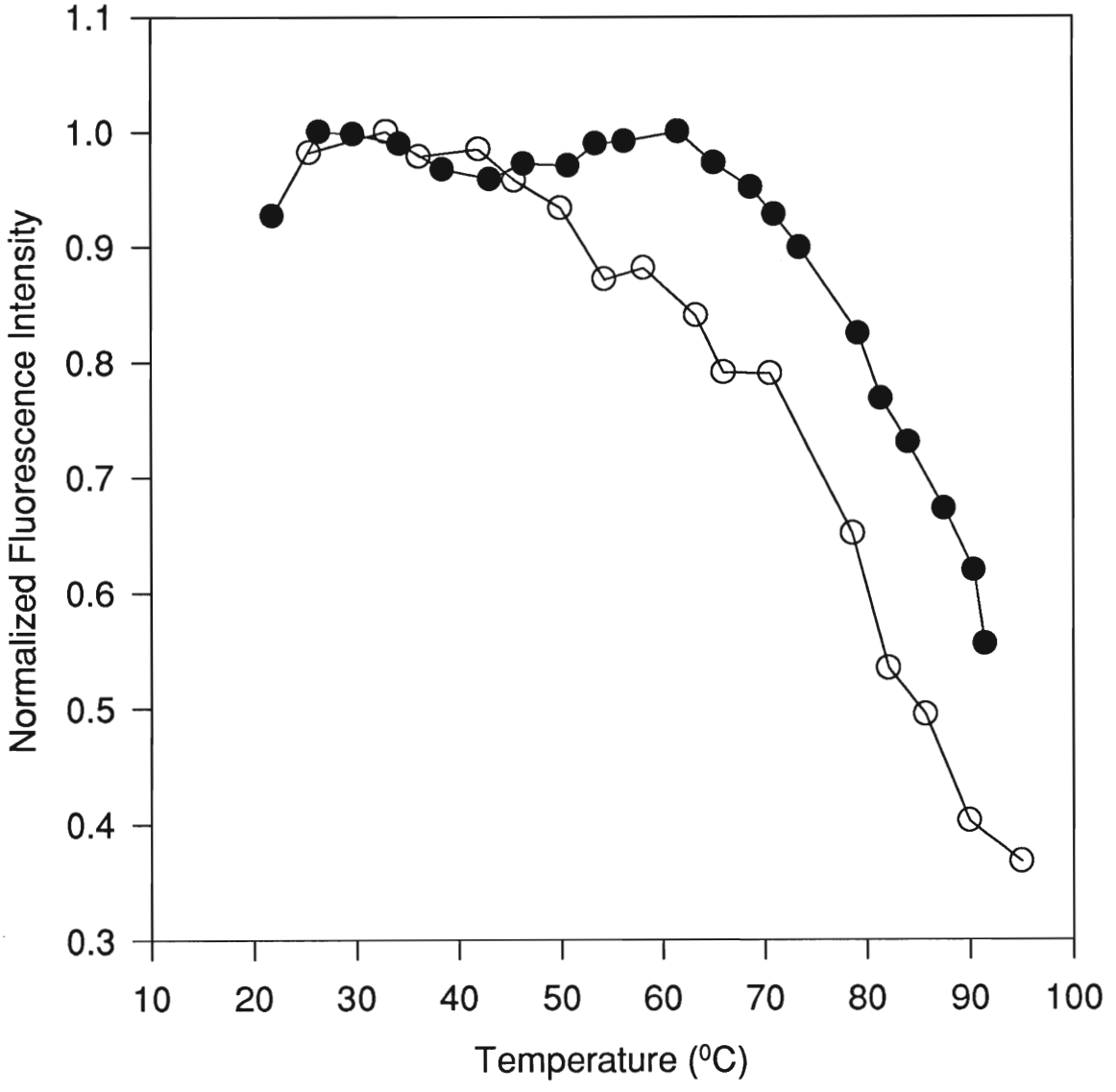

Figure 6.6. Monitoring the changes in Ac fluorescence intensity of free (●) and entrapped (○) HSA-Ac by direct excitiation at 360 nm.

6.4 Conclusions

HSA can be successfully entrapped into sol-gel derived matrices with retention of structure and binding ability. Thermal denaturation of entrapped HSA showed an increase in the thermal stability of domain II about 20°C in comparison to free protein. The stability of domain I was similar to that obtained in solution. This preliminary work provides a basis for further studies which must be done to characterize the changes in stability and dynamics for the two domains on entrapment.

6.5 References for Chapter 6

1)Jordon, J. D.; Dunbar, R. A.; Bright, F. V. *Anal. Chem.* **1995**, *67*, 2436.

2)Edminston, P. L.; Wambolt, C. L.; Smith, M. K.; Saavedra, S. S. *J. Coll. Int. Sci.* **1994**, *163*, 395.

3)Ingersoll, C. M.; Jordon, J. D.; Bright, F. V. *Anal. Chem.* **1996**, *68*, 3194.

4)Wang, R.; Sun, S.; Bekos, E. J.; Bright, F. V. *Anal. Chem.* **1996**, *67*, 149.

5)Narazaki, R.; Maruyama, T.; Otagiri, M. *Biochim. Biophys. Acta.* **1997**, *1338*, 275.

6)Zheng, L; Brennan, J.D. *The Analyst.* **1998**, *123*, 1735.

Chapter 7: Conclusions and Future Work

7.1 Conclusions

Although the field of biosensors has grown rapidly over the past decade, many obstacles still exist in the efficient interfacing of biomolecules to physical transducers. In this work, we have been able to successfully advance the understanding of structure-function relationships of proteins, both in solution and when entrapped in sol-gel derived matrices. Solution studies have provided new information regarding the unfolding pathway of HSA, by labelling domain I with acrylodan to obtain further information during stability studies. Although this highly abundant protein had been studied for decades, the model we have proposed and the method by which we investigated the unfolding was novel.

HSA and HSA labelled with acrylodan (HSA-Ac), which is a much larger protein molecule, was also able to be entrapped in their native state. Even though a distribution of environments is evident for the entrapped proteins, an increase in T_{un} of 20° was evident for HSA. This indicates an increase in thermal stability of the entrapped protein . Entrapped HSA-Ac thermal stability results showed that the region containing the Trp residue is stabilized and the region containing the Ac was as stable as in solution. This indicates that perhaps entrapment has resulted in only the stabilizing of domain II. The protein may be able to unfold, although instrumentation limits with temperature do not allow the monitoring of this. These results need to be investigated further.

By the time this thesis was written, the structure-function relationships as well as the stability and unfolding of cod III parvalbumin were already well understood in

solution. Once the proteins were characterized in solution, we were able to successfully encapsulate them into sol-gel derived silicate monoliths to examine how they behave while encapsulated. Cod III parvalbumin was able to maintain its structure, stability as well as binding ability when entrapped. In fact, the stability was improved in terms of chemical denaturation by urea. In terms of binding Ca^{2+}, the process was reversible, although the binding capacity decreases as the number of detection cycles increased. This is most likely due to the fact that some fraction of the protein is irreversibly denaturing in each cycle. It was also found that the k_d value decreased as a function of aging. The optimal aging time was found to be 15-20 days.

We took these studies a step further to investigate the structure, function and binding ability of cod III parvalbumin labelled with acrylodan and iodoacetoxy-nitrobenzoxadiazole. The purpose of labelling this protein was to be able to detect Ca^{2+} without having to excite the protein in the UV region. Results showed that Ac was too large a probe to allow refolding of the protein after labelling. However, the protein was able to refold in the presence of NBD. Thermal stability studies indicated that C3P-NBD was as stable a free C3P, whereas C3P-Ac was not. Preliminary work showed that NBD was the better probe to use for Ca^{2+} detection.

Preliminary fiber optic work indicated that free and entrapped C3P-NBD can be excited at 442 nm to detect the binding of Ca^{2+}, via distal end sensing. The results obtained from Ca^{2+} sensing using entrapped C3P-NBD were very promising. It was shown that C3P-NBD entrapped into sol-gel derived matrix on the end of a fiber is capable of reversibly sensing Ca^{2+} with good sensitivity and a LOD of less than 5 μM

(based on sensitivity and S/N levels), and also is capable of undergoing the FAST process for fluorescently labelled proteins.

The results in this thesis show that proteins, both large and small, can be successfully encapsulated into TEOS derived matrices to retain their structure, function and in some cases improve the stability of the entrapped protein.

7.2 Future Work

Low temperature sol-gel processing is proving to be a successful method for entrapment of biomolecules. Many proteins have been reported to have actually been further stabilized when entrapped in comparison to in solution. However, the harsh initial conditions posed by the sol-gel process can immediately decide whether or not the entrapment will be detrimental to the protein.

The first suggestion for future work is to better control and aim to minimize the amount of alcohol present during entrapment. Alcohol is known to be detrimental to many proteins. This could perhaps be done by choosing different precursors or conducting washing steps. Of course washing steps are not an option for small proteins since leaching can result. Thus other alternatives are needed to remove the alcohol, such as rotary evaporation of the hydrolyzed silane prior to addition of buffer.

Another large problem with using sol-gel entrapped molecules as sensors is that 100% of the protein is not usually native after encapsulation. Some fraction of the protein is not able to retain its structure, stability and or activity. This is possibly due to a distribution of environments which is produced as a result of the sol-gel process. Control

of stability and minimization of the number of environments is a key component in developing regenerable biosensors.